

**Mathematical Modeling of Bone Mineralization: Incorporating Biological and  
Physicochemical Dynamics**

Hossein Poorhemati

Biological and Biomedical Engineering

McGill University, Montreal

April 2024

A thesis submitted to McGill University in partial fulfillment of the requirements of the  
degree of Doctor of Philosophy

© Hossein Poorhemati, 2024

## **Abstract**

Bone is a composite material with specific physical properties dictated by its biological function. Formation of mineralized bone tissue includes production of collagenous organic matrix by bone-forming osteoblasts, matrix maturation in the extracellular space, and controlled deposition of hydroxyapatite onto the mature matrix. In certain human diseases, such as osteogenesis imperfecta and osteomalacia, bone mineralization is affected, resulting in the formation of tissue which is either too brittle or too soft. Appropriate calcium and phosphate levels are important for bone formation and regulated in terrestrial animals by the number of hormones, including parathyroid hormone (PTH), vitamin D, and fibroblast growth factor 23 (FGF23). Alongside cellular and hormonal mechanisms, the mineralization process is inherently controlled by physicochemical factors, including ion composition and pH of the surrounding biological fluid. Understanding the contribution of biological and physicochemical factors to the process of bone formation is crucial for developing treatment strategies for diseases that affect bone health.

Computational modeling provides a way to mathematically represent our understanding of underlying processes, thus allowing an overarching control over multiple factors. Carefully built mathematical models provide an ability to explore diverse scenarios that may not be feasible to replicate experimentally, thus allowing comprehensive analysis of complex systems. The goal of my research was to use mathematical modeling to explore the role of the physicochemical regulation of calcium and phosphate homeostasis in regulation of bone mineralization.

Previous mathematical models of bone formation omitted the physicochemical aspects of the process. To overcome this gap, I simulated the environment, also known as bone interstitial fluid, is where all ions required for the mineral formation are accumulated. The environment composition of 7 major components and 22 chemical species was defined according to published literature. I mathematically described the chemical processes resulting in the equilibrium established prior to the mineral precipitation, then examined if this solution is supersaturated regarding hydroxyapatite and other calcium phosphate species, and finally modeled the mineral precipitation. Model analysis demonstrated a significant role of pH and phosphate levels in regulating the dynamics of interstitial fluid, by adjusting ions availability, saturation level and precipitation rate.

Next, I integrated the physicochemical regulation of bone formation with the biological regulation described in the previously developed models. The comprehensive model included the transition of collagen matrix from naïve to mature form, the action of biomineralization inhibitors and nucleators, the physicochemical processes occurring in the interstitial fluid and the mineral formation rate that was informed by both physicochemical and biological regulation. After fine tuning the integrated model to describe the experimentally observed dynamics of bone formation, we were able to investigate and compare the contribution of different factors, their importance, and their synergic influence in the outcome of mineralization. Importantly, to fully explain experimental data, the model required assuming that inhibitors of mineralization are removed proportionally to the mineral formation, thus suggesting a new testable hypothesis.

The integrated model enables comprehensive exploration of the dynamics of bone formation within specific physiological contexts, thus deciphering the underlying mechanisms driving observed phenotypes. These conditions may be rooted in disruptions of ion levels in disorders like X-linked hypophosphatemia, or they may stem from biological factors such as abnormalities in collagen type I, as seen in cases of osteogenesis imperfecta.

## Résumé

L'os est un matériau composite dont les propriétés physiques spécifiques sont dictées par sa fonction biologique. La formation du tissu osseux minéralisé comprend la production d'une matrice organique collagénique par les ostéoblastes formant l'os, la maturation de la matrice dans l'espace extracellulaire et le dépôt contrôlé d'hydroxyapatite sur la matrice mature. Dans certaines maladies humaines, telles que l'ostéogenèse imparfaite et l'ostéomalacie, la minéralisation osseuse est affectée, ce qui entraîne la formation de tissus trop fragiles ou trop mous. Des niveaux appropriés de calcium et de phosphate sont importants pour la formation des os et sont régulés chez les animaux terrestres par un certain nombre d'hormones, dont l'hormone parathyroïdienne (PTH), la vitamine D et le facteur de croissance des fibroblastes 23 (FGF23). Outre les mécanismes cellulaires et hormonaux, le processus de minéralisation est intrinsèquement contrôlé par des facteurs physico-chimiques, notamment la composition ionique et le pH du liquide biologique environnant. La compréhension de la contribution des facteurs biologiques et physico-chimiques au processus de formation osseuse est cruciale pour le développement de stratégies de traitement des maladies qui affectent la santé osseuse.

La modélisation informatique permet de représenter mathématiquement notre compréhension des processus sous-jacents, permettant ainsi un contrôle global sur de multiples facteurs. Des modèles mathématiques soigneusement construits permettent d'explorer divers scénarios qu'il n'est peut-être pas possible de reproduire expérimentalement, ce qui permet une analyse complète de systèmes complexes. L'objectif de ma recherche était d'utiliser la modélisation mathématique pour explorer le rôle de la

régulation physico-chimique de l'homéostasie du calcium et du phosphate dans la régulation de la minéralisation osseuse.

Les modèles mathématiques précédents de la formation osseuse omettaient les aspects physico-chimiques du processus. Pour combler cette lacune, j'ai simulé l'environnement, également connu sous le nom de fluide interstitiel de l'os, où s'accumulent tous les ions nécessaires à la formation du minéral. La composition de l'environnement en 7 composants majeurs et 22 espèces chimiques a été définie en fonction de la littérature publiée. J'ai décrit mathématiquement les processus chimiques aboutissant à l'équilibre établi avant la précipitation minérale, puis j'ai examiné si cette solution était sursaturée en hydroxyapatite et autres espèces de phosphate de calcium, et enfin j'ai modélisé la précipitation minérale. L'analyse du modèle a démontré un rôle significatif du pH et des niveaux de phosphate dans la régulation de la dynamique du fluide interstitiel, en ajustant la disponibilité des ions, le niveau de saturation et le taux de précipitation.

Ensuite, j'ai intégré la régulation physico-chimique de la formation osseuse à la régulation biologique décrite dans les modèles développés précédemment. Le modèle complet comprenait la transition de la matrice de collagène de la forme naïve à la forme mature, l'action des inhibiteurs de biominéralisation et des nucléateurs, les processus physicochimiques se produisant dans le fluide interstitiel et le taux de formation minérale qui était informé à la fois par la régulation physicochimique et la régulation biologique. Après avoir affiné le modèle intégré pour décrire la dynamique de la formation osseuse observée expérimentalement, nous avons pu étudier et comparer la contribution des différents facteurs, leur importance et leur influence synergique sur le résultat de la minéralisation. Il

est important de noter que pour expliquer pleinement les données expérimentales, le modèle a nécessité de supposer que les inhibiteurs de la minéralisation sont éliminés proportionnellement à la formation du minéral, suggérant ainsi une nouvelle hypothèse vérifiable.

Le modèle intégré permet une exploration complète de la dynamique de la formation osseuse dans des contextes physiologiques spécifiques, déchiffrant ainsi les mécanismes sous-jacents à l'origine des phénotypes observés. Ces conditions peuvent être enracinées dans des perturbations des niveaux d'ions dans des troubles tels que l'hypophosphatémie liée au chromosome X, ou elles peuvent découler de facteurs biologiques tels que des anomalies dans le collagène de type I, comme on le voit dans les cas d'ostéogenèse imparfaite.

*To my beloved partner, Faezeh, your love and unwavering support carried me through every triumph and doubt. This journey is ours.*

*To my incredible parents, Farideh and Ebrahim, your wisdom, sacrifices, and endless belief in my abilities have fueled this achievement.*

*To my cherished siblings, Ali and Neda, your constant cheer enriched this journey. Your presence has made the challenges more bearable and the successes more joyful.*

## Contents

|   |      |
|---|------|
| List of Figures.....  | iii  |
| List of Tables.....   | xi   |
| Abbreviations.....  | xiii |
| Acknowledgements .....  | xvii |
| Contribution to original knowledge.....   | xix  |
| Contribution of Authors.....  | xxi  |
| Chapter 1. Introduction.....  | 1    |
| Chapter 2. Biology, physical chemistry, and mathematics of Bone .....   | 3    |
| 1. Introduction.....  | 3    |
| 2. Bone biology .....   | 3    |
| 2.1. Bone composition .....   | 3    |
| 2.2. Bone physiology.....   | 4    |
| 2.3. Bone functions.....  | 8    |
| 2.4. Bone formation .....   | 12   |
| 3. Physicochemical Aspects of Bone Mineralization.....  | 15   |
| 3.1. Solubility and Precipitation .....   | 16   |
| 3.2. Crystal Nucleation and Growth .....  | 20   |
| 3.3. Role of Non-collagenous Proteins .....   | 23   |
| 4. Mathematical modeling of Bone Homeostasis.....   | 26   |
| References .....  | 30   |
| Chapter 3. Mathematical modeling of the role of bone turnover in pH regulation in bone interstitial fluid ..... | 37   |
| Abstract.....   | 38   |
| 1. Introduction.....  | 39   |
| 2. Model Development.....   | 40   |
| 3. Results and Discussion .....   | 47   |
| 4. Conclusions .....  | 58   |
| References .....  | 60   |
| Bridging chapter 3 and 4.....   | 63   |
| Chapter 4. Mathematical model of physicochemical regulation of precipitation of bone hydroxyapatite.....        | 64   |
| Abstract.....   | 65   |
| 1. Introduction.....  | 66   |

|   |     |
|---|-----|
| 2. Model Development and Simulations .....  | 67  |
| 3. Results .....  | 75  |
| 4. Discussion .....   | 86  |
| 5. Additional Resources .....   | 89  |
| References .....  | 91  |
| Bridging Chapter 4 and 5 .....  | 94  |
| Chapter 5. Mathematical Model Capturing Physicochemical and Biological Regulation of Bone Mineralization..... | 95  |
| Abstract.....   | 96  |
| 1. Introduction.....  | 98  |
| 2. Model Development.....   | 99  |
| 3. Results.....   | 108 |
| 4. Discussion.....  | 117 |
| 5. Conclusion .....   | 120 |
| References .....  | 122 |
| Chapter 6. Final Discussion, Conclusion, and Future Directions .....  | 125 |
| 6.1. Advancing the mathematical modeling of bone formation.....   | 125 |
| 6.2. Application of the model .....   | 129 |
| 6.3. Accessibility of research.....   | 133 |
| References .....  | 135 |

## List of Figures

### Chapter 3.

**Figure 1.** Graphical presentation of the model. A) Schematics of modeled compartments. Interstitial fluid compartment was assumed to be a cuboid with a constant volume of 3 mm<sup>3</sup> and a side of 1 mm<sup>2</sup> that is next to bone tissue. The volume of bone involved in resorption/formation varies in thickness 0.1-3 mm. B) The flow of information in the model.

**Figure 2.** Characteristics of phosphate buffer. The model was reduced to phosphate only and included equations 1, 7-9, as well as relevant terms in equations 13-14, and 17-20. First, the level of total phosphate (TPO<sub>4</sub>) was specified, then total hydrogen (TH) was varied, and the equilibrium state was calculated in the model. A, B) Changes in pH (A) and free equilibrium hydrogen ion (B) as a function of total hydrogen (TH) for three levels of TPO<sub>4</sub>, low (0.9 mM, solid line), physiological (1.2 mM, dashed line), and high (1.6 mM, dotted line). The inflection point pH<sub>c</sub> corresponding to buffers pK<sub>a</sub> and the buffering range (pH<sub>c</sub> ± 1) are depicted on panel A. C) Changes in buffering capacity as a function of TPO<sub>4</sub>.

**Figure 3.** Characteristics of carbonate buffer and a combined carbonate/phosphate buffer.

A) The model was reduced to carbonate only and included equations 1, 10-11, and relevant terms in equations 13, 15, 17-20. The level of total carbonate (TCO<sub>3</sub>) was specified, then total hydrogen (TH) was varied, and the equilibrium pH was calculated. B, C) The model was reduced to carbonate and phosphate only and included equations 1, 7-11, and relevant terms in equations 13-15, and 17-20. The levels of total carbonate (TCO<sub>3</sub>) and total phosphate (TPO<sub>4</sub>) were specified, then total hydrogen (TH) was varied, and the equilibrium state was calculated. B) Changes in pH as a function of total hydrogen; C) Buffering capacity of carbonate buffer with TPO<sub>4</sub> = 0 (circles) or increasing TPO<sub>4</sub> (crosses) to the maximum concentration of 4 mM (top-most cross). For A and B: low: TCO<sub>3</sub>=30 mM, TPO<sub>4</sub>=0.9 mM, physiological (medium): TCO<sub>3</sub>=35 mM, TPO<sub>4</sub>=1.2 mM, high: TCO<sub>3</sub>= 40 mM, TPO<sub>4</sub>=1.6 mM.

**Figure 4.** Characteristics of the interstitial fluid buffer. A) The levels of total phosphate (TPO<sub>4</sub>), total carbonate (TCO<sub>3</sub>), and total calcium (TCa), were specified, then total hydrogen (TH) was varied, and the equilibrium state was calculated using equations 1-20. Plotted are changes in pH as a function of added hydrogen (TH) for low (TCO<sub>3</sub>=30 mM, TPO<sub>4</sub>=0.9 mM, TCa=2.1 mM), physiological (TCO<sub>3</sub>=35 mM, TPO<sub>4</sub>=1.2 mM, TCa=2.5 mM), and high (TCO<sub>3</sub>= 40 mM, TPO<sub>4</sub>=1.6 mM, TCa=2.8 mM) concentrations. B) Free equilibrium hydrogen as a function of TH for the physiological concentrations for carbonate buffer only (same as dashed line on figure 3A), carbonate/phosphate buffer (same as dashed line on figure 3B), and carbonate/phosphate buffer plus calcium species (same as dashed line on figure 4A).

**Figure 5.** Contribution of hydroxyapatite dissolution to pH control in interstitial fluid. The levels of total phosphate (TPO<sub>4</sub>), total carbonate (TCO<sub>3</sub>), and total calcium (TCa), were specified as physiological (table 2) without or with the additions due to dissolution of hydroxyapatite contained in 1-3 μm<sup>3</sup> of bone adjacent to interstitial fluid, then the total hydrogen (TH) was varied, and the equilibrium state was calculated using equations 1-20. A, B) Changes in pH (A) and free equilibrium hydrogen (B) as a function of added hydrogen (TH) for an interstitial fluid without hydroxyapatite dissolution (solid line, same as Fig 4A), and the interstitial fluid after resorption of 3 μm<sup>3</sup> of bone into a 3 μm<sup>3</sup> volume of interstitial fluid (dashed line). C) Change in the buffering capacity of interstitial fluid due to dissolution of 0-3 mm<sup>3</sup> of bone. D) Buffering capacity of interstitial fluid without dissolution (dashed line), with 3 mm<sup>3</sup> hydroxyapatite dissolution (dotted line) or after the addition of phosphate, calcium or hydroxide in amounts contained in 3 mm<sup>3</sup> of hydroxyapatite (grey bars).

**Figure 6.** Contribution of hydroxyapatite precipitation to pH control in interstitial fluid. The levels of total phosphate (TPO<sub>4</sub>), total carbonate (TCO<sub>3</sub>), and total calcium (TCa), were specified as physiological (table 2) without or with the reduction due to precipitation of hydroxyapatite in 0.1-0.4 mm<sup>3</sup> of bone adjacent to interstitial fluid, then the total hydrogen (TH) was varied, and the equilibrium state was calculated using equations 1-20. A, B) Changes in pH (A) and free equilibrium hydrogen (B) as a function of added hydrogen (TH) for an interstitial fluid without hydroxyapatite precipitation (solid line, same as Fig 4A), and the interstitial fluid after precipitation of 0.4 μm<sup>3</sup> of bone using chemical compounds from a 3 μm<sup>3</sup> volume of interstitial fluid (dashed line). C) Change in the buffering capacity of interstitial fluid due to formation of 0.1-0.4 mm<sup>3</sup> of bone. D) Buffering capacity of interstitial fluid without formation (solid line), after 0.4 mm<sup>3</sup> hydroxyapatite precipitation (dashed line) or after the removal of phosphate, calcium or hydroxide in amounts contained in 0.4 mm<sup>3</sup> of hydroxyapatite.

#### **Chapter 4.**

**Figure 1** Schematic representation of the model and its different compartments and their functions. Arrows show the flow of data between compartments

**Figure 2** Effect of physiological and pathophysiological total concentration of calcium (A,B), phosphate (B,D), and carbonate (E,F) on the equilibrium concentration of ionized calcium (A,C,E), and ionized phosphate (B,D,E) at physiological pH 7.4 (solid line), low pH 7.3 (dashed line) and high pH 7.55 (dashed-dotted line). The vertical lines are the mild and severe levels for low and high total concentrations (Table 3)

**Figure 3** Effect of physiological and pathophysiological total concentration of calcium (A,D), phosphate (B,E), and carbonate (C,F) on the solution supersaturation (equation 5) of hydroxyapatite (A-C) in the ISF at physiological pH 7.4 (solid line), low pH 7.3 (dashed line) and high pH 7.55 (dash-dotted line), and brushite (D-F, solid line), octacalcium phosphate (D-F, dashed line), tricalcium phosphate (D-F, dotted line), and calcium carbonate (D-F, dash-dotted line) in the ISF at physiological pH 7.4. The vertical lines are the mild and sever levels for low and high total concentrations (Table 3)

**Figure 4** Effect of physiological and pathophysiological total concentration of calcium (A), phosphate (B), and carbonate (C) on the precipitation rate of hydroxyapatite in the ISF, at physiological pH7.4 (solid line), low pH 7.3 (dashed line) and high pH 7.55 (dished-dotted line). The vertical lines are the mild and sever levels for low and high total concentrations (Table 3)

**Figure 5** Solution supersaturation (A) and precipitation rate (B) influenced by simultaneous changes in total calcium and total phosphate concentration in physiologically relevant concentrations at normal 7.4 pH

**Figure 6** Hydroxyapatite precipitation rate in a 24-hour precipitation period of the isolated ISF (A) and the accumulated mass of hydroxyapatite in a cube of 1  $\mu\text{m}^3$  volume (B) at physiological pH7.4 (solid line), low pH 7.3 (dashed line) and high pH 7.55 (dished-dotted line)

**Figure 7** Model validation with prior experimental data. Simulations were performed with experimental data reported by (A) Miyajima et al [41] or (B) Boistelle et al [42]. Model predictions are plotted as solid line and published data (circles with experimental errors for A and dashed lines for B,C) were extracted from the published papers and replotted with permission

## Chapter 5.

**Figure 1.** Schematic representation of the integrated model and governing equations

**Figure 2.** Bone mineralization model behavior influenced by changes in pH level of the BIF. Plotted are changes in time in naïve and mature collagen (A), inhibitors (B), nucleators (C), hydroxyapatite (D), and the rate of mineral formation (E) at physiological pH 7.4 (solid line) and physiologically relevant levels of acidic pH 6.8 (dotted line) and basic pH 8.0 (dashed line). (F) pH dependence for mineralization delay (solid line, right scale) identified from plots in E as time to reach maximal rate of mineralization, and mineralization degree (dashed line, left scale) identified as mineralization level at  $t=200$  normalized to that observed in standard physiological conditions.

**Figure 3.** Sensitivity analysis for the parameter changes in the integrated model. Model parameters, including characteristic rates of matrix maturation,  $k_1$  (A, B), inhibitors production  $v_1$  (C, D), inhibitors removal  $r_1$  (E, F), nucleator production  $k_2$  (G, H), nucleator removal  $r_2$  (I, J) as well as the maximum physicochemical precipitation rate  $f(R)$  (K, L) were varied as indicated on the corresponding plots, and the mineralization dynamics (A, C, E, G, I, K), delay (B, D, F, H, J, L, solid lines, right axes) and degree (B, D, F, H, J, L, dashed lines, left axes) were examined.

**Figure 4.** Mineralization dynamics under normal, hypo- and hyper- physiological calcium and phosphate levels at BIF. BIF phosphate (A, B) or calcium (C, B) were varied as indicated on the corresponding plots, and the mineralization dynamics (A, C), delay (B, D, solid lines, right axes) and degree (B, D, dashed lines, left axes) were examined.

**Figure 5.** Bone mineralization model behavior with an alternative inhibitor removal term. Plotted are changes in time in naïve and mature collagen (A), inhibitors (B), nucleators (C), hydroxyapatite (D), and the rate of mineral formation (E) at indicated levels of  $t_1$ . (F) Mineralization delay (solid line, right scale), and mineralization degree (dashed line, left scale) as function of  $t_1$ .

**Figure 6.** Comparison of model predictions with different inhibitor removal terms at severe hypo- and hyperphosphatemia. Plotted are changes in time in inhibitors (A), nucleators (B), hydroxyapatite (C) at indicated levels of BIF phosphate. (F) Mineralization delay (solid line, right scale), and mineralization degree (dashed line, left scale) as function of BIF phosphate levels.

**Figure 7.** Predictions of the updated model for the effects of physicochemical factors on bone mineralization. BIF pH (A, B), phosphate (C, D) or calcium (E, F) were varied as indicated on the corresponding plots, and the mineralization dynamics (A, C, E), delay (B, D, F, solid lines, right axes) and degree (B, D, F, dashed lines, left axes) were examined.

## **Chapter 6.**

**Figure 1.** Breakdown of different bone mineralization phenotype based on model outcome measures: mineralization delay and mineralization degree

**Figure 2.** A Screen shot of the beta version of the graphical user interface of the integrated model of bone mineralization

## List of Tables

### Chapter 3.

**Table 1.** Parameter values and corresponding references

**Table 2.** Levels of total phosphate, total carbonate and total calcium used in the model. Medium level represents physiological concentrations (mM), low and high are extremes of the physiological range.

**Table 3.** Buffering capacity and range for different solutions. Physiological concentrations of corresponding components (Table 2) were used for calculations. For the effect of bone, hydroxyapatite dissolution from 3 mm<sup>3</sup> of bone and requirement for hydroxyapatite formation for 0.4 mm<sup>3</sup> of bone, were accounted for.

### Chapter 4.

**Table 1** Model components and their effect on the ionic strength of the solution. Reported are solution components in their ionic forms, nomenclature for their total concentrations, physiological total plasma concentrations and ionic strength of the solution following the inclusion of the specific component from top to down of the list. The reported ionic strength of human plasma is 0.15-0.16 [12]. Systemic pH was set to 7.4

**Table 2** ISF Reactions and their equilibrium constants

**Table 3** physiological and pathophysiological levels of total calcium, total phosphate, total carbonate, and systemic pH

**Table 4** Percentage of saturation ratio changes in hypo/hyper levels of blood calcium, phosphate, and carbonate compared to normal concentrations at physiological pH (7.4)

**Table 5** Percentage of hydroxyapatite precipitation rate change in hypo/hyper levels of blood calcium, phosphate, and carbonate compared to normal concentrations at physiological pH (7.4)

## **Chapter 5.**

**Table 1.** Physicochemical compartment variables, parameters, and values

**Table 2.** Variables and parameters of the biology compartment

## Abbreviations

| <b>Abbreviation</b>   | <b>Definition</b>   |
|-----------------------|---|
| <b>ATP</b>            | Adenosine triphosphate                                    |
| <b>BIF</b>            | Bone interstitial fluid                                   |
| <b>BMDD</b>           | Bone mineral density distribution                         |
| <b>BMPs</b>           | Bone morphogenetic proteins                               |
| <b>BMUs</b>           | Basic multicellular units                                 |
| <b>BSP</b>            | Bone sialoprotein   |
| <b>CFI</b>            | Canada Foundation for Innovation                          |
| <b>CHAp</b>           | Carbonated hydroxyapatite                                 |
| <b>CKD</b>            | Chronic kidney disease                                    |
| <b>DMP1</b>           | Dentin Matrix Protein 1                                   |
| <b>ECM</b>            | Extracellular matrix                                      |
| <b>FGF23</b>          | Fibroblast growth factor 23                               |
| <b>FRQNT</b>          | Fonds de recherche du Québec - Nature et technologies     |
| <b>HA</b>             | Hydroxyapatite  |
| <b>IP</b>             | Ionic product   |
| <b>ISF</b>            | Interstitial fluid  |
| <b>K<sub>SP</sub></b> | Solubility product  |
| <b>MESI</b>           | Ministère de l'Économie, de la science et de l'innovation |
| <b>MGP</b>            | Matrix Gla protein  |
| <b>mRNA</b>           | Messenger ribonucleic acid                                |

|                        |   |
|------------------------|---|
| <b>NCPs</b>            | Non-collagenous proteins                                    |
| <b>NR</b>              | Newton-Raphson  |
| <b>NSERC</b>           | Natural Sciences and Engineering Research Council of Canada |
| <b>O.Th.</b>           | Osteoid thickness   |
| <b>OCP</b>             | Octacalcium phosphate                                       |
| <b>OI</b>              | Osteogenesis imperfecta                                     |
| <b>OPG</b>             | Osteoprotegrin  |
| <b>OPN</b>             | Osteopontin   |
| <b>OV/BV</b>           | Osteoid volume per bone volume                              |
| <b>P<sub>i</sub></b>   | Phosphate   |
| <b>PP<sub>i</sub></b>  | Pyrophosphate   |
| <b>PTH</b>             | Parathyroïdienne  |
| <b>RGD</b>             | Arginine-glycine-aspartic acid                              |
| <b>T<sub>c</sub></b>   | Temperature in Celsius                                      |
| <b>TCa</b>             | Total calcium   |
| <b>TCl</b>             | Total chloride  |
| <b>TCO<sub>3</sub></b> | Total carbonate   |
| <b>TGFβ</b>            | Transforming growth factor β                                |
| <b>TH</b>              | Total hydrogen  |
| <b>TK</b>              | Total potassium   |
| <b>TMg</b>             | Total magnesium   |
| <b>TNa</b>             | Total sodium  |

---

**TPO<sub>4</sub>**

Total phosphate

---



## **Acknowledgements**

First and foremost, I would like to express my deepest gratitude to my supervisor, Dr. Svetlana Komarova. She provided me with this invaluable opportunity and guided me through every step of my PhD journey. Dr. Komarova fostered my confidence and development as a researcher, never limiting my intellectual curiosity and always supporting my professional growth. Her mentorship extended beyond research, offering valuable advice, and sharing her experiences that shaped me not only as a researcher but also as a person.

I am also grateful to my PhD committee members, Dr. Bettina Wille, and Dr. Ives Levesque. Their continuous direction and guidance throughout these years ensured that I remained on track and completed the research process successfully. Their insightful feedback helped me identify areas for improvement and refine my research focus.

My sincere thanks go to the staff of the department of Biological and Biomedical Engineering and Faculty of Dentistry, particularly Pina Sorrini and Sabrina Teoli. Their responsiveness and support were invaluable. They helped me navigate departmental policies and procedures, making my research experience much smoother. I am particularly grateful to the BBME department for recognizing my work by awarding me the Excellence Award on multiple occasions.

I would like to acknowledge the Shriners Hospitals for Children - Montreal for providing a fantastic research environment. The supportive atmosphere allowed me to focus on my research without undue stress.

A special thank you to all my colleagues in the Beaver lab: Gulzhakhan Sadvakassova, Kerstin Tiedemann, Josephine Tauer, Chrisanne D'souza, Mahmoud Moussa, Priyesh Patel, Sirion Aksornthong, Karina Zhang, Mattias Neset, Sara Shalviry, Madalina Patron, Mari Mielkozorova. Their constant support, encouragement, and friendship were instrumental in my success. Their valuable feedback throughout the years helped me refine my research and maintain a positive outlook, especially during challenging times.

Finally, my deepest gratitude goes to my partner, Faezeh Pazoki. Her unwavering support throughout this journey was invaluable. Her encouragement during challenging moments, and her presence when I felt exhausted kept me going.

This research would not have been possible without the contributions of all these individuals. Thank you.

## **Contribution to original knowledge**

Findings represented in the current thesis yield significant contributions to the current understanding of bone mineral formation. Specifically, my research findings include:

1. Characterization of the bone microenvironment and examination of its behavior under distinct scenarios that alter its composition.
2. Emphasizing on the relative importance of carbonate and phosphate buffers in bone interstitial fluid
3. A demonstration of how hydroxyapatite mineralization is regulated by factors defining the interstitial fluid, which can be locally or systematically influenced.
4. Introducing an approach to include physicochemical aspects of bone mineralization in mathematical modeling of bone
5. An evaluation of the relative contribution of biological versus physicochemical factors in regulating hydroxyapatite precipitation under physiological and pathophysiological conditions.
6. A demonstration of how a more realistic depiction of bone mineralization processes can enhance our comprehension of scenarios in which blood levels of various ions, particularly calcium and phosphate, deviate from normal ranges.
7. An illustration of how a more realistic depiction of bone mineralization processes can facilitate the treatment of diseases exhibiting phenotypes of mineralization abnormalities.

8. An easily available and re-usable tool that can help researcher further investigate various scenarios of abnormal mineralization, hypothesize on the cause and direct experimental and clinical efforts to validate their hypothesis.

The research presented herein stems from a structured approach that entailed the pursuit of three distinct objectives, as defined and executed during my PhD in Biological and Biomedical Engineering at McGill University.

## **Contribution of Authors**

In all chapters of this thesis the contributions of authors are as follows:

**Hossein Poorhemati:** Conceptualization, Formal analysis, Investigation, Methodology, Software, Validation, Visualization, Writing—original draft, Writing—review & editing.

**Svetlana Komarova:** Conceptualization, Funding acquisition, Methodology, Project administration, Writing—review & editing.

## **Chapter 1. Introduction**

In certain human diseases, such as osteogenesis imperfecta and osteomalacia, problems with bone mineralization drive pathophysiology. These serious medical conditions resulting in bone deformities or fractures can be caused by increased (osteogenesis imperfecta) [1] or decreased (osteomalacia) [2] bone mineralization. Regulation of bone mineralization is complex and includes physicochemical factors relevant to availability of calcium and phosphorus for mineral precipitation as well as biological factors which determine the bone matrix structure and the availability of mineralization inhibitors [3]. Together, physicochemical and biological factors determine the dynamics of mineral formation and the resulting quality and quantity of bone tissue.

Plasma level of ionic minerals forming hydroxyapatite - calcium and phosphate - and their regulators such as parathyroid hormone (PTH), vitamin D and fibroblast growth factor 23 (FGF23) play a critical role in bone mineralization [4]. Global regulation of calcium and phosphate balances the demands of bone tissue with those of other organs, such as production of breast milk, which contains high levels of calcium in mammals, or production of calcium carbonate containing eggshell in egg-laying birds. Both local and systemic regulation of calcium and phosphate homeostasis are complex and non-linear. Therefore, mathematical modeling represents an important tool to decipher the complex consequences arising from changes in physicochemical, cellular, and hormonal modes of regulation. Previously, computational models describing the biological aspects of bone mineralization and hormonal regulation of calcium and phosphate homeostasis have been developed [5-9].

However, the physicochemical aspects and most importantly their influence on the mineralization process have not yet been considered.

The goal of this work was to develop a mathematical description of bone mineralization that incorporates major biological and physicochemical factors. To do so, I first had to explore the chemistry of the bone interstitial fluid, then develop a mathematical description of physicochemical regulation of mineral precipitation and later integrate it with biological regulation of this process. Thus, this project had three main objectives:

1. To mathematically model chemical processes occurring in the bone interstitial fluid
2. To mathematically model the physicochemical regulation of bone mineralization in the defined environment of bone interstitial fluid.
3. To develop a model integrating the physicochemical and biological aspects of regulation of bone mineralization.

The integrated model developed in this thesis enables comprehensive exploration of the dynamics of bone formation within specific physiological and pathophysiological contexts, thus allowing to investigate potential mechanisms leading to the development of clinically relevant mineralization problems, such as in osteomalacia and osteogenesis imperfecta.

## **Chapter 2. Biology, physical chemistry, and mathematics of Bone**

### **1. Introduction**

Bone tissue exemplifies the intricate synergy between biological and physicochemical processes, resulting in a material with exceptional strength and adaptability. Bone mineralization, at the center of this study, involves the orchestrated production of an organic collagenous matrix by osteoblast bone cells, followed by its maturation and the deposition of hydroxyapatite, the key mineral responsible for bone rigidity. Disruptions in this process, as seen in osteogenesis imperfecta (brittle bones) and osteomalacia (soft bones), highlight the critical roles of both biological and physicochemical factors in skeletal health.

This chapter explores three key aspects relevant to bone: the intricate biology of bone, the physicochemical processes governing bone mineralization, and the application of mathematical modeling to understand and further investigate bone processes. This chapter provides the foundational concepts required to better understand the research presented in the following chapters.

### **2. Bone biology**

#### **2.1. Bone composition**

Bone is a biological composite material that includes three different phases, a mineral phase, an organic phase, and water [10]. The mature bone mineral phase is made up of nanosized crystalline hydroxyapatite with chemical formula of  $\text{Ca}_{10}(\text{PO}_4)_6(\text{OH})_2$  [11-13]. Affected by

diet and environment, some ions in this molecule could be substituted by carbonate ( $\text{CO}_3^{2-}$ ), magnesium ( $\text{Mg}^{2+}$ ), acid phosphate ( $\text{HPO}_4^{2-}$ ), etc. [11, 12]. Although it is not clear why primitive terrestrial organism bodies replaced calcium carbonate with calcium phosphate, the physiological advantages of this change in providing a stronger and more stable skeleton under acidic conditions was previously suggested [14]. The mineral phase of bone functions to provide a strong structure for the organic phase, mechanical resistance for the tissue, and an abundant number of ions (particularly calcium and phosphate) for whole body homeostasis [12].

The organics phase of the bone consists of almost 90% type I collagen, 5% non-collagenous proteins (NCPs), and 2% lipids by weight [10]. The levels of these proteins vary with age, skeletal site, gender, ethnicity, and health status [15-18]. We will discuss the organic phase in more detail later when we get to the Extracellular Matrix section.

Finally, the water phase is responsible for cell and matrix nutrition, filling the pores, interacting with collagen fibrils, controlling ion flux, and binding to minerals [12, 19]. There are also some suggestions on how water content could be associated with bone mechanical properties, however, more studies are needed to determine the exact role [20]. Depending on the species and bone age water could take up to 10% of bone weight [12].

## **2.2. Bone physiology**

### **Bone cells**

As for any other organ, bones have their own specific cell types, osteoblast or bone forming cells, osteoclasts or bone resorbing cells, osteocytes, and bone lining cells. These cells communicate with one another and with different parts of the body by direct contact or through secreted molecular signaling [12].

### **Osteoblasts**

Synthesis of the extracellular matrix and its subsequent mineralization is the primary responsibility of osteoblasts. They are also involved in regulating the activation and maturation of osteoclasts [21]. Various biomarkers distinguish different stages of osteoblast differentiation. Early osteoblast differentiation (preosteoblast) is characterized by the presence of type I collagen and alkaline phosphatase, whereas the late stage of osteoblastic differentiation is indicated by the expression of osteocalcin [22]. Osteoblasts are connected to other adjacent bone cells, including other osteoblasts, osteocytes and bone lining cells and mediate and propagate signaling among them. They are connected through cytoplasmic processes with other osteoblasts and through gap junctions with osteocytes [23, 24].

### **Osteoclasts**

Unlike osteoblasts, osteoclasts are giant multinucleated cells with the primary role of resorbing the bone matrix. These cells attach to the bone and make a sealed resorption pit. Later, by actively transferring hydrogen ions from the cell to the sealed zone using their proton pumps they decrease the pH down to 4.5 to accommodate bone resorption [21].

These pumps are coupled with Cl<sup>-</sup> channel and introduce HCL to the sealed zone. HCL dissolves the bone mineral whereas proteolytic enzymes resorb the organic components [21]. Osteoblasts and bone marrow stromal cells regulate osteoclasts maturation and proliferation through expression of different factors such as RANKL (receptor activator for nuclear factor kappa B ligand) and M-CSF (Macrophage colony stimulating factor) [25, 26]. Expression of osteoprotegrin (OPG) which acts as a decoy receptor and binds to RANKL, prevents activation and development of osteoclasts [26, 27].

### **Osteocytes**

Osteocytes are formed from the osteoblasts which were entrapped in the mineralized matrix. Osteocytes are the most abundant bone cell type, they have a half-life of 25 years [28]. Through their long processes osteocytes are connected to each other as well as to osteoblasts and bone lining cells. This complex network of osteocytes processes makes them able to sense strain stimuli and respond to the mechanical demands of the organism by influencing the osteoblast and osteoclast activities [29, 30]. Osteocytes also play an important role in mineral homeostasis by sensing variation in ion concentration and initiating movement of ion between bone matrix and extracellular fluid [31]. It is also shown that osteocytes in some vertebrates have a limited bone resorption capability. This phenomenon which is known as osteocytic osteolysis is particularly important in states of increased demand for mineral mobilization, which is observed during pregnancy and lactation [28].

### **Bone lining cells**

Only a small proportion (almost one third) of osteoblasts become trapped as osteocytes, the rest will undergo apoptosis or transform into bone lining cells [28]. These inactive osteoblasts have a flat spindle shape and cover bone surfaces [21]. They separated the lacunae and canaliculi from the interstitial fluids and are also involved in bone marrow barrier formation and regulation of other bone cells [32].

## **Remodeling**

Bone remodeling is a process to ensure bone is constantly renewed to maintain its strength and mineral homeostasis [33]. This process requires tightly coupled actions of osteoclasts and osteoblasts to sequentially resorb the old bone packets and form new ones to prevent accumulation of microfractures [33] and ensure new tissue adaptation to mechanical forces [34]. This necessary coordination is organized by local signaling among groups of osteoclasts and osteoblasts known as basic multicellular units (BMUs) [35]. Imbalance in the BMU in the form of limited reconstruction leads to bone loss [36, 37]. BMUs organization has morphological differences in cortical and trabecular bones. While 2-5% of cortical bone undergoes remodeling every year, trabecular bone due to higher surface to volume ratio is remodeled more actively [34].

Bone remodeling has three major steps: resorption, reversal, and formation. Resorption stage is characterized by formation of multinucleated osteoclasts on the bone surface. This stage could take almost 2 weeks. Following the osteoclastic bone resorption, the reversal stage begins. Here, new mononuclear cells appear on the bone surface preparing it for bone formation process and also signaling osteoblasts to differentiate and migrate to that surface.

The reversal stage lasts for 4-5 weeks. The cycle will be completed when eventually osteoblasts replace the resorbed bone, and the surface becomes covered with bone lining cells for an extended resting period until the time next remodeling happens. The formation is known to be the longest stage and could take up to 4 months to complete [34].

Bone remodeling must be a strictly regulated process to ensure there is a balance between the bone resorption and following formation. Bone remodeling happens at several anatomically distinct sites. This means that besides the systemic regulatory factors, there must be a local regulation to attain such a balanced activity [38]. RANKL/RANK/OPG and Wnt/ $\beta$ -catenin are two of many pathways that play a significant role in transducing systemic and local signals, which can affect the activity of osteoclasts and osteoblasts. As a result, they impact the balance and timing of bone resorption and formation during the remodeling cycle [38-40].

### **2.3. Bone functions**

Bones are mostly known for their role in supporting body mass, protecting internal organs and making locomotion possible. However, their role is not limited to only structure and motion. Bones store a considerable amount of essential minerals, especially calcium and phosphate, which are indispensable for various physiological activities and mineral homeostasis [21, 41]. Human body relies on bone tissue to restore variation in blood calcium and phosphate levels back to the normal range [32]. Lastly, bones provide a considerable surface area that could absorb toxins and heavy metals that may damage other organs if circulated in blood [42].

## **Mechanotransduction**

Within the environment, all living organisms are constantly exposed to external physical forces. This interaction triggers a process known as mechanotransduction, where these physical forces are translated into biochemical signals, thereby initiating a functional response. At the cellular level, mechanical stimuli instigate the generation of biochemical signals, initiating a cascade of intracellular processes. These processes encompass activation of complex signaling pathways, adjustments in gene expression, and modifications in protein synthesis. As a result, both the intracellular and extracellular environments undergo adaptation in response to the initial mechanical stimulus [43]. This mechanosensitive feedback loop plays a critical role in regulating various cellular functions such as migration, proliferation, differentiation, and apoptosis, ultimately influencing organ development and maintaining homeostasis [43, 44]. Bone mechanotransduction has a pivotal role in different bone processes such as formation, maintenance and skeletal adaptation to its environment.

Osteocytes, as the primary inhabitants of bone tissue, are thought to play a pivotal role in detecting and reacting to mechanical stimuli. Originating from osteoblasts embedded within the bone matrix, osteocytes form an intricate network of lacunae and canaliculi, facilitating chemical and fluid exchange with cells on the bone surface [45]. Variations in mechanical forces experienced by bone tissue induce changes in fluid flow within this network, serving as discernible signals which is captured by osteocytes long processes [46, 47]. It is also speculated that osteocytes may directly respond to the matrix strains [48]. Although the exact mechanism by which different external forces are transmitted to these bone cells is

still incompletely understood, it leads to the activation of osteoblasts and osteoclasts to initiate the adaptation process. The coordinated activity of these cell bones results in the organization of the bone tissue according to the direction of the mechanical forces [21, 49].

### **Mineral homeostasis**

Almost 98% of body's calcium, 85% of phosphorous, 95% of sodium and 50% of magnesium are stored in bones [21]. Interactions between the whole body homeostasis of these elements and the processes of bone formation and resorption are complex and include hormonal regulation by PTH, vitamin D, FGF23, and calcitonin. These chemical elements are also available in intracellular and extracellular environments and contribute to a variety of biological processes making their homeostasis a systemic challenge. Among these, calcium and phosphorous, being the major bone constituents, receive a greater attention.

Of the 2% of calcium available in the serum, approximately 50% is in ionized form under the normal serum protein concentration, 10% is in the form of different acid complexes, and the remaining 40% is bound to proteins such as albumins and globulins [50, 51]. This protein bound portion is biologically inactive, however, it could function as a rapid source of available calcium [52].

The approximately 15% of the whole-body phosphorus content that is not stored in bone is involved in different biological processes such as energy metabolism, cellular signalling, membrane composition, nucleotide structure and of course bone mineralization. In soft tissues it is in the form of phosphate esters while it appears as inorganic phosphate ions in the extracellular fluids [52].

Global regulation of calcium and phosphate balances the demand of bone tissue with those of other organs, such as production of breast milk, which contains high levels of calcium in mammals, or production of calcium carbonate containing eggshell in egg-laying birds. Calcium and phosphate homeostasis is achieved by a complex system of interactions whose major players are bone, kidney and intestine through hormonal regulations particularly by parathyroid hormone (PTH), Fibroblast Growth Factor 23 (FGF23), and biologically active vitamin D. Vitamin D precursor derived from the diet or synthesized in the skin under UV-B undergoes two hydroxylation reactions in the liver and the kidneys, to produce the biologically active calcitriol (1,25-dihydroxyvitamin D; 1,25(OH)<sub>2</sub>D<sub>3</sub>). FGF23 is a phosphate-regulating hormone produced by osteocytes. PTH, calcitriol and FGF23 regulation is strongly interconnected, with each of the hormones affecting and being affected by the others. Following a drop in blood calcium level, parathyroid gland works toward elevating PTH level in the serum to stimulates bone resorption by osteoclasts, calcium reabsorption and production of active vitamin D in the kidney. The elevated level of active vitamin D then increases the intestinal absorption of calcium and phosphate [53, 54]. Later, FGF23 signalling in response to elevated levels of phosphate works toward increasing phosphate excretion and vitamin D production in the kidney to prevent further intestinal phosphate absorption. Eventually, elevated levels of FGF23 inhibits PTH production [53]. When bone is changed due to the demands in mineral homeostasis, the needs of the organism override the needs of bone as a tissue, resulting in severe bone loss in conditions associated with imbalance in calcium and phosphate regulating hormones, such as hyperparathyroidism [55].

## **2.4. Bone formation**

Vertebrate mineralization necessitates a suitable extracellular matrix, functioning as a scaffold receptive to mineral deposition [56]. Osteoblasts synthesize the extracellular matrix which provides the nucleation sites for the hydroxyapatite crystal to form [57]. This heterogeneous mineral deposition occurs within, at the surface or between collagen fibers [58, 59]. Besides this matrix, the adequate concentration of ions particularly calcium and phosphate and low concentration of different mineralization inhibitors is needed. Enzymes coordinate bone mineralization initiation and process. For example, alkaline phosphatase is the enzyme responsible for the breakdown of inorganic pyrophosphate (PP<sub>i</sub>), a potent inhibitor of mineralization, to produce inorganic phosphate (P<sub>i</sub>) which is a promoter of mineralization. Alkaline phosphatase level is used as a biomarker of osteoblast activity and bone formation [57].

### **Extracellular matrix**

Bone tissue is composed of different bone cells (~8% of bone weight) and the bone extracellular matrix (ECM) produced by osteoblasts [60, 61]. The inorganic hydroxyapatite is deposited and later mineralized in the empty space provided by the collagen type I fibril in a process which is mediated by non-collagenous proteins [62, 63]. The inorganic (mineral) phase holds the majority of the extracellular matrix (~67% of bone weight), while the organic matrix only accounts for almost 25% of the weight of bone tissue [21, 61]. The organic matrix, is mostly composed of collagen type I that is organized in a layer-by-layer

structure called lamellae [64]. In addition, non-collagenous proteins (NCPs) account for almost 5% of the total bone weight (or 10-15% of total bone protein content) [10, 12].

Collagen type I is the building block of bone matrix fiber network [12]. Collagen type I exists in bone ECM in a triple helix structure formed by two  $\alpha 1$  and one  $\alpha 2$  chains [41]. Collagen's crosslinking abilities make it the ideal lattice for its different functions. Collagen lattice stabilizes the extracellular matrix, makes the tissue elastic, and supports the initial mineral deposition and binding with other macromolecules [10]. Other than structural functions, collagen is also reported to be involved in regulating apoptosis, proliferation, and differentiation of bone cells [64].

NCPs are known to be involved in cell-mineral-matrix interactions, in organizing the ECM, and in regulation of mineralization process [12]. For example, osteocalcin, the most abundant bone NCP, is a known regulator of mineralization and its serum level is being used as a biomarker of bone formation [64]. Lipids, accounting for less than 3% of bone tissue, surround the cells controlling the flux of ions and other signaling molecules between the cell and extracellular environment [10].

### **Matrix mineralization**

Bone matrix deposition by osteoblasts precedes bone mineralization. This leads to presence of unmineralized bone matrix in the locations undergoing active bone formation [21]. This unmineralized bone matrix is called osteoid. Excessive amount of osteoid is observed in diseases such as osteomalacia and is often associated with bone mineralization deficiency [32]. Once mineralization starts in the osteoid, only in a few days approximately 70% of the

final mineral content will be crystallized [65, 66]. This is referred to as the *primary mineralization* characterized by a fast mineralization rate compared to the next phase. During the subsequent *secondary mineralization* phase, the mineral content keeps increasing in an extended time scale of years [67].

A number of inhibitors of mineralization are employed to precisely regulate mineral formation. The balance action of these inhibitors keeps the body capable of controlled mineralization as physiological needs emerge. Pyrophosphate (PP<sub>i</sub>) [60], Matrix Gla Protein (MGP) [68, 69], Osteopontin (OPN) [70], and Dentin Matrix Protein 1 (DMP1) [71] are among the most important mineralization inhibitors. Pyrophosphate is produced during different intracellular metabolic reaction and is found extracellularly [72, 73]. Both PP<sub>i</sub> and OPN prevent the formation and growth of calcium and phosphate crystals and their inhibitory properties could be eliminated by the action of tissue non-specific alkaline phosphatase [70, 74, 75]. MGP is a circulating inhibitor. Its over expression leads to moderate osteomalacia and its ablation causes ectopic calcification [68, 69]. DMP1 has a unique behavior where its presence in the solution causes mineralization inhibition, however, attached to the collagen surface of the matrix it promotes mineralization [71, 76, 77].

The matrix vesicle theory proposes that in addition to nucleation centers that occur on mature bone matrix, mineralization is also controlled by vesicles released by mature osteoblasts [78]. This theory proposed that matrix vesicles create a confined microenvironment conducive to the initial formation (nucleation) of hydroxyapatite crystals. These crystals enlarge within the vesicles through the accumulation of calcium (Ca<sup>2+</sup>) and phosphate (Pi) ions, eventually rupturing the vesicle membrane and depositing

the resulting crystal onto the surrounding collagen scaffold [41]. Nevertheless, it can be generalized that in order for bone mineralization to occur, *i*) there should be a proper extracellular matrix which provides the nucleation sites on specific molecules or as part of matrix vesicles; *ii*) the concentration of mineralization inhibitors should decrease, and *iii*) appropriate concentration of calcium and phosphate should be present. The first two aspects are controlled biologically, while the availability of calcium and phosphate also depends on the physicochemical processes occurring in the bone interstitial fluid.

### **3. Physicochemical Aspects of Bone Mineralization**

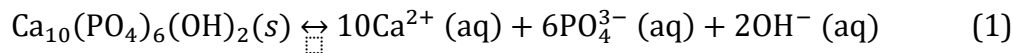
Physicochemical principles dictate the solubility and precipitation of calcium phosphate salts, including hydroxyapatite, the key mineral component of bone. Extracellular matrix components, particularly collagen fibrils, act as a template for mineral nucleation. Their intricate structure, governed by electrostatic interactions and controlled by collagen crosslinking, dictates the initial formation and subsequent growth of hydroxyapatite crystals [79]. Additionally, the size, morphology, and orientation of these crystals are determined by a complex interplay of physicochemical factors. Supersaturation, the degree to which the local environment exceeds the equilibrium concentration for hydroxyapatite formation, plays a crucial role. A precisely controlled level of supersaturation is necessary for controlled crystal growth [80, 81]. The ionic environment surrounding the nascent crystals also exerts a strong influence. For example, certain divalent cations like magnesium can become incorporated into the hydroxyapatite lattice, potentially influencing its mechanical

properties [82]. Understanding these physicochemical aspects is crucial for a comprehensive description of bone mineralization.

### 3.1. Solubility and Precipitation

#### Solubility Product ( $K_{sp}$ ) and Hydroxyapatite Precipitation

The concept of solubility product ( $K_{sp}$ ) plays a vital role in understanding the precipitation of ionic compounds, including hydroxyapatite (HA), the primary mineral component of bone.  $K_{sp}$  represents the equilibrium constant for a specific dissolution reaction. In the context of bone mineralization, the relevant reaction is the dissolution of hydroxyapatite:



where  $s$  denotes the solid phase (hydroxyapatite) and  $aq$  denotes the aqueous phase (dissolved ions) [83].

The  $K_{sp}$  of hydroxyapatite is the product of the individual ion concentrations raised to their respective stoichiometric coefficients in the dissolution reaction at equilibrium state:

$$K_{sp} = [\text{Ca}^{2+}]^{10} [\text{PO}_4^{3-}]^6 [\text{OH}^{-}]^2 \quad (2)$$

This constant value signifies the specific concentration product at which a saturated solution exists. If the product of the ion concentrations, known as ionic product (IP) (calculated similar to  $K_{sp}$ , however at a specific solution condition), exceeds the  $K_{sp}$ , the solution becomes supersaturated, and hydroxyapatite precipitation occurs to re-establish

equilibrium. Conversely, if the product falls below the  $K_{sp}$ , the solution is undersaturated, and existing hydroxyapatite crystals may dissolve [84].

The physiological value of the  $K_{sp}$  for hydroxyapatite in body fluids is not a precisely defined constant due to factors like ionic strength and the presence of complexing agents that can influence the apparent solubility [85, 86]. However, the concept of  $K_{sp}$  remains a valuable tool. Biological regulators cause changes in the concentrations of calcium and phosphate ions, as well as the pH, in the vicinity of the extracellular matrix. By manipulating these factors, they can influence the local ion product and promote conditions favorable for hydroxyapatite precipitation or dissolution [87].

### **Influence of local ion concentrations on mineralization**

Calcium ( $Ca^{2+}$ ) and phosphate ( $PO_4^{3-}$ ) concentrations play a crucial role in regulating hydroxyapatite precipitation through their direct influence on the IP value. An increase in either  $Ca^{2+}$  or  $PO_4^{3-}$  concentration in the local environment surrounding osteoblasts can elevate the ionic product of their concentrations, potentially pushing the solution towards supersaturation and promoting hydroxyapatite precipitation. Conversely, a decrease in either ion concentration can lead to undersaturation and dissolution of existing hydroxyapatite crystals [81].

Osteoblasts actively regulate the concentrations of these ions within the extracellular matrix through various mechanisms. They possess ion channels and transporters on their cell membranes that facilitate the movement of calcium and phosphate ions between the

extracellular fluid and the intracellular space. Additionally, osteoblasts produce enzymes such as alkaline phosphatase, which hydrolyzes pyrophosphate, a natural inhibitor of hydroxyapatite precipitation, while at the same time producing phosphate [88]. This tight control over ion concentrations allows for the controlled formation and growth of hydroxyapatite crystals within the bone matrix [89].

The concentration of hydroxyl ions ( $\text{OH}^-$ ) is another factor influencing the ionic product and, consequently, hydroxyapatite precipitation. A higher pH (more alkaline environment) leads to a lower concentration of  $\text{H}^+$  ions, which can combine with  $\text{PO}_4^{3-}$  to form less soluble complexes like  $\text{HPO}_4^{2-}$  and  $\text{H}_2\text{PO}_4^-$ . This effectively frees up more  $\text{PO}_4^{3-}$  ions, potentially increasing the ionic product and driving hydroxyapatite precipitation. Conversely, a lower pH can promote the formation of these complexes, reducing the availability of free  $\text{PO}_4^{3-}$  ions and potentially hindering hydroxyapatite precipitation [90].

### **Role of substituent ions in hydroxyapatite structure**

While hydroxyapatite has the formula  $\text{Ca}_{10}(\text{PO}_4)_6(\text{OH})_2$ , the structure can accommodate the substitution of other ions for  $\text{Ca}^{2+}$  and  $\text{PO}_4^{3-}$  in limited amounts. These substitutions can influence the chemical and physical properties of the hydroxyapatite crystals, potentially impacting bone quality. Magnesium ions can replace some calcium ions within the hydroxyapatite lattice. This substitution can influence the mechanical properties of the mineral, potentially affecting bone strength. Studies have shown that magnesium incorporation can enhance fracture toughness, making the bone more resistant to cracking [91]. However, excessive magnesium substitution can also lead to defects in the

hydroxyapatite structure, potentially weakening the bone [92]. Carbonate ions can substitute for phosphate ions in the hydroxyapatite structure, forming a mineral known as carbonated hydroxyapatite (CHAp). CHAp is more similar to the mineral component of natural bone compared to pure hydroxyapatite [93]. The presence of carbonate can improve the biocompatibility of the material and may also influence its resorption rate within the body [94]. The extent of ion substitutions depends on various factors, including the availability of the substitute ions in the local environment and the physiological state of the organism. Dietary intake, hormonal factors, and age can all influence the concentration of these ions, affecting the composition of the hydroxyapatite crystals deposited in the bone matrix [81, 95]. Understanding the role of these substituent ions provides valuable insights into the diverse physicochemical properties of bone minerals and their potential contribution to bone health and disease.

### **Bone activity and acid-base balance**

Another factor that can affect mineralization is the acidity level of the extracellular fluid. Elimination of acids which are the result of metabolic activities is a must in multicellular organisms. The skeleton of vertebrates, having hydroxide containing hydroxyapatite, is a massive reserve of base and contributes to maintaining acid-base balance within narrow limits [96]. Longstanding evidence shows the association between bone loss and acidosis. Systemic acidosis can happen as a result of renal, bronchial, gastrointestinal disease, severe (anaerobic) exercise, excessive protein intake, ageing, or menopause. Local acidosis happens as a result of inflammation, infection, wounds, tumors or ischemia [96]. These conditions will

affect the activation of osteoblastic and osteoclastic bone cells. Although it was thought before that skeleton is a passive ion exchange column which buffers the acidosis [97, 98], it became apparent that osteoclasts bone resorption is stimulated by protons [99, 100]. In fact, acidosis is required for the initiation of resorption and it's only after this initial activation that other pro-osteoclastic agents such as RANKL, 1,25(OH)<sub>2</sub> vitamin D, PTH and ATP can further stimulate resorptive activity [96, 101, 102]. In the case of osteoblast cells, decreasing pH from 7.4 to 6.9 caused remarkable reduction in osteoblast alkaline phosphatase activity and downregulated its mRNA which is a major regulator of bone mineralization, and upregulated mRNA for matrix gla protein which is an inhibitor of mineralization [103]. Altogether, it is safe to say that in continued acidosis, the deposition of alkaline mineral from interstitial fluid into the bone by osteoblast cells is reduced and the resorptive activity of osteoclasts is promoted to ensure the introduction of the necessary hydroxyl ions into the environment to buffer protons [96].

### **3.2. Crystal Nucleation and Growth**

#### **Nucleation Sites and Mineralization Control**

The intricate process of bone mineralization hinges on the formation and subsequent growth of hydroxyapatite crystals within the collagenous matrix secreted by osteoblasts [104]. This delicate process of mineralization begins with nucleation, the initial formation of organized ions from a supersaturated solution. In the context of bone, hydroxyapatite precipitation occurs when the local concentration product of calcium and phosphate ions exceeds the solubility product ( $K_{sp}$ ) of hydroxyapatite in the bone interstitial fluid [105]. However,

simply exceeding the  $K_{sp}$  is not enough for spontaneous precipitation to occur. Nucleation presents an energetic barrier, requiring a specific minimum amount of energy, known as the activation energy, in order to form the first stable hydroxyapatite clusters. This activation energy barrier can be significantly reduced by the presence of nucleation sites. It has been known that bone formation is a heterogenous mineralization [106]. In bone, the collagen fibrils, the primary structural component of the extracellular matrix, serve as a crucial template for hydroxyapatite nucleation. The specific arrangement of amino acid residues within the collagen molecule, particularly the presence of negatively charged phosphate groups, creates a favorable electrostatic environment for attracting positively charged calcium ions [107]. These initial calcium ions can then act as a foundation for the subsequent recruitment of phosphate ions, initiating the formation of hydroxyapatite nuclei. Additionally, non-collagenous proteins (NCPs) further enhance the nucleation process [108]. These NCPs possess specific binding domains for both calcium and phosphate ions, facilitating their interaction and promoting the assembly of hydroxyapatite clusters on the collagen fibrils [109]. The interplay between collagen fibrils and NCPs provides a highly organized and controlled microenvironment that significantly reduces the activation energy for hydroxyapatite nucleation, ultimately dictating the rate and location of mineral deposition within the bone matrix.

## **Crystal Growth**

Following the initial nucleation event, hydroxyapatite crystals undergo a process of growth, gradually increasing in size and perfecting their crystalline structure. This growth process is

governed by a delicate interplay between the diffusion of ions in the surrounding solution and the surface energy of the growing crystals.

Diffusion refers to the random thermal movement of ions in the extracellular fluid. For hydroxyapatite crystal growth to occur, calcium and phosphate ions must continuously reach the crystal surface and integrate into the crystal lattice. The rate of diffusion is directly proportional to the concentration gradient of these ions in the vicinity of the crystals. Osteoblasts, through their active regulation of ion concentrations and the production of enzymes like alkaline phosphatase, can create a favorable environment for diffusion, promoting the continuous supply of ions required for crystal growth [88].

However, simply reaching the crystal surface is not enough for an ion to become incorporated. The surface energy of a crystal refers to the energy associated with its surface area. In the context of hydroxyapatite, there is an inherent energetic penalty associated with creating new crystal surfaces. To minimize this energy penalty, crystals tend to grow in a preferential manner, favoring the expansion of existing faces with lower surface energy. Additionally, specific NCPs can interact with the growing crystal surfaces, potentially influencing their growth habit and morphology [110]. This interplay between diffusion, surface energy, and NCP interactions dictates the final size, shape, and orientation of the hydroxyapatite crystals within the bone matrix.

Understanding the factors influencing crystal growth is crucial for bone health. Abnormalities in the diffusion of ions, changes in surface energy due to the presence of impurities, or dysregulation of NCP expression can all lead to the formation of hydroxyapatite crystals with altered properties. These altered crystals may compromise the

mechanical integrity of the bone or hinder its proper remodeling, potentially contributing to bone diseases like osteoporosis.

### **3.3. Role of Non-collagenous Proteins**

NCPs play a critical role in orchestrating the intricate process of bone mineralization. While collagen fibrils provide the structural framework for hydroxyapatite deposition, NCPs act as essential modulators, influencing various aspects of crystal formation, growth, nucleation, and the overall physicochemical properties of the mineral phase. Here, we explore the functions of two key NCPs: osteopontin (OPN) and bone sialoprotein (BSP) in modulating physicochemical environment.

*Osteopontin (OPN):* OPN is a highly abundant NCP found throughout the bone matrix. It possesses several functionalities relevant to bone mineralization. Firstly, OPN binds to both calcium and phosphate ions through specific integrin binding motifs (RGD) and phosphorylated serine residues, respectively [111]. This ability allows OPN to act as a bridge, facilitating the interaction and co-localization of these ions in the vicinity of the collagen fibrils, promoting the initiation of hydroxyapatite nucleation [112]. Additionally, OPN can interact with the growing hydroxyapatite crystals, potentially influencing their morphology and size [70]. Studies suggest that OPN may preferentially bind to specific crystal faces, potentially directing their growth along a particular axis [113]. This preferential binding could influence the overall mechanical properties of the bone by affecting the packing and organization of the hydroxyapatite crystals within the collagen matrix.

OPN also acts as a strong biological regulator of mineralization. It exhibits an affinity for other bone matrix components, including collagen and other NCPs, contributing to the overall organization and stability of the mineralized matrix [114]. OPN's interaction with collagen may also influence the mechanical properties of the bone by acting as a sacrificial bond during fracture events, dissipating energy and preventing crack propagation [115]. Finally, OPN is implicated in various cellular processes related to bone remodeling. Its interaction with specific cell surface receptors on osteoclasts can modulate their activity, influencing the resorption of old bone tissue [116]. Therefore, OPN acts as a multifaceted regulator, that influences both the physicochemical aspects of mineral formation and bone homeostasis and remodeling.

*Bone Sialoprotein (BSP):* BSP is another crucial NCP, particularly abundant at the initial stages of mineralization. Similar to OPN, BSP possesses binding sites for calcium ions and may play a role in attracting these ions to the collagen surface, promoting nucleation [117]. However, BSP's primary function is believed to be related to directing the initial orientation and growth of hydroxyapatite crystals [118]. Studies have shown that BSP binds preferentially to specific regions along the collagen fibril, potentially acting as a template for the ordered assembly of hydroxyapatite crystals along the long axis of the collagen molecules [119]. This oriented growth is essential for maintaining the anisotropic mechanical properties of bone, allowing it to withstand forces from different directions.

Beyond its role in nucleation and crystal orientation, BSP may also influence the overall crystallinity of hydroxyapatite. Some studies suggest that BSP interactions with the growing crystals can promote the formation of more mature and perfect crystals with enhanced

mechanical strength [120]. The interplay between BSP and other NCPs, like OPN, further regulates the mineralization process. For instance, while OPN may influence the overall size and morphology of the crystals, BSP could dictate their specific orientation within the collagen matrix [109]. Together, these proteins create a finely tuned microenvironment that governs the formation of a highly organized and functional bone mineral phase.

Numerous other NCPs contribute to bone mineralization. These include dentin matrix protein 1 (DMP1), matrix Gla protein (MGP), and bone morphogenetic proteins (BMPs). DMP1, similar to OPN, can bind calcium ions and may influence nucleation events [121, 122]. MGP exhibits inhibitory effects on calcification, potentially regulating the progression of mineralization and preventing excessive crystal growth [123]. BMPs, on the other hand, are signaling molecules that play a crucial role in osteoblast differentiation and activity, indirectly influencing bone mineralization by regulating the cellular environment [124]. Understanding the specific functions of these diverse NCPs and their interactions is essential for a comprehensive picture of bone development and mineralization.

Non-collagenous proteins, with their diverse functionalities, orchestrate a complex dance during bone mineralization. These proteins not only provide nucleation sites but also actively influence crystal formation, growth, orientation, and ultimately the physicochemical properties of the mineral phase within the bone matrix. A deeper understanding of the intricacies of NCP function promises the development of novel therapeutic strategies for bone diseases characterized by abnormal mineralization.

#### 4. Mathematical modeling of Bone Homeostasis

The previous sections clearly established that regulation of bone formation is a complex process. An intricate orchestration of local and systemic functions is required for the bone to perform its diverse role in the body from facilitating locomotion to keeping the calcium and phosphate homeostasis. Bone impacts other organs and processes and is impacted by them. Understanding bone requires conducting studies at different dimensions and scales. Mathematical modeling has already proved to be extremely useful in assisting to better understand such processes. Pivonka and Komarova [125] discussed multiple scenarios in bone research where mathematical modeling could be useful. One example is in predicting the system behavior when multiple events contribute simultaneously, such the outcome of action of transforming growth factor  $\beta$  (TGF $\beta$ ) which is known to directly affect osteoblasts and osteoclasts and to modulate expression of osteoclast-regulatory molecules [126]. Another situation is when different events under study have significantly different time scales, such as when investigating the relationship between PTH receptor-mediated signaling of bone cells and consequent changes in bone mass [6]. The important roles of computational models in understanding such complex phenomena is now well acknowledged for multiscale bone structure [127] bone fracture healing [128], bone mechanobiology [129], as well as mineralization in biological systems [130].

Understanding the interactions among bone cells, bone resorption and formation under the influence of systemic hormones PTH, FGF23, or vitamin D is another example of complex phenomena that was shown to strongly benefit from computational approaches. Bone as an organ is involved in the systemic homeostasis of calcium and phosphate alongside with kidney and intestine. Raposo et al. [9] developed a model of calcium homeostasis that

includes hormones (PTH and calcitriol) and the effector organs (parathyroids, bone, kidney, and intestine). In a later work Raposo et al. included also phosphorus metabolism in a model to investigate hyperparathyroidism [131]. Different researchers have developed similar models that consider bone as an essential, although simplified component [5, 8, 132, 133]. A complementary approach to better understand bone contribution through mathematical modeling focused on developing models of bone remodeling [134-136]. Based on these studies, Peterson et al. [7] presented a physiologically based mathematical model that integrates calcium homeostasis and bone biology. The model in addition to relevant cellular aspects of bone remodeling regulation, is capable to describe a range of clinical and therapeutic conditions leading to changes in ion concentration, PTH, calcitriol, and some bone remodeling markers observed in hypo- or hyperthyroidism. This modeling work demonstrates potential usefulness of mathematical biology in addressing clinical problems.

At the core of research around bone is the mineralization process and how it is impacted by various biological or non-biological or local or systemic factors. The first model of bone mineralization was developed and published by Komarova et al. in 2015 [6]. This model was made of five different ordinary differential equations each describing one component of bone mineralization. The five components are naïve and mature matrix, inhibitors, nucleators and minerals. The equations describe the production and removal of components during the process. In this study, the model outcome is used to determine two characteristics of the mineralization process under each given condition: degree of mineralization and mineralization lag time. Degree of mineralization is defined as the amount of mineral formed at a specific time passed the initiation of the process. On the other hand, mineralization lag time is defined as the time passed before the fast mineralization phase begins, i.e. the time

that osteoid is formed but not yet calcified. Using these two measures the model provides easily understandable and physiologically interpretable measures to describe mineralization behavior. This model was later fully investigated by a different group for its stability, uniqueness and boundedness of the solution [137]. The bone mineralization model as it is, can successfully predict the behavior of healthy mineralization and changes in different diseases such as osteogenesis imperfecta. However, it assumes that the ions and particularly calcium and phosphate required for hydroxyapatite formation are always available at normal physiological levels. Since many diseases of mineralization are caused by abnormal levels of plasma calcium and phosphate, accounting for the physicochemical processes relevant to calcium and phosphate chemical species would significantly improve model applicability to pathophysiological conditions.

A proper model of bone mineralization must take into account both biological and physicochemical factors that can significantly affect the mineralization behavior. While the major factors of the biological regulation of the process are well presented in the Komarova et al. model [6], only by including physicochemical regulation of bone interstitial fluid we would be able to truly describe the intricate process of bone formation. My research objective was to address these limitations and develop a model that describes both biological and physicochemical aspects of bone mineralization. The following 3 chapters are the three models developed to achieve this goal. The first model was an effort to understand the effect of pH on bone processes by making a preliminary simulated interstitial fluid. The second model simulates bone interstitial fluid where the environment is permissive to precipitation of hydroxyapatite. This model captures the physicochemical regulation of bone

mineralization. Lastly, the third model is an integration of the physicochemical model and the biological model [6].

## References

1. Rauch, F. and F.H. Glorieux, *Osteogenesis imperfecta*. The Lancet, 2004. **363**(9418): p. 1377-1385.
2. Cianferotti, L., *Osteomalacia is not a single disease*. International Journal of Molecular Sciences, 2022. **23**(23): p. 14896.
3. Donnelly, E. and A.L. Boskey, *Mineralization*, in *Vitamin D*. 2011, Elsevier. p. 381-401.
4. Bonjour, J.-P., *Calcium and phosphate: a duet of ions playing for bone health*. Journal of the American College of Nutrition, 2011. **30**(sup5): p. 438S-448S.
5. Granjon, D., O. Bonny, and A. Edwards, *Coupling between phosphate and calcium homeostasis: a mathematical model*. American Journal of Physiology-Renal Physiology, 2017. **313**(6): p. F1181-F1199.
6. Komarova, S.V., et al., *Mathematical model for bone mineralization*. Front Cell Dev Biol, 2015. **3**: p. 51.
7. Peterson, M.C. and M.M. Riggs, *A physiologically based mathematical model of integrated calcium homeostasis and bone remodeling*. Bone, 2010. **46**(1): p. 49-63.
8. Powell, T., *A mathematical model for calcium homeostasis*. The Bulletin of mathematical biophysics, 1972. **34**: p. 483-502.
9. Raposo, J.F., L.G. Sobrinho, and H.G. Ferreira, *A minimal mathematical model of calcium homeostasis*. Journal of Clinical Endocrinology & Metabolism, 2002. **87**(9): p. 4330-4340.
10. Boskey, A.L., *Bone composition: relationship to bone fragility and antiosteoporotic drug effects*. BoneKEY reports, 2013. **2**.
11. Von Euw, S., et al., *Bone mineral: new insights into its chemical composition*. Scientific reports, 2019. **9**(1): p. 8456.
12. Boskey, A.L. and P.G. Robey, *The composition of bone*. Primer on the metabolic bone diseases and disorders of mineral metabolism, 2013: p. 49-58.
13. Rey, C., et al., *Bone mineral: update on chemical composition and structure*. Osteoporosis international, 2009. **20**: p. 1013-1021.
14. Wagner, D.O. and P. Aspenberg, *Where did bone come from? An overview of its evolution*. Acta orthopaedica, 2011. **82**(4): p. 393-398.
15. Boskey, A.L. and R. Coleman, *Aging and bone*. J Dent Res, 2010. **89**(12): p. 1333-48.
16. Donnelly, E., et al., *Bone tissue composition varies across anatomic sites in the proximal femur and the iliac crest*. Journal of orthopaedic research, 2012. **30**(5): p. 700-706.
17. Gregson, C.L., et al., *Analysis of body composition in individuals with high bone mass reveals a marked increase in fat mass in women but not men*. The Journal of Clinical Endocrinology & Metabolism, 2013. **98**(2): p. 818-828.
18. Leslie, W.D., *Ethnic differences in bone mass—clinical implications*. The Journal of Clinical Endocrinology & Metabolism, 2012. **97**(12): p. 4329-4340.
19. Yoder, C.H., et al., *Structural water in carbonated hydroxylapatite and fluorapatite: Confirmation by solid state <sup>2</sup>H NMR*. Calcified Tissue International, 2012. **90**: p. 60-67.
20. Techawiboonwong, A., et al., *Cortical bone water: in vivo quantification with ultrashort echo-time MR imaging*. Radiology, 2008. **248**(3): p. 824-833.
21. Vassiliou, V., E. Chow, and D. Kardamakis, *Bone metastases: a translational and clinical approach*. Vol. 21. 2013: Springer Science & Business Media.

22. Cohen Jr, M.M., *The new bone biology: pathologic, molecular, and clinical correlates*. American journal of medical genetics part A, 2006. **140**(23): p. 2646-2706.
23. Stains, J.P. and R. Civitelli, *Cell-cell interactions in regulating osteogenesis and osteoblast function*. Birth Defects Research Part C: Embryo Today: Reviews, 2005. **75**(1): p. 72-80.
24. Stains, J.P. and R. Civitelli, *Gap junctions in skeletal development and function*. Biochimica et Biophysica Acta (BBA)-Biomembranes, 2005. **1719**(1-2): p. 69-81.
25. Chambers, T., *Regulation of the differentiation and function of osteoclasts*. The Journal of pathology, 2000. **192**(1): p. 4-13.
26. Teitelbaum, S.L., *Bone resorption by osteoclasts*. Science, 2000. **289**(5484): p. 1504-1508.
27. Blair, H.C., L.J. Robinson, and M. Zaidi, *Osteoclast signalling pathways*. Biochemical and biophysical research communications, 2005. **328**(3): p. 728-738.
28. Franz-Odenaal, T.A., B.K. Hall, and P.E. Witten, *Buried alive: how osteoblasts become osteocytes*. Developmental dynamics: an official publication of the American Association of Anatomists, 2006. **235**(1): p. 176-190.
29. Tate, M.L.K., et al., *The osteocyte*. The international journal of biochemistry & cell biology, 2004. **36**(1): p. 1-8.
30. Iqbal, J. and M. Zaidi, *Molecular regulation of mechanotransduction*. Biochemical and biophysical research communications, 2005. **328**(3): p. 751-755.
31. Cullinane, D., *The role of osteocytes in bone regulation: mineral homeostasis versus mechanoreception*. Journal of Musculoskeletal and Neuronal Interactions, 2002. **2**(3): p. 242-244.
32. Shea, J.E. and S.C. Miller, *Skeletal function and structure: implications for tissue-targeted therapeutics*. Advanced drug delivery reviews, 2005. **57**(7): p. 945-957.
33. Clarke, B., *Normal bone anatomy and physiology*. Clinical journal of the American Society of Nephrology, 2008. **3**(Supplement\_3): p. S131-S139.
34. Hadjidakis, D.J. and I.I. Androulakis, *Bone remodeling*. Annals of the New York academy of sciences, 2006. **1092**(1): p. 385-396.
35. Frost, H.M., *Mathematical Elements of Lamellab Bone Remodeling*. Plastic and Reconstructive Surgery, 1964. **34**(3): p. 315.
36. Parfitt, A.M., *The coupling of bone formation to bone resorption: a critical analysis of the concept and of its relevance to the pathogenesis of osteoporosis*. 1982, Elsevier. p. 1-6.
37. Juliet, E. and M. Compston, R. & McClung, *WDL Osteoporosis*. Lancet, 2019. **393**: p. 364-376.
38. Kenkre, J. and J. Bassett, *The bone remodelling cycle*. Annals of clinical biochemistry, 2018. **55**(3): p. 308-327.
39. Kearns, A.E., S. Khosla, and P.J. Kostenuik, *Receptor activator of nuclear factor  $\kappa$ B ligand and osteoprotegerin regulation of bone remodeling in health and disease*. Endocrine reviews, 2008. **29**(2): p. 155-192.
40. Clevers, H. and R. Nusse, *Wnt/ $\beta$ -catenin signaling and disease*. Cell, 2012. **149**(6): p. 1192-1205.
41. Murshed, M., *Mechanism of Bone Mineralization*. Cold Spring Harb Perspect Med, 2018. **8**(12).
42. Raisz, L.G., *Physiology and pathophysiology of bone remodeling*. Clinical chemistry, 1999. **45**(8): p. 1353-1358.
43. Jaalouk, D.E. and J. Lammerding, *Mechanotransduction gone awry*. Nature reviews Molecular cell biology, 2009. **10**(1): p. 63-73.

44. Stewart, S., et al., *Mechanotransduction in osteogenesis*. Bone & joint research, 2020. **9**(1): p. 1-14.
45. Robling, A.G. and L.F. Bonewald, *The osteocyte: new insights*. Annual review of physiology, 2020. **82**: p. 485-506.
46. Kamel, M.A., et al., *Activation of  $\beta$ -catenin signaling in MLO-Y4 osteocytic cells versus 2T3 osteoblastic cells by fluid flow shear stress and PGE2: Implications for the study of mechanosensation in bone*. Bone, 2010. **47**(5): p. 872-881.
47. Fritton, S.P. and S. Weinbaum, *Fluid and solute transport in bone: flow-induced mechanotransduction*. Annual review of fluid mechanics, 2009. **41**: p. 347-374.
48. Klein-Nulend, J., et al., *Sensitivity of osteocytes to biomechanical stress in vitro*. The FASEB Journal, 1995. **9**(5): p. 441-445.
49. Burger, E.H. and J. Klein-Nulend, *Mechanotransduction in bone—role of the lacunocanalicular network*. The FASEB journal, 1999. **13**(9001): p. S101-S112.
50. Rigo, J., M. Mohamed, and M. DE CURTIS, *Disorders of calcium, phosphorus, and magnesium metabolism*, in *Neonatal-Perinatal Medicine*. 2010, Elsevier Mosby. p. 1523-1556.
51. Hsu, S.C. and M.A. Levine. *Perinatal calcium metabolism: physiology and pathophysiology*. in *Seminars in Neonatology*. 2004. Elsevier.
52. Rigo, J., et al., *Calcium and phosphorus homeostasis: pathophysiology*. Neonatology: A practical approach to neonatal diseases, 2012: p. 333-353.
53. DiGirolamo, D.J., T.L. Clemens, and S. Kousteni, *The skeleton as an endocrine organ*. Nature Reviews Rheumatology, 2012. **8**(11): p. 674-683.
54. Bilezikian, J.P., et al., *The parathyroids: basic and clinical concepts*. 2014: academic Press.
55. Mackiewicz, Z., et al., *Bone as a source of organism vitality and regeneration*. Folia histochemica et cytobiologica, 2011. **49**(4): p. 558-569.
56. McKee, M.D. and W.G. Cole, *Chapter 2 - Bone Matrix and Mineralization*, in *Pediatric Bone (Second Edition)*, F.H. Glorieux, J.M. Pettifor, and H. Jüppner, Editors. 2012, Academic Press: San Diego. p. 9-37.
57. Jannin, A., V. Kerlan, and R. Desaillood. *Endocrinology of bone mineralization: An update*. in *Annales d'Endocrinologie*. 2022. Elsevier.
58. Glimcher, M.J., *Bone: nature of the calcium phosphate crystals and cellular, structural, and physical chemical mechanisms in their formation*. Reviews in mineralogy and geochemistry, 2006. **64**(1): p. 223-282.
59. Landis, W.J., et al., *Structural relations between collagen and mineral in bone as determined by high voltage electron microscopic tomography*. Microscopy research and technique, 1996. **33**(2): p. 192-202.
60. Sapir-Koren, R. and G. Livshits, *Bone Mineralization and Regulation of Phosphate Homeostasis*. Ibm Bonekey, 2011. **8**(6).
61. Walsh, W.R., et al., *Cell structure and biology of bone and cartilage*. Handbook of histology methods for bone and cartilage, 2003: p. 35-58.
62. Gajjeraman, S., et al., *Matrix macromolecules in hard tissues control the nucleation and hierarchical assembly of hydroxyapatite*. Journal of Biological Chemistry, 2007. **282**(2): p. 1193-1204.
63. Roberts, S., et al., *Functional involvement of PHOSPHO1 in matrix vesicle-mediated skeletal mineralization*. Journal of Bone and Mineral Research, 2007. **22**(4): p. 617-627.

64. Young, M.F., *Bone matrix proteins: their function, regulation, and relationship to osteoporosis*. Osteoporosis international, 2003. **14**: p. 35-42.
65. Misof, B.M., et al., *Effects of intermittent parathyroid hormone administration on bone mineralization density in iliac crest biopsies from patients with osteoporosis: a paired study before and after treatment*. The Journal of Clinical Endocrinology & Metabolism, 2003. **88**(3): p. 1150-1156.
66. Boivin, G. and P.J. Meunier, *Methodological considerations in measurement of bone mineral content*. Osteoporosis international, 2003. **14**(Suppl 5): p. 22-28.
67. Roschger, P., et al., *Bone mineralization density distribution in health and disease*. Bone, 2008. **42**(3): p. 456-466.
68. Marulanda, J., et al., *Matrix Gla protein deficiency impairs nasal septum growth, causing midface hypoplasia*. Journal of Biological Chemistry, 2017. **292**(27): p. 11400-11412.
69. Murshed, M., et al., *Extracellular matrix mineralization is regulated locally; different roles of two gla-containing proteins*. The Journal of cell biology, 2004. **165**(5): p. 625-630.
70. Boskey, A., et al., *Osteopontin-hydroxyapatite interactions in vitro: inhibition of hydroxyapatite formation and growth in a gelatin-gel*. Bone and mineral, 1993. **22**(2): p. 147-159.
71. He, G., et al., *Spatially and temporally controlled biomineralization is facilitated by interaction between self-assembled dentin matrix protein 1 and calcium phosphate nuclei in solution*. Biochemistry, 2005. **44**(49): p. 16140-16148.
72. Fleisch, H. and S. Bisaz, *Isolation from urine of pyrophosphate, a calcification inhibitor*. American Journal of Physiology-Legacy Content, 1962. **203**(4): p. 671-675.
73. Russell, R., et al., *Inorganic pyrophosphate in plasma in normal persons and in patients with hypophosphatasia, osteogenesis imperfecta, and other disorders of bone*. The Journal of clinical investigation, 1971. **50**(5): p. 961-969.
74. McKEE, M.D. and A. Nanci, *Osteopontin and the bone remodeling sequence. Colloidal-gold immunocytochemistry of an interfacial extracellular matrix protein*. Annals of the new York Academy of Sciences, 1995. **760**: p. 177-189.
75. Nanci, A., et al., *Ultrastructural characterization and immunolocalization of osteopontin in rat calvarial osteoblast primary cultures*. Microscopy research and technique, 1996. **33**(2): p. 214-231.
76. He, G., et al., *Nucleation of apatite crystals in vitro by self-assembled dentin matrix protein I*. Nature materials, 2003. **2**(8): p. 552-558.
77. Hunter, G.K. and H.A. Goldberg, *Nucleation of hydroxyapatite by bone sialoprotein*. Proceedings of the National Academy of Sciences, 1993. **90**(18): p. 8562-8565.
78. Anderson, H.C., *Mineralization by matrix vesicles*. Scanning electron microscopy, 1984(Pt 2): p. 953-964.
79. Beniash, E., *Biomaterials—hierarchical nanocomposites: the example of bone*. Wiley Interdisciplinary Reviews: Nanomedicine and Nanobiotechnology, 2011. **3**(1): p. 47-69.
80. Onuma, K., T. Tsuji, and M. Iijima, *Biomaterialization: Mechanisms of hydroxyapatite crystal growth*. Bioinspiration: From Nano to Micro Scales, 2012: p. 107-134.
81. Wang, L. and G.H. Nancollas, *Calcium orthophosphates: crystallization and dissolution*. Chemical reviews, 2008. **108**(11): p. 4628-4669.
82. Laurencin, D., et al., *Magnesium incorporation into hydroxyapatite*. Biomaterials, 2011. **32**(7): p. 1826-1837.

83. Rey, C., et al., *1.11 Bioactive calcium phosphate compounds: physical chemistry*. Compr. Biomater. II, 2017. **1**: p. 187-221.
84. Guan, X., *Kinetics studies of reactions at solid-liquid interface: Simulation of biomineralization*. 2007: State University of New York at Buffalo.
85. Luo, L., et al., *Mechanism of inhibition of human KSP by monastrol: insights from kinetic analysis and the effect of ionic strength on KSP inhibition*. Biochemistry, 2004. **43**(48): p. 15258-15266.
86. Ibis, F., et al., *A combined experimental and modelling study on solubility of calcium oxalate monohydrate at physiologically relevant pH and temperatures*. Crystals, 2020. **10**(10): p. 924.
87. Cruz, M.A.E., *Studies on the role of matrix vesicles in bone mineralization: observations from micro to nanoscale*. 2023, Universidade de São Paulo.
88. Pujari-Palmer, M., et al., *Pyrophosphate stimulates differentiation, matrix gene expression and alkaline phosphatase activity in osteoblasts*. PloS one, 2016. **11**(10): p. e0163530.
89. Lakhkar, N.J., et al., *Bone formation controlled by biologically relevant inorganic ions: role and controlled delivery from phosphate-based glasses*. Advanced drug delivery reviews, 2013. **65**(4): p. 405-420.
90. Lee, I.-H., et al., *Effects of pH and reaction temperature on hydroxyapatite powders synthesized by precipitation*. Journal of the Korean Ceramic Society, 2020. **57**: p. 56-64.
91. Castellani, C., et al., *Bone-implant interface strength and osseointegration: Biodegradable magnesium alloy versus standard titanium control*. Acta biomaterialia, 2011. **7**(1): p. 432-440.
92. Zhang, J., et al., *Dual function of magnesium in bone biomineralization*. Advanced healthcare materials, 2019. **8**(21): p. 1901030.
93. Landi, E., et al., *Carbonated hydroxyapatite as bone substitute*. Journal of the European Ceramic Society, 2003. **23**(15): p. 2931-2937.
94. Garskaite, E., et al., *Effect of processing conditions on the crystallinity and structure of carbonated calcium hydroxyapatite (CHAp)*. CrystEngComm, 2014. **16**(19): p. 3950-3959.
95. Cacciotti, I., *Cationic and anionic substitutions in hydroxyapatite*, in *Handbook of bioceramics and biocomposites*. 2016, Springer International Publishing Cham, Switzerland. p. 145-211.
96. Arnett, T.R. *Acid-base regulation of bone metabolism*. in *International Congress Series*. 2007. Elsevier.
97. Barzel, U.S., *The skeleton as an ion exchange system: Implications for the role of acid-base imbalance in the genesis of osteoporosis*. Journal of Bone and Mineral Research, 1995. **10**(10): p. 1431-1436.
98. Bushinsky, D., et al., *Effects of pH on bone calcium and proton fluxes in vitro*. American Journal of Physiology-Renal Physiology, 1983. **245**(2): p. F204-F209.
99. ARNETT, T.R. and D.W. DEMPSTER, *A comparative study of disaggregated chick and rat osteoclasts in vitro: effects of calcitonin and prostaglandins*. Endocrinology, 1987. **120**(2): p. 602-608.
100. Brandao-Burch, A. and T. Arnett. *Normal human osteoclasts are activated by acidosis*. 2004. AMER SOC BONE & MINERAL RES.
101. Hoebertz, A. and T.R. Arnett, *Isolated osteoclast cultures*, in *Bone research protocols*. 2003, Springer. p. 53-64.

102. Morrison, M.S., et al., *ATP is a potent stimulator of the activation and formation of rodent osteoclasts*. The Journal of physiology, 1998. **511**(2): p. 495-500.
103. Brandao-Burch, A., et al., *Acidosis inhibits bone formation by osteoblasts in vitro by preventing mineralization*. Calcified tissue international, 2005. **77**: p. 167-174.
104. Tavafoghi, M. and M. Cerruti, *The role of amino acids in hydroxyapatite mineralization*. Journal of The Royal Society Interface, 2016. **13**(123): p. 20160462.
105. Ito, A., et al., *Solubility product of OH-carbonated hydroxyapatite*. Journal of Biomedical Materials Research: An Official Journal of The Society for Biomaterials and The Japanese Society for Biomaterials, 1997. **36**(4): p. 522-528.
106. Campi, G., et al., *Heterogeneous and self-organizing mineralization of bone matrix promoted by hydroxyapatite nanoparticles*. Nanoscale, 2017. **9**(44): p. 17274-17283.
107. Urry, D., *Neutral sites for calcium ion binding to elastin and collagen: a charge neutralization theory for calcification and its relationship to atherosclerosis*. Proceedings of the National Academy of Sciences, 1971. **68**(4): p. 810-814.
108. Roach, H., *Why does bone matrix contain non-collagenous proteins? The possible roles of osteocalcin, osteonectin, osteopontin and bone sialoprotein in bone mineralisation and resorption*. Cell biology international, 1994. **18**(6): p. 617-628.
109. Hong, M.-H., et al., *Biomineralization of bone tissue: calcium phosphate-based inorganics in collagen fibrillar organic matrices*. Biomaterials Research, 2022. **26**(1): p. 42.
110. Jahromi, M.T., G. Yao, and M. Cerruti, *The importance of amino acid interactions in the crystallization of hydroxyapatite*. Journal of the Royal Society Interface, 2013. **10**(80): p. 20120906.
111. Icer, M.A. and M. Gezmen-Karadag, *The multiple functions and mechanisms of osteopontin*. Clinical biochemistry, 2018. **59**: p. 17-24.
112. Hunter, G.K., *Role of osteopontin in modulation of hydroxyapatite formation*. Calcified tissue international, 2013. **93**: p. 348-354.
113. Wang, Z., et al., *A potential mechanism for amino acid-controlled crystal growth of hydroxyapatite*. Journal of materials chemistry B, 2015. **3**(47): p. 9157-9167.
114. Petersson, U., *Studies on three matrix molecules in bone and dentin*. 2003: Institutionen för odontologi/Department of Odontology.
115. Fantner, G.E., et al., *Nanoscale ion mediated networks in bone: osteopontin can repeatedly dissipate large amounts of energy*. Nano letters, 2007. **7**(8): p. 2491-2498.
116. Si, J., et al., *Osteopontin in bone metabolism and bone diseases*. Medical science monitor: international medical journal of experimental and clinical research, 2020. **26**: p. e919159-1.
117. Malaval, L., et al., *Bone sialoprotein plays a functional role in bone formation and osteoclastogenesis*. The Journal of experimental medicine, 2008. **205**(5): p. 1145-1153.
118. Marinovich, R., et al., *The role of bone sialoprotein in the tendon–bone insertion*. Matrix Biology, 2016. **52**: p. 325-338.
119. Fujisawa, R., Y. Nodasaka, and Y. Kuboki, *Further characterization of interaction between bone sialoprotein (BSP) and collagen*. Calcified tissue international, 1995. **56**: p. 140-144.
120. Morgan, S., A.A. Poundarik, and D. Vashishth, *Do non-collagenous proteins affect skeletal mechanical properties?* Calcified tissue international, 2015. **97**: p. 281-291.
121. Carvalho, M.S., et al., *Bone matrix non-collagenous proteins in tissue engineering: Creating new bone by mimicking the extracellular matrix*. Polymers, 2021. **13**(7): p. 1095.

122. Gericke, A., et al., *Different forms of DMP1 play distinct roles in mineralization*. Journal of dental research, 2010. **89**(4): p. 355-359.
123. Schurgers, L.J., E.C. Cranenburg, and C. Vermeer, *Matrix Gla-protein: the calcification inhibitor in need of vitamin K*. Thrombosis and haemostasis, 2008. **100**(10): p. 593-603.
124. Sánchez-Duffhues, G., et al., *Bone morphogenetic protein signaling in bone homeostasis*. Bone, 2015. **80**: p. 43-59.
125. Pivonka, P. and S.V. Komarova, *Mathematical modeling in bone biology: From intracellular signaling to tissue mechanics*. Bone, 2010. **47**(2): p. 181-189.
126. Vilar, J.M.G., R. Jansen, and C. Sander, *Signal processing in the TGF- $\beta$  superfamily ligand-receptor network*. PLoS computational biology, 2006. **2**(1): p. e3.
127. Podshivalov, L., A. Fischer, and P.Z. Bar-Yoseph, *On the road to personalized medicine: multiscale computational modeling of bone tissue*. Archives of Computational Methods in Engineering, 2014. **21**: p. 399-479.
128. Wang, M., N. Yang, and X. Wang, *A review of computational models of bone fracture healing*. Medical & biological engineering & computing, 2017. **55**: p. 1895-1914.
129. Boaretti, D., et al., *Perspectives on in silico bone mechanobiology: computational modelling of multicellular systems*. European Cells & Materials, 2022. **44**: p. 56-73.
130. Ostapienko, B.I., D. Lopez, and S.V. Komarova, *Mathematical modeling of calcium phosphate precipitation in biologically relevant systems: scoping review*. Biomech Model Mechanobiol, 2019. **18**(2): p. 277-289.
131. Raposo, J., et al., *A mathematical model of calcium and phosphorus metabolism in two forms of hyperparathyroidism*. Endocrine, 2012. **41**: p. 309-319.
132. Granjon, D., O. Bonny, and A. Edwards, *A model of calcium homeostasis in the rat*. American Journal of Physiology-Renal Physiology, 2016. **311**(5): p. F1047-F1062.
133. Hurwitz, S., et al., *Simulation of calcium homeostasis: modeling and parameter estimation*. American Journal of Physiology-Regulatory, Integrative and Comparative Physiology, 1983. **245**(5): p. R664-R672.
134. Komarova, S.V., et al., *Mathematical model predicts a critical role for osteoclast autocrine regulation in the control of bone remodeling*. Bone, 2003. **33**(2): p. 206-215.
135. Ryser, M.D., N. Nigam, and S.V. Komarova, *Mathematical modeling of spatio-temporal dynamics of a single bone multicellular unit*. Journal of bone and mineral research, 2009. **24**(5): p. 860-870.
136. Lemaire, V., et al., *Modeling the interactions between osteoblast and osteoclast activities in bone remodeling*. Journal of theoretical biology, 2004. **229**(3): p. 293-309.
137. Agarwal, R. and C. Midha, *Study and mathematical analysis of the novel fractional bone mineralization model*. Journal of Computational Analysis & Applications, 2024. **33**(1).

**Chapter 3. Mathematical modeling of the role of bone turnover in pH regulation in bone interstitial fluid**

**Mathematical modeling of the role of bone turnover in pH regulation in bone interstitial fluid**

Hossein Poorhemati<sup>a,b</sup>, Svetlana V. Komarova<sup>a,b,c\*</sup>

<sup>a</sup>Department of Biological and Biomedical Engineering, McGill University, Montreal, QC, Canada

<sup>b</sup>Shriners Hospital for Children – Canada, Montreal, QC, Canada

<sup>c</sup>Faculty of Dentistry, McGill University, Montreal, QC, Canada

Email addresses:

Hossein Poorhemati: [hossein.poorhemati@mail.mcgill.ca](mailto:hossein.poorhemati@mail.mcgill.ca)

Svetlana V. Komarova: [svetlana.komarova@mcgill.ca](mailto:svetlana.komarova@mcgill.ca)

\*Corresponding author: Svetlana V. Komarova, Shriners Hospital for Children – Canada, 1003 Decarie Boulevard, Montreal, Quebec, Canada H4A 0A9. Tel: (514) 282-7153, Email: [svetlana.komarova@mcgill.ca](mailto:svetlana.komarova@mcgill.ca)

## **Abstract**

**Background and aims:** Bone turnover is strongly affected by pH of surrounding fluid, and in turn plays a role in maintaining systemic pH, however the quantitative contribution of bone processes to pH regulation is not known. Our goal was to develop a mathematical model describing pH regulation in the interstitial fluid and to examine the contribution of hydroxyapatite dissolution and precipitation to pH regulation.

**Materials and methods:** We modeled twelve reversible equilibrium reactions of sixteen calcium, phosphate, hydrogen and carbonate species in the interstitial fluid and examined the buffering capacity and range. The effect of hydroxyapatite dissolution and precipitation was modeled by assuming that the calcium, phosphate and hydroxide contained in the bone volume adjacent to the interstitial fluid is instantaneously added to or removed from the interstitial fluid.

**Results:** The carbonate buffer was found to dominate electrochemical buffering system of the bone interstitial fluid. Nevertheless, the phosphate added during dissolution of bone hydroxyapatite significantly improved the interstitial fluid buffering capacity. In contrast, hydroxyapatite precipitation had limited effect on the interstitial fluid pH regulation.

**Conclusion:** This study provides mechanistic insights into the physicochemical processes underlying the known role of bone turnover processes in regulation of body pH homeostasis.

## **Keywords**

pH regulation, hydroxyapatite, mathematical modeling, interstitial fluid, bone, resorption

## 1. Introduction

Precise regulation of pH homeostasis is critical for the animal survival in environmental conditions that constantly challenge acid-base balance through respiratory or metabolic acidosis [1]. Changes in pH in the interstitial fluid that immediately surrounds cells has been implicated in regulating insulin resistance in diabetes [2], tumor progression [3], and muscle blood flow during exercise [4]. Bone turnover is strongly affected by the pH of surrounding fluid [5], and it has been suggested that bone remodeling, in particular bone resorption in turn plays a role in maintaining systemic pH [6]. However, how much bone turnover can contribute to the pH regulation is not clear.

In blood, fast regulation of pH includes physicochemical buffers, such as carbonate and phosphate buffers, proteins and hemoglobin [1, 7]. However, in the interstitial fluid surrounding tissues, including bone, there are no red blood cells, and therefore the hemoglobin-based pH regulation is absent, and protein content is significantly reduced [7, 8]. Therefore, the main pH regulation in the interstitial fluid occurs through the carbonate and phosphate buffers. Importantly, dissolution or precipitation of hydroxyapatite,  $\text{Ca}_{10}(\text{PO}_4)_6(\text{OH})_2$ , the mineral component of bone, can change the concentrations of  $\text{Ca}^{2+}$ ,  $\text{PO}_4^{3-}$  and  $\text{OH}^-$  in the interstitial fluid, thus potentially affecting its buffering capacity. However, the quantitative analysis of potential contribution of bone turnover processes to pH regulation has not yet been performed.

The goal of this study was to develop a mathematical model describing the regulation of pH in the interstitial fluid environment and to examine the potential role in pH regulation of

dissolution and precipitation of hydroxyapatite during bone resorption and formation. Following the analysis of approaches used to model mineralization and associated processes [9], we based our model of the biochemistry of interstitial fluid on the published models of the chemical equilibrium in the aqueous phase of biological fluids [10, 11]. The computation incorporation of bone processes was based on our previous study of biological regulation of bone mineralization [12].

## 2. Model Development

### 2.1 Aqueous Phase Equilibrium Model

We modeled the equilibrium state of calcium, phosphate, hydrogen and carbonate in the interstitial fluid in bone proximity. We modeled the chemical interactions among 16 chemical species that had at least one of these four core components in its structure. The 16 species were linked together with 12 reversible reactions with corresponding equilibrium constants, the value of which was obtained from previous studies (**Table 1**). Additional 4 equations described the principle of mass conservation for total hydrogen (TH), total calcium (TCa), total phosphate (TPO<sub>4</sub>) and total carbonate (TCO<sub>3</sub>) (Table 1). These four total concentrations also served as inputs of the aqueous phase equilibrium model. The ranges for the total values of the four core components were obtained from their reported physiological serum levels (**Table 1**).

$$K_{\text{H}_2\text{O}} = [\text{H}^+] \times [\text{OH}^-] \tag{1}$$

$$K_{\text{CaOH}} \times [\text{CaOH}^+] = [\text{OH}^-] \times [\text{Ca}^{2+}]$$

(2)

$$K_{\text{CaH}_2\text{PO}_4} \times [\text{CaH}_2\text{PO}_4^+] = [\text{Ca}^{2+}] \times [\text{H}_2\text{PO}_4^-]$$

(3)

$$K_{\text{CaHPO}_4} \times [\text{CaHPO}_4] = [\text{Ca}^{2+}] \times [\text{HPO}_4^{2-}]$$

(4)

$$K_{\text{CaPO}_4} \times [\text{CaPO}_4^-] = [\text{Ca}^{2+}] \times [\text{PO}_4^{3-}] \quad (5)$$

$$K_{\text{CaHCO}_3} \times [\text{CaHCO}_3^+] = [\text{Ca}^{2+}] \times [\text{HCO}_3^-] \quad (6)$$

$$K_{\text{H}_3\text{PO}_4} \times [\text{H}_3\text{PO}_4] = [\text{H}^+] \times [\text{H}_2\text{PO}_4^-] \quad (7)$$

$$K_{\text{H}_2\text{PO}_4} \times [\text{H}_2\text{PO}_4^-] = [\text{H}^+] \times [\text{HPO}_4^{2-}] \quad (8)$$

$$K_{\text{HPO}_4} \times [\text{HPO}_4^{2-}] = [\text{H}^+] \times [\text{PO}_4^{3-}] \quad (9)$$

$$K_{\text{H}_2\text{CO}_3} \times [\text{H}_2\text{CO}_3] = [\text{H}^+] \times [\text{HCO}_3^-] \quad (10)$$

$$K_{\text{HCO}_3} \times [\text{HCO}_3^-] = [\text{H}^+] \times [\text{CO}_3^{2-}] \quad (11)$$

$$K_{\text{CaCO}_3} \times [\text{CaCO}_3] = [\text{Ca}^{2+}] \times [\text{CO}_3^{2-}] \quad (12)$$

$$\begin{aligned} \text{TH} = & [\text{H}^+] + 2 \times [\text{CaH}_2\text{PO}_4^+] + [\text{CaHPO}_4] + [\text{CaHCO}_3^+] + 3 \times [\text{H}_3\text{PO}_4] + 2 \times [\text{H}_2\text{PO}_4^-] + \\ & [\text{HPO}_4^{2-}] + 2 \times [\text{H}_2\text{CO}_3] + [\text{HCO}_3^-] - [\text{OH}^-] - [\text{CaOH}^+] \end{aligned} \quad (13)$$

$$\begin{aligned} \text{TPO}_4 = & [\text{CaH}_2\text{PO}_4^+] + [\text{CaHPO}_4] + [\text{CaPO}_4^-] + [\text{H}_3\text{PO}_4] + [\text{H}_2\text{PO}_4^-] + [\text{HPO}_4^{2-}] + [\text{PO}_4^{3-}] \end{aligned} \quad (14)$$

$$\text{TCO}_3 = [\text{CaHCO}_3^+] + [\text{H}_2\text{CO}_3] + [\text{HCO}_3^-] + [\text{CaCO}_3] \quad (15)$$

$$\begin{aligned} \text{TCa} = & [\text{Ca}^{2+}] + [\text{CaOH}^+] + [\text{CaH}_2\text{PO}_4^+] + [\text{CaHPO}_4] + [\text{CaPO}_4^-] + [\text{CaHCO}_3^+] + [\text{CaCO}_3] \end{aligned} \quad (16)$$

**Table 1.** Parameter values and corresponding references.

| Parameter       | Value or range | Reference |
|-----------------|----------------|-----------|
| $K_{H_2O}$      | 1.01E – 14     | [13]      |
| $K_{CaOH}$      | 3.98E – 02     | [14]      |
| $K_{CaH_2PO_4}$ | 3.13E – 02     | [15]      |
| $K_{CaHPO_4}$   | 1.47E – 03     | [15]      |
| $K_{CaPO_4}$    | 2.89E – 07     | [16]      |
| $K_{CaHCO_3}$   | 6.92E – 02     | [10]      |
| $K_{H_3PO_4}$   | 6.37E – 03     | [10]      |
| $K_{H_2PO_4}$   | 6.53E – 08     | [10]      |
| $K_{HPO_4}$     | 6.46E – 13     | [10]      |
| $K_{H_2CO_3}$   | 4.90E – 07     | [10]      |
| $K_{HCO_3}$     | 5.62E – 11     | [10]      |
| $K_{CaCO_3}$    | 4.17E – 04     | [10]      |
| $TPO_4$         | 0.9 – 1.6 mM   | [17]      |
| $TCO_3$         | 30-40 mM       | [17]      |
| $TCa$           | 2.1-2.8 mM     | [17, 18]  |

The aqueous phase equilibrium of a solution containing ions is affected by the presence of electrolytes in the solution, due to the electrostatic forces between the electrolytes and ions participating in the equilibrium [19]. To account for this effect, the effective concentration of each species needs to be calculated. Effective concentration for the species  $i$  is defined by

$$Q_i = c_i \cdot \gamma_i \quad (17)$$

where  $c_i$  is the molar concentration and  $\gamma_i$  is the activity coefficient of that species [19]. To calculate the activity coefficient for different species in a solution we need to first calculate the ionic strength,  $I$ , of the solution. The ionic strength for a solution is calculated from equation (18), where  $n$  is the number of species and  $c_i$  and  $z_i$  are the molar concentration and charge of the  $i$ th species in the solution.

$$I = \frac{1}{2} \sum_{i=1}^n c_i \cdot z_i^2 \quad (18)$$

Considering the value of ionic strength in human plasma (0.16 M [20]), to calculate the activity coefficient, we used Davies equation which is acceptable for  $I \leq 0.5 M$  [21]:

$$\log \gamma_i = -Az_i^2 \left( \frac{\sqrt{I}}{(1+\sqrt{I})} - 0.3I \right) \quad (19)$$

where  $A$  is the activity coefficient constant. The value of  $A$  depends on temperature and the dielectric constant of water [22]. The dependence of  $A$  on temperature ( $T_c$  is temperature in Celsius, 37 °C in our study) was later approximated as follows [23, 24]:

$$A = 0.486 + 6.07 \times 10^{-4}T_c + 6.43 \times 10^{-6}T_c^2 \quad (20)$$

To calculate the final equilibrium concentrations in the aqueous phase model, we used an iterative method. First, we assumed all activity coefficients to be equal to 1 and calculated equilibrium concentrations and ionic strength, which allowed us to update the values for the activity coefficients. Then we used the updated values of activity coefficients to calculate the updated equilibrium concentrations and ionic strength, followed by the newly updated activity coefficients. In all iterations, the ionic strength value and the activity coefficients were assessed to be less than 0.1 and 1, respectively. This iterative process continued until the maximum difference (L-infinity norm) between the last two iterative values of activity coefficients were smaller than  $\varepsilon = 10E - 8$ .

## 2.2 Buffer characteristic method

The behavior of phosphate and carbonate buffering systems in interstitial fluid was studied individually and in combination. In each specific case, all inputs of the relevant aqueous phase equilibrium model other than the total hydrogen were kept constant, total hydrogen concentration (TH) was changed over a range of concentrations (simulating adding protons to the environment), and an effective concentration of free proton and the resulting pH was calculated by the aqueous phase equilibrium model. To calculate the buffering range, first we found the inflection points ( $\frac{\partial^2 pH}{\partial TH^2} = 0$ ) of the  $pH = f(TH^+)$  graph, from which we selected an inflection point that *i*) was in the physiological range of pH values, and *ii*) demonstrated the minimal change in pH with the change in TH. This point,  $pH_c$ , corresponds to the highest buffering capacity and is equivalent to the  $pK_a$  of the simple buffers. The buffering range was calculated as  $\pm$  one pH unit from the  $pH_c$  ( $pH^{+/-} = pH_c \pm 1$ ). Finally, the buffering capacity was calculated as  $DTH/DpH$  between the  $pH^{+/-}$  points.

## 2.3 Bone processes

We studied the effects of dissolution of hydroxyapatite due to bone resorption or its precipitation due to bone formation on interstitial fluid pH regulation. We assumed that a unit volume of interstitial fluid is a cuboid with the thickness of 3  $\mu m$  and a surface area of 1  $\mu m^2$  neighbouring bone (Fig. 1A). The volume of resorbing or forming bone was assumed to differ depending on the thickness of bone involved in an active process. We next assumed that bone volume contains  $0.8E+9$  molecules/ $mm^3$  [12] of hydroxyapatite,  $Ca_{10}(PO_4)_6(OH)_2$ . In this study, we ignored the mass transfer limitations and assumed that minerals

transferred from bone to interstitial fluid or vice versa instantaneously at time 0 and that mineral distribution in bone and interstitial fluid remained homogeneous. Therefore, hydroxyapatite dissolution and precipitation were defined as changes in the initial inputs of four total concentrations, TH, TCa, TPO<sub>4</sub>, TCO<sub>3</sub>, in the equilibrium aqueous phase model, and the resulting interstitial fluid equilibrium concentrations and pH was quantified.

## **2.4 Model as a whole**

Figure 1B demonstrates the schematic representation of how different parts of the model work together. In the *Bone processes* compartment, the scenario of interest was defined as quiescent, dissolution and precipitation. Then this scenario was mathematically translated to provide the input values for the *Aqueous phase equilibrium compartment*, which includes three sub-compartments: chemical equilibrium calculator, activity calculator and validity check functions, such as recalculating equilibrium constants from the calculated equilibrium concentrations and checking their consistency with reported values, checking the values of ionic strength to be less than or equal to 0.1, and activity coefficients to be less than or equal to 1. *Aqueous phase equilibrium compartment* calculates the equilibrium concentrations of sixteen species, which then allows the *Buffer characterization* compartment to report the buffering behavior of interstitial fluid in the defined scenario.

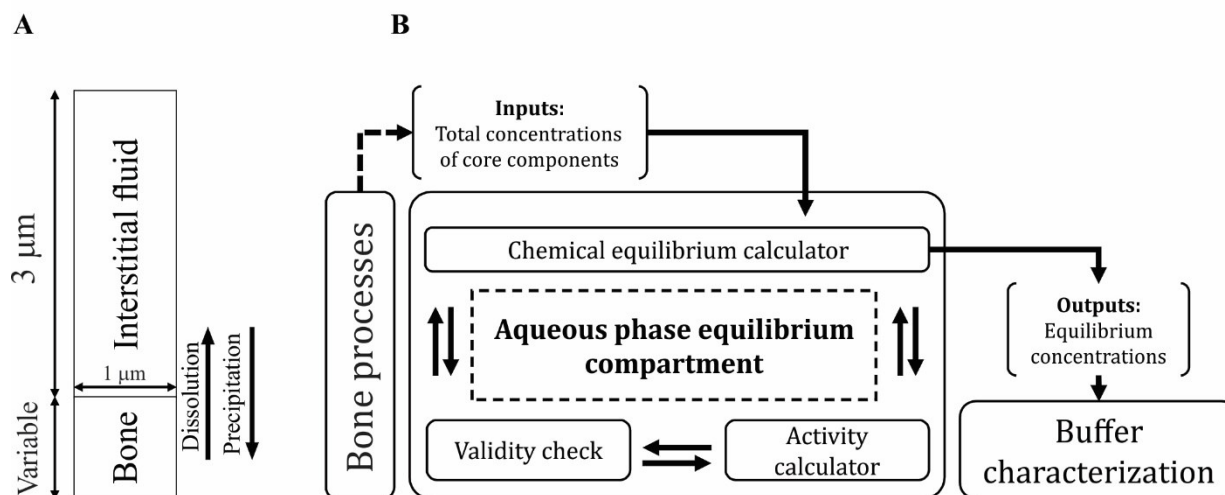


**Figure 1.** Graphical presentation of the model. A) Schematics of modeled compartments. Interstitial fluid compartment was assumed to be a cuboid with a constant volume of 3 mm<sup>3</sup> and a side of 1 mm<sup>2</sup> that is next to bone tissue. The volume of bone involved in resorption/formation varies in thickness 0.1-3 mm. B) The flow of information in the model.

#### 2.4.1. Solving the system of non-linear equations

The preliminary models of phosphate, carbonate and combined phosphate and carbonate buffering systems were calculated with MATLAB fsolve solver. However, the implementation of the complete model including all 16 species led to extensively time-consuming computations. To facilitate solving the system of 16 non-linear equations, we used the Newton-Raphson numerical method, based on the works by Morel [25] and Carrayrou [26]. Briefly, using equations 1 to 12 and equilibrium constants, we defined every one of the 16 species as a combination of concentration of 4 different components: H<sup>+</sup>, Ca<sup>2+</sup>, H<sub>3</sub>PO<sub>4</sub>, and H<sub>2</sub>CO<sub>3</sub> in the form of  $K_i[H^+]^\alpha[Ca^{2+}]^\beta[H_3PO_4]^\gamma[H_2CO_3]^\delta$  where  $K_i$  could be the combination of several equilibrium constants and the power of each concentration could be negative,

positive or zero. Then in the conservation equation (equations 13 to 16) each term was replaced with its corresponding form of combination of these 4 main components. The whole model was then collapsed into a system of 4 equations and 4 unknowns, which was solved using Newton-Raphson method by formulating its corresponding Jacobine matrix and defining an initial guess for the values of these four components. As suggested by Morel [25] to avoid negative solutions in our iterative procedure, wherever the Newton-Raphson method resulted in a negative solution for a component concentration, it was replaced with its corresponding positive value from the previous NR iteration divided by 10. Finally, the values of the remaining 12 species were recalculated from the four numerically estimated values. The implementation of this model in MATLAB is available on the corresponding github repository at: [https://github.com/Hosseinpoorhemati/Bone\\_aqueous\\_phase.git](https://github.com/Hosseinpoorhemati/Bone_aqueous_phase.git)

## **2.5 Modeling and computational resources**

The modeling and part of preliminary computations were conducted using MATLAB R2019b, provided by McGill university license. Computations for the complete model were initially conducted on the supercomputer Béluga from the École de technologie supérieure in Montreal, managed by Calcul Québec ([www.calculquebec.ca](http://www.calculquebec.ca)) and Compute Canada ([www.computecanada.ca](http://www.computecanada.ca)). The improved analysis of the complete model using Newton Raphson method was fast enough to run on a desktop computer.

## **3. Results and Discussion**

### **3.1. Contribution of phosphate and carbonate to the buffering capacity of interstitial fluid**

To understand the relative role of phosphate and carbonate buffers in maintaining pH in interstitial fluid, we examined the properties of these buffers independently or in combination, at variable levels of total phosphate and carbonate, which were chosen to represent the extremes and medium values of the physiological range (**Table 2**). Changes in equilibrium pH after total hydrogen (TH) was varied over a broad range of values were examined for the phosphate buffer alone (equations 1, 7-9, relevant terms in 13-14, and 17-20), carbonate buffer alone (equations 1, 10-11, relevant terms in 13 and 15, and 17-20), or the combination of phosphate and carbonate buffers (equations 1, 7-11, relevant terms in 13-15, and 17-20). The phosphate buffer had a buffering range between pH6.17 and pH8.17 (**Table 3**), and the buffering capacity of 0.5 mM H<sup>+</sup>/pH (**Fig. 2A**). Plotting the concentration of free H<sup>+</sup> as a function of total hydrogen allows to clearly visualize the limit of buffering behaviour in solutions with different concentrations of total phosphate (TPO<sub>4</sub>) (**Fig. 2B**), demonstrating increase in buffering capacity with increase in TPO<sub>4</sub> (**Fig. 2C**).

**Table 2.** Levels of total phosphate, total carbonate and total calcium used in the model. Medium level represents physiological concentrations (mM), low and high are extremes of the physiological range.

|                  | <b>Low</b> | <b>Medium</b> | <b>High</b> |
|------------------|------------|---------------|-------------|
| <b>Phosphate</b> | 0.9        | 1.2           | 1.6         |
| <b>Carbonate</b> | 30         | 35            | 40          |
| <b>Calcium</b>   | 2.1        | 2.5           | 2.8         |

**Table 3.** Buffering capacity and range for different solutions. Physiological concentrations of corresponding components (Table 2) were used for calculations. For the effect of bone, hydroxyapatite dissolution from 3 mm<sup>3</sup> of bone and requirement for hydroxyapatite formation for 0.4 mm<sup>3</sup> of bone, were accounted for.

| Buffering system                          | Buffering range | Buffering capacity (mM H <sup>+</sup> /pH) |
|---|-----------------|--|
| Phosphate buffer                          | 6.17 - 8.17     | 0.5  |
| Carbonate buffer                          | 5.25 - 7.25     | 14.9                                       |
| Phosphate and carbonate buffer            | 5.24 - 7.24     | 15.0                                       |
| Interstitial buffer                       | 5.40 - 7.40     | 14.7                                       |
| Interstitial buffer after bone resorption | 5.35 - 7.35     | 18.2                                       |
| Interstitial buffer after bone formation  | 5.40 - 7.40     | 14.3                                       |

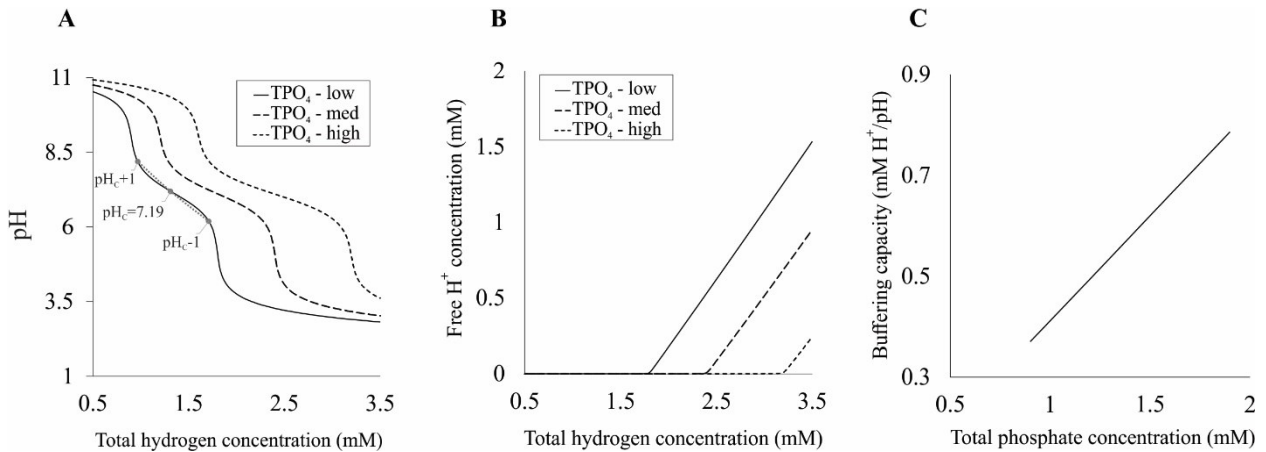


**Figure 2.** Characteristics of phosphate buffer. The model was reduced to phosphate only and included equations 1, 7-9, as well as relevant terms in equations 13-14, and 17-20. First, the level of total phosphate (TPO<sub>4</sub>) was specified, then total hydrogen (TH) was varied, and the equilibrium state was calculated in the model. A, B) Changes in pH (A) and free equilibrium hydrogen ion (B) as a function of total hydrogen (TH) for three levels of TPO<sub>4</sub>, low (0.9 mM, solid line), physiological (1.2 mM, dashed line), and high (1.6 mM, dotted line). The inflection point pH<sub>c</sub> corresponding to buffers pK<sub>a</sub> and the buffering range (pH<sub>c</sub> ± 1) are depicted on panel A. C) Changes in buffering capacity as a function of TPO<sub>4</sub>.

The carbonate buffer had a buffering capacity of 14.9 mM H<sup>+</sup>/pH, almost 30-fold higher than that of the phosphate buffer (**Fig. 3A**). When the two buffers were combined, the buffering properties of the solution were dominated by the carbonate buffer (**Fig. 3B, Table 3**). Nevertheless, adding increasing concentrations of phosphate to the carbonate buffer resulted in improved buffering capacity of the solution, although supraphysiological concentrations of PO<sub>4</sub><sup>3-</sup> (4 mM) were required for a noticeable effect (**Fig. 3C**). In all three cases, while increase in the concentrations of total phosphate and total carbonate resulted in increased buffering capacity, the buffering range was not considerably affected. Thus, the electrochemical buffering system of the bone interstitial fluid is dominated by the carbonate buffer, likely due to much higher physiological concentrations of total carbonate (30-40 mM) compared to total phosphate (1-2 mM) [17]. Nevertheless, the influence of phosphate buffer is evident at supraphysiological yet biologically observable concentrations of ~4 mM, which correspond to the levels observed in patients with hyperphosphatemia [17, 27].

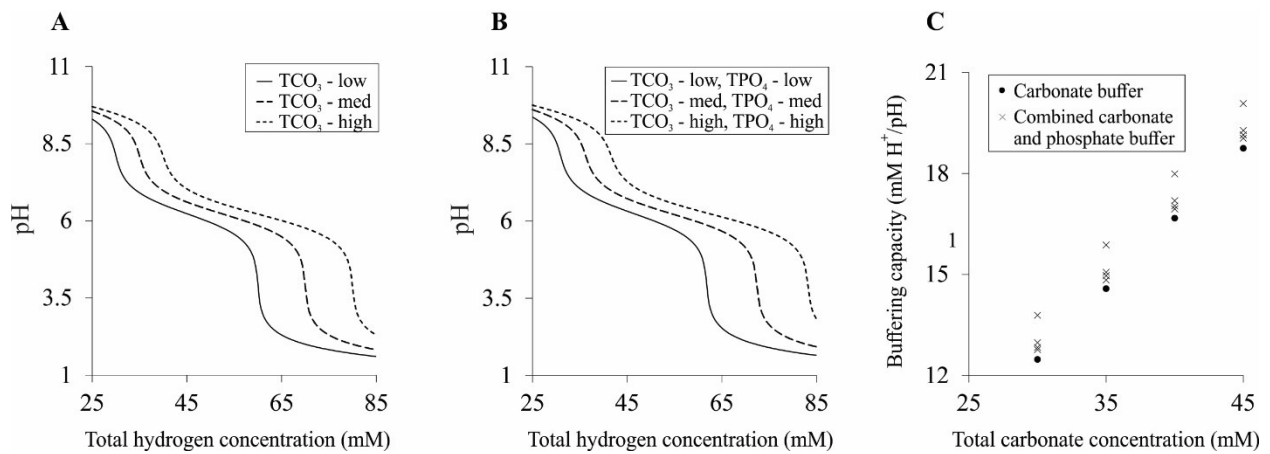


**Figure 3.** Characteristics of carbonate buffer and a combined carbonate/phosphate buffer.

A) The model was reduced to carbonate only and included equations 1, 10-11, and relevant terms in equations 13, 15, 17-20. The level of total carbonate (TCO<sub>3</sub>) was specified, then total hydrogen (TH) was varied, and the equilibrium pH was calculated. B, C) The model was reduced to carbonate and phosphate only and included equations 1, 7-11, and relevant terms in equations 13-15, and 17-20. The levels of total carbonate (TCO<sub>3</sub>) and total phosphate (TPO<sub>4</sub>) were specified, then total hydrogen (TH) was varied, and the equilibrium state was calculated. B) Changes in pH as a function of total hydrogen; C) Buffering capacity of carbonate buffer with TPO<sub>4</sub> = 0 (circles) or increasing TPO<sub>4</sub> (crosses) to the maximum concentration of 4 mM (top-most cross). For A and B: low: TCO<sub>3</sub>=30 mM, TPO<sub>4</sub>=0.9 mM, physiological (medium): TCO<sub>3</sub>=35 mM, TPO<sub>4</sub>=1.2 mM, high: TCO<sub>3</sub>= 40 mM, TPO<sub>4</sub>=1.6 mM.

### 3.2. Contribution of calcium to buffering system in the interstitial fluid

While calcium is not directly involved in buffering, it interacts with phosphate and carbonate species and thus may potentially affect the pH regulation. Therefore, we examined how addition of calcium species to the environment affects the buffering properties of the solution containing both phosphate and carbonate buffers. For total calcium values in the extremes and medium of the physiological range (**Table 2**), changes in equilibrium pH after total hydrogen (TH) was varied over a broad range of values were examined for the complete aqueous phase model (equations 1-20). Addition of calcium species decreased the buffering capacity and resulted in the shift of buffering range to higher values (from 5.24 - 7.24 to 5.40 - 7.40) (**Fig. 4B-dashed line, Table 3**).

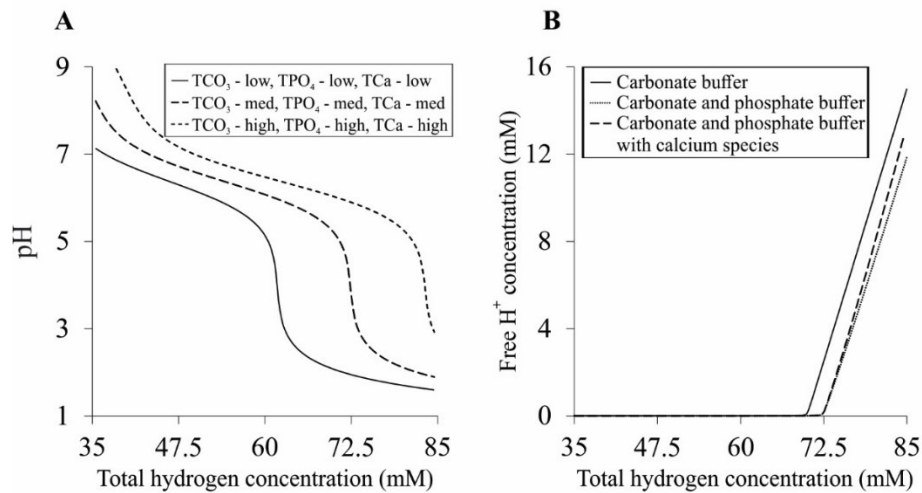


**Figure 4.** Characteristics of the interstitial fluid buffer. A) The levels of total phosphate (TPO<sub>4</sub>), total carbonate (TCO<sub>3</sub>), and total calcium (TCa), were specified, then total hydrogen (TH) was varied, and the equilibrium state was calculated using equations 1-20. Plotted are changes in pH as a function of added hydrogen (TH) for low (TCO<sub>3</sub>=30 mM, TPO<sub>4</sub>=0.9 mM, TCa=2.1 mM), physiological (TCO<sub>3</sub>=35 mM, TPO<sub>4</sub>=1.2 mM, TCa=2.5 mM), and high (TCO<sub>3</sub>=40 mM, TPO<sub>4</sub>=1.6 mM, TCa=2.8 mM) concentrations. B) Free equilibrium hydrogen as a function of TH for the physiological concentrations for carbonate buffer only (same as

dashed line on figure 3A), carbonate/phosphate buffer (same as dashed line on figure 3B), and carbonate/phosphate buffer plus calcium species (same as dashed line on figure 4A).

### **3.3. Contribution of hydroxyapatite dissolution to pH regulation in interstitial fluid**

Since bone consists of large amounts of hydroxyapatite,  $\text{Ca}_{10}(\text{PO}_4)_6(\text{OH})_2$ , its dissolution leads to addition of the corresponding chemical species, phosphate, calcium, and hydroxide, to interstitial fluid, which may affect its buffering properties. To study the potential effect of hydroxyapatite dissolution on pH regulation in interstitial fluid, we assumed that bone with a surface area of  $1 \mu\text{m}^2$  neighbors a unit volume of interstitial fluid (a cuboid with the thickness of  $3 \mu\text{m}$ ). The volume of actively dissolving bone was assumed to differ depending on the thickness. The dissolution of  $1 \text{ mm}^3$  of bone containing  $0.8\text{E}+9$  hydroxyapatite molecules/ $\text{mm}^3$  [12] is estimated to release 4.4, 2.7, and 0.9 mM of total calcium, total phosphate and total hydroxide respectively to the interstitial fluid. Assuming instantaneous transfer of minerals from bone to interstitial fluid, we defined the effect of bone dissolution as a change in the initial inputs of TH, TCa, and  $\text{TPO}_4$ , and examined the buffering properties of the resulting solution. Interstitial fluid buffering capacity noticeably increased after hydroxyapatite dissolution (**Table 3, Fig. 5A,B**) proportionally to amount of dissolved hydroxyapatite (**Fig. 5C**). To assess which of the hydroxyapatite components affect the interstitial fluid buffering capacity, we compared the effect of hydroxyapatite dissolution to individually adding phosphate, calcium or hydroxide to the interstitial fluid in amounts contained in the same volume of hydroxyapatite. While addition hydroxide did not considerably affect the interstitial fluid buffering capacity, addition of calcium and phosphate resulted in increase in buffering capacity. Addition of phosphate and calcium

together increased buffering capacity to approximately the same extent as hydroxyapatite dissolution (**Fig. 5D**). Thus, dissolution of hydroxyapatite present in bone can noticeably improve the buffering capacity of interstitial fluid solution. Our assumptions of immediate hydroxyapatite dissolution mostly reflect the cell-independent dissolution/precipitation of bone that is known to occur relatively fast [28, 29]. While the osteoclast-mediated bone resorption likely occurs much slower, at estimated 0.027 - 0.060 mm<sup>3</sup>/day [28], it is plausible that the resorbed hydroxyapatite and organic matrix is initially accumulated in the sealing zone underneath actively resorbing osteoclasts [30], and then instantaneously released in the environment when osteoclast moves to the new location. Taken together, we conclude that bone dissolution/resorption can participate in pH homeostasis by improving interstitial fluid buffering capacity.

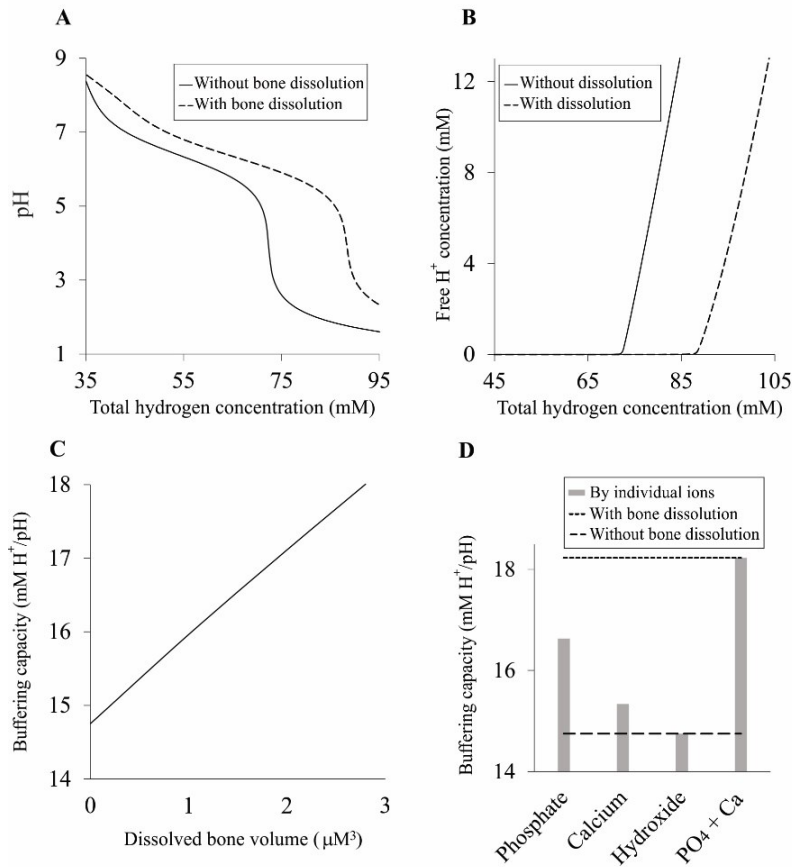


**Figure 5.** Contribution of hydroxyapatite dissolution to pH control in interstitial fluid. The levels of total phosphate (TPO<sub>4</sub>), total carbonate (TCO<sub>3</sub>), and total calcium (TCa), were specified as physiological (table 2) without or with the additions due to dissolution of hydroxyapatite contained in 1-3  $\mu m^3$  of bone adjacent to interstitial fluid, then the total hydrogen (TH) was varied, and the equilibrium state was calculated using equations 1-20. A, B) Changes in pH (A) and free equilibrium hydrogen (B) as a function of added hydrogen (TH) for an interstitial fluid without hydroxyapatite dissolution (solid line, same as Fig 4A), and the interstitial fluid after resorption of 3  $\mu m^3$  of bone into a 3  $\mu m^3$  volume of interstitial fluid (dashed line). C) Change in the buffering capacity of interstitial fluid due to dissolution of 0-3  $\mu m^3$  of bone. D) Buffering capacity of interstitial fluid without dissolution (dashed

line), with 3 mm<sup>3</sup> hydroxyapatite dissolution (dotted line) or after the addition of phosphate, calcium or hydroxide in amounts contained in 3 mm<sup>3</sup> of hydroxyapatite (grey bars).

### **3.4. Contribution of bone formation to pH regulation in interstitial fluid**

In contrast to resorption, bone formation would remove ions from interstitial fluid which will lead to decrease in phosphate and calcium concentrations and may potentially affect the buffering capacity of interstitial fluid. To study the potential effect of bone formation on pH regulation in interstitial fluid, we assumed that hydroxyapatite precipitates in the bone matrix along the surface area of 1  $\mu\text{m}^2$  adjacent to interstitial fluid. In this scenario, the amount of bone that can be formed instantaneously is limited by the amount of calcium and phosphate in the volume of interstitial fluid, which we estimated is sufficient to form up to 0.4-0.5 mm<sup>3</sup>. We defined the effect of hydroxyapatite precipitation as a change in the initial inputs of TH, TCa, and TPO<sub>4</sub>, and examine the buffering properties of the resulting solution. Interstitial fluid buffering capacity slightly decreased after hydroxyapatite precipitation in maximal amounts (**Table 3, Fig. 6 A,B**). We have found that the decrease in buffering capacity was proportional to the amount of hydroxyapatite precipitation (**Fig. 6C**). Investigation of which component of hydroxyapatite is responsible for the change in the buffering capacity demonstrated that removal of hydroxide did not considerably affect the interstitial fluid buffering capacity, while decrease in Ca and PO<sub>4</sub> resulted in a decrease in buffering capacity. The combined effect of decrease in calcium and phosphate decreased the buffering capacity to approximately the same extent as hydroxyapatite precipitation (**Fig. 6D**). These data indicate that the precipitation of hydroxyapatite does not strongly affect the buffering capacity of interstitial fluid due to the fact that hydroxyapatite precipitation is

limited by the amounts of chemical species immediately available in the adjacent volume of interstitial fluid. Moreover, since hydroxyapatite precipitation can only reduce the concentration of phosphate buffer, it can only reduce the buffering capacity to that of the carbonate buffer, which is almost 30 times stronger. While our assumption of instantaneous precipitation may appear contradictory to known slow rates of bone formation,  $\sim 0.5 \text{ mm}^3/\text{mm}^2/\text{day}$  [31], it is important to note that the limiting step of bone formation is deposition and maturation of extracellular matrix, while actual mineral precipitation occurs after the specific conditions are met and occurs at the physicochemical rates [12].

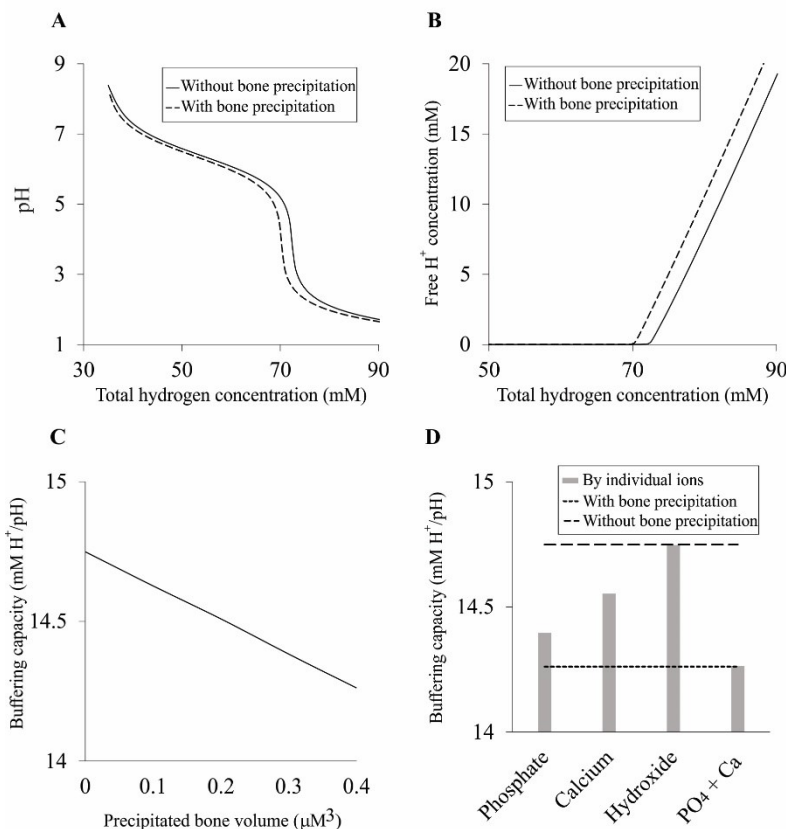


**Figure 6.** Contribution of hydroxyapatite precipitation to pH control in interstitial fluid. The levels of total phosphate (TPO4), total carbonate (TCO3), and total calcium (TCa), were

specified as physiological (table 2) without or with the reduction due to precipitation of hydroxyapatite in 0.1-0.4 mm<sup>3</sup> of bone adjacent to interstitial fluid, then the total hydrogen (TH) was varied, and the equilibrium state was calculated using equations 1-20. A, B) Changes in pH (A) and free equilibrium hydrogen (B) as a function of added hydrogen (TH) for an interstitial fluid without hydroxyapatite precipitation (solid line, same as Fig 4A), and the interstitial fluid after precipitation of 0.4 μm<sup>3</sup> of bone using chemical compounds from a 3 μm<sup>3</sup> volume of interstitial fluid (dashed line). C) Change in the buffering capacity of interstitial fluid due to formation of 0.1-0.4 mm<sup>3</sup> of bone. D) Buffering capacity of interstitial fluid without formation (solid line), after 0.4 mm<sup>3</sup> hydroxyapatite precipitation (dashed line) or after the removal of phosphate, calcium or hydroxide in amounts contained in 0.4 mm<sup>3</sup> of hydroxyapatite.

#### **4. Conclusions**

In this study we modeled the reactions occurring in the interstitial fluid adjacent to the bone surface and investigated the contribution of phosphate and carbonate buffers to regulation of pH, as well as a potential effects of the processes of bone resorption and formation on pH regulation in the interstitial fluid. We have demonstrated that while the electrochemical buffering system of the bone interstitial fluid is dominated by the carbonate buffer, the contributions of phosphate buffer cannot be discarded. In particular, during the process of precipitation and dissolution of hydroxyapatite of the bone tissue, changes in phosphate concentration in interstitial fluid due to its incorporation into or release from hydroxyapatite resulted in noticeable changes in interstitial fluid buffering capacity. While these changes

were relatively limited in case of bone formation, the dissolution of hydroxyapatite present in bone significantly improved the buffering capacity of interstitial fluid solution. Thus, this study provides mechanistic insights into the physicochemical processes underlying the known role of bone turnover in regulation of body pH homeostasis [5, 6], which can be validated in the future experimental studies. While to our knowledge, variation in pH of the interstitial fluid compartment in bone has not yet been characterized, it has been successfully studied in the soft tissues [2-4]. It can be anticipated that the development of novel methods, such as in vivo pH monitoring [32], will provide the opportunity to investigate the function of interstitial fluid in bone. Previous models of bone turnover [33-36] assumed unlimited reservoir producing or receiving hydroxyapatite components. The more detailed models of bone resorption [2] and formation [12] are now being developed, and together with the current study will help in developing a more precise theoretical description of elemental processes important for integration of bone turnover with other physiological functions of the organism.

### **CRedit authorship contribution statement**

Hossein Poorhemati: Data curation, Formal analysis, Investigation, Software, Visualization, Writing – original draft. Svetlana V. Komarova: Conceptualization, Funding acquisition, Supervision, Writing – review & editing.

### **Declaration of Competing Interest**

The authors declare that they have no known competing financial interests or personal relationships that could have appeared to influence the work reported in this paper.

## Acknowledgements

The operation of the supercomputer is funded by the Canada Foundation for Innovation (CFI), the ministère de l'Économie, de la science et de l'innovation du Québec (MESI) and the Fonds de recherche du Québec - Nature et technologies (FRQNT). The project is supported by the operating grant from Natural Sciences and Engineering Research Council of Canada (NSERC, [RGPIN-288253](#)).

## Data Availability

The code describing implementation of current bone aqueous phase model in MATLAB is available on github: [https://github.com/Hosseinpoorhemati/Bone\\_aqueous\\_phase.git](https://github.com/Hosseinpoorhemati/Bone_aqueous_phase.git).

## References

1. Burggren, W. and N. Bautista, *Invited review: Development of acid-base regulation in vertebrates*. Comparative Biochemistry and Physiology a-Molecular & Integrative Physiology, 2019. **236**.
2. Marunaka, Y., *Roles of interstitial fluid pH and weak organic acids in development and amelioration of insulin resistance*. Biochemical Society Transactions, 2021. **49**(2): p. 715-726.
3. Kolosenko, I., et al. *Therapeutic implications of tumor interstitial acidification*. in *Seminars in Cancer Biology*. 2017. Elsevier.
4. Juel, C., *Changes in interstitial K<sup>+</sup> and pH during exercise: implications for blood flow regulation*. Applied Physiology, Nutrition, and Metabolism, 2007. **32**(5): p. 846-851.
5. Arnett, T.R. *Acid-base regulation of bone metabolism*. in *International Congress Series*. 2007. Elsevier.
6. Bushinsky, D.A., *Acid-base imbalance and the skeleton*. Eur J Nutr, 2001. **40**(5): p. 238-44.
7. Seifter, J.L. and H.Y. Chang, *Extracellular Acid-Base Balance and Ion Transport Between Body Fluid Compartments*. Physiology (Bethesda), 2017. **32**(5): p. 367-379.
8. Ren, L., et al., *Biomechanical and biophysical environment of bone from the macroscopic to the pericellular and molecular level*. J Mech Behav Biomed Mater, 2015. **50**: p. 104-22.

9. Ostapienko, B.I., D. Lopez, and S.V. Komarova, *Mathematical modeling of calcium phosphate precipitation in biologically relevant systems: scoping review*. Biomech Model Mechanobiol, 2019. **18**(2): p. 277-289.
10. Oyane, A., et al., *Preparation and assessment of revised simulated body fluids*. Journal of Biomedical Materials Research Part A: An Official Journal of The Society for Biomaterials, The Japanese Society for Biomaterials, and The Australian Society for Biomaterials and the Korean Society for Biomaterials, 2003. **65**(2): p. 188-195.
11. Barat, R., et al., *Modelling biological and chemically induced precipitation of calcium phosphate in enhanced biological phosphorus removal systems*. Water Res, 2011. **45**(12): p. 3744-52.
12. Komarova, S.V., et al., *Mathematical model for bone mineralization*. Front Cell Dev Biol, 2015. **3**: p. 51.
13. Harned, H.S., B.B. Owen, and C. King, *The physical chemistry of electrolytic solutions*. Journal of The Electrochemical Society, 1959. **106**(1): p. 15C.
14. Koutsoukos, P. and G. Nancollas, *Crystal growth of calcium phosphates-epitaxial considerations*. Journal of crystal growth, 1981. **53**(1): p. 10-19.
15. Chughtai, A.R., R. Marshall, and G.H. Nancollas, *Complexes in calcium phosphate solutions*. The Journal of physical chemistry, 1968. **72**(1): p. 208-211.
16. Sillen, L.G., A.E. Martell, and J. Bjerrum, *Stability constants of metal-ion complexes*. 1964, Chemical Society: London.
17. McKee, T.J. and S.V. Komarova, *Is it time to reinvent basic cell culture medium?* Am J Physiol Cell Physiol, 2017. **312**(5): p. C624-C626.
18. Goldstein, D.A., *Serum Calcium*, in *Clinical Methods: The History, Physical, and Laboratory Examinations*, rd, et al., Editors. 1990: Boston.
19. Skoog, D.A., et al., *Fundamentals of analytical chemistry*. 2013: Nelson Education.
20. Forsen, S. and J. Kordel, *Calcium in biological systems*. 1994, University Science Books: Mill Valley, CA. p. 107.
21. C, D., *Ion associations*. 1st edn ed. 1962: Butterworths, London.
22. Huckel, E. and P. Debye, *Zur theorie der elektrolyte. i. gefrierpunkterniedrigung und verwandte erscheinungen*. Phys. Z, 1923. **24**: p. 185-206.
23. Drake, F., G. Pierce, and M. Dow, *Measurement of the dielectric constant and index of refraction of water and aqueous solutions of KCl at high frequencies*. Physical Review, 1930. **35**(6): p. 613.
24. Wyman Jr, J., *Measurements of the dielectric constants of conducting media*. Physical Review, 1930. **35**(6): p. 623.
25. Morel, F. and J. Morgan, *A Numerical Method for Computing Equilibria in Aqueous Chemical Systems Environmental Science & Technology*. 1972.
26. Carrayrou, J., R. Mose, and P. Behra, *New efficient algorithm for solving thermodynamic chemistry*. Aiche Journal, 2002. **48**(4): p. 894-904.
27. Mozar, A., et al., *High extracellular inorganic phosphate concentration inhibits RANK–RANKL signaling in osteoclast-like cells*. Journal of cellular physiology, 2008. **215**(1): p. 47-54.
28. Parfitt, A., *Misconceptions (3): calcium leaves bone only by resorption and enters only by formation*. Bone (New York, NY), 2003. **33**(3): p. 259-263.

29. Dedic, C., et al., *Calcium fluxes at the bone/plasma interface: Acute effects of parathyroid hormone (PTH) and targeted deletion of PTH/PTH-related peptide (PTHrP) receptor in the osteocytes*. *Bone*, 2018. **116**: p. 135-143.
30. Blangy, A., et al., *The osteoclast cytoskeleton—current understanding and therapeutic perspectives for osteoporosis*. *Journal of Cell Science*, 2020. **133**(13).
31. Parfitt, A.M., et al., *Structural and cellular changes during bone growth in healthy children*. *Bone*, 2000. **27**(4): p. 487-94.
32. Li, Y., et al., *FITC-labeled alendronate as an in vivo bone pH sensor*. *BioMed research international*, 2020. **2020**.
33. Komarova, S.V., et al., *Mathematical model predicts a critical role for osteoclast autocrine regulation in the control of bone remodeling*. *Bone*, 2003. **33**(2): p. 206-215.
34. Lemaire, V., et al., *Modeling the interactions between osteoblast and osteoclast activities in bone remodeling*. *Journal of theoretical biology*, 2004. **229**(3): p. 293-309.
35. Lerebours, C., et al., *A multiscale mechanobiological model of bone remodelling predicts site-specific bone loss in the femur during osteoporosis and mechanical disuse*. *Biomechanics and modeling in mechanobiology*, 2016. **15**(1): p. 43-67.
36. Ryser, M.D. and K.A. Murgas, *Bone remodeling as a spatial evolutionary game*. *Journal of theoretical biology*, 2017. **418**: p. 16-26.

## **Bridging chapter 3 and 4**

As described in the introduction of this thesis, one of the objectives of my research was to simulate bone microenvironment permissive to hydroxyapatite precipitation. This required understanding the chemical reactions governing the environment. In chapter 3, a preliminary environment was simulated assuming the environment is a solution of specific ions of major importance in defining the observed characteristics of bone interstitial fluid which keep reacting until an equilibrium is achieved following any perturbation. This model was used to investigate particularly two objectives. First, considering the known effect of acid-base balance on bones, given the physiological concentration of relevant ions the model provided insights on how the environment behaved, which buffer dominated, and whether there was any influence of abnormal concentrations of specific ions on the buffering behavior of the system. Secondly, it was used to investigate if a more detailed description of the environment was needed, i.e. if inclusion of more ions and chemical species were required before introducing the precipitation kinetics into the system.

Building on the findings of chapter 3, in chapter 4 a modified description of the bone interstitial fluid is presented. The new model not only includes more ions and chemical components, but also accommodates hydroxyapatite precipitation backed up by empirical equations of hydroxyapatite precipitation at physiological pH and performs the operation much faster. In this work the implementation of systemic pH as a separate component of the model provides a more straightforward way to investigate the impact of chronic abnormal pH levels on physical chemistry of hydroxyapatite precipitation in bone, which was not an option in the initial model presented in chapter 3.

**Chapter 4. Mathematical model of physicochemical regulation of precipitation of bone hydroxyapatite**

**Mathematical model of physicochemical regulation of precipitation of bone hydroxyapatite**

**Hossein Poorhemati<sup>1,2</sup>, Svetlana Komarova<sup>1,2,3\*</sup>**

<sup>1</sup>Department of Biological and Biomedical Engineering, McGill University, Canada

<sup>2</sup>Shriners Hospital for Children, Montreal, QC, Canada McGill University

<sup>3</sup>Faculty of Dental Medicine and Oral Health Sciences, McGill University, Canada

**\* Correspondence:**

Svetlana V. Komarova

[svetlana.komarova@mcgill.ca](mailto:svetlana.komarova@mcgill.ca)

**Keywords:** Bone, Mineralization, Mathematical Modeling, Physiochemistry, Hydroxyapatite

## **Abstract**

Formation of hydroxyapatite in bone, dentin and enamel occurs at restricted molecular sites of specific extracellular matrix proteins and is controlled by multiple mineralization inhibitors. However, the role of physicochemical factors, such as the availability of required ions and the saturation status of the aqueous environment in biological mineralization, is not fully understood. The goal of this study was to use mathematical modelling to describe the complex physicochemical environment permissive to the precipitation of biological hydroxyapatite. We simulated the processes occurring in the bone interstitial fluid (ISF) defined as an aqueous environment containing seven chemical components (calcium, phosphate, carbonate, sodium, potassium, magnesium, and chloride) that form 30 chemical species. We simulated reversible equilibrium reactions among these chemical species, and calculated supersaturation for hydroxyapatite and its precipitation rate using kinetic theory. The simulated ISF was of correct ionic strength and predicted the equilibrium component concentrations that were consistent with the experimental findings. Supersaturation of physiological ISF was  $\sim 16$ , which is consistent with prior findings that mineralization inhibitors are required to prevent spontaneous mineral precipitation. Only total calcium, total phosphate and to a lesser degree total carbonate affected ion availability, solution supersaturation and hydroxyapatite precipitation rate. Both calcium and phosphate levels directly affected hydroxyapatite precipitation, and phosphate was affected by pH, which additionally influenced hydroxyapatite precipitation. Integrating mathematical models capturing the physiochemical and biological factors regulating bone mineralization will allow in silico studies of complex clinical scenarios associated with alterations in ISF ion composition, such as rickets, hypophosphatemia, and chronic kidney disease.

## 1. Introduction

Bone is a biological composite material including three different phases, a mineral phase, an organic phase, and water [1]. The mature bone mineral phase is made up of nanosized crystalline hydroxyapatite (HAP) with chemical formula of  $\text{Ca}_{10}(\text{PO}_4)_6(\text{OH})_2$  [1]. The mineral phase of bone provides a strong structure for the mechanical resistance for the tissue [2], and an abundant number of ions (particularly calcium and phosphate) for whole body homeostasis [3]. The organic phase of the bone consists of almost 90% type I collagen, 5% non-collagenous proteins (NCPs), and 2% lipids by weight [1]. Finally, the aqueous phase is responsible for cell and matrix nutrition, mediating interactions between collagen fibrils and minerals, and controlling ion flux [3]. Bone formation starts with deposition of organic matrix by osteoblasts, which happens at a much faster rate than bone mineralization [4]. The unmineralized bone matrix, osteoid, is mineralized through physicochemical processes regulated by the presence of nucleation centers that can be provided by matrix vesicles [5] and can arise with the maturation of extracellular matrix [6], and the concentrations of mineralization inhibitors produced by osteoblasts or present in the circulation. Thus, complex biological and physicochemical phenomena are involved in regulating hydroxyapatite mineralization.

Mathematical models provide a deeper understanding of how different components interact and influence each other in complex environments [7]. We have previously modeled the role of biological factors in bone mineralization [8], and have examined a simplified model of pH regulation in bone microenvironment [9]. Building on the concept of simulated interstitial fluid (ISF) introduced in the previous work [9], in the current study, we aimed to develop a mathematical model describing the complex physicochemical environment permissive to

the precipitation of biological hydroxyapatite. The aqueous environment of ISF was defined to contain seven commonly reported chemical components (calcium, phosphate, carbonate, sodium, potassium, magnesium, and chloride) that form 30 chemical species. Computing the outcomes of reversible equilibrium reactions among these chemical species allowed us to calculate solution supersaturation for HAP and assess HAP precipitation rate using kinetic theory.

## **2. Model Development and Simulations**

### **2.1. Model assumptions**

In this study, we have simulated the processes occurring in the interstitial fluid (ISF) in the bone vicinity. It is assumed that the environment is homogenous, and ions are immediately distributed evenly in the environment. The following assumptions regarding the biological components of the system were made: 1) the effects of biological factors on equilibrium reactions in ISF are minimal; 2) the presence of biological inhibitors of mineralization increases the precipitation threshold [10]; 3) the nucleation of biological mineral is controlled by biological processes [11], and physicochemical aspects are involved in crystal growth. Efforts have been made to keep the model working with the minimum number of components and complexity while ensuring the predictions are reliable and close enough to the actual processes happening in the body.

Figure 1 provides a map of the model, its different compartments, and the flow of data in the model. A detailed description of how the model is constructed is provided in the following sections.

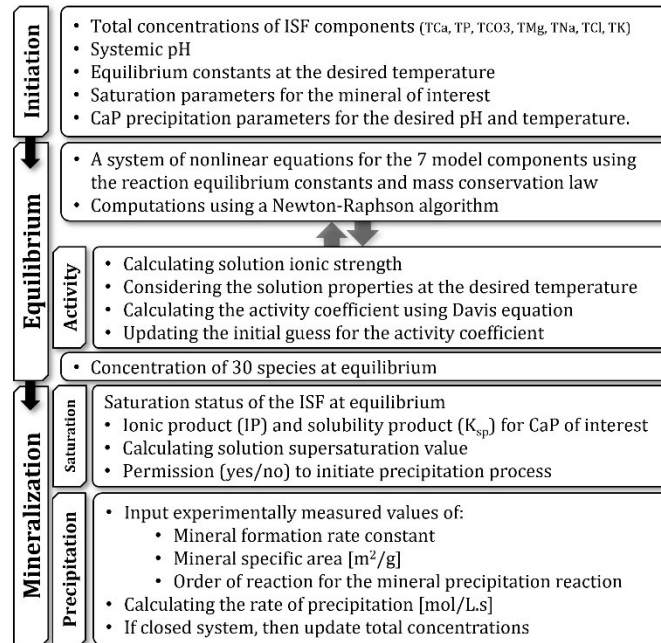


**Figure 1** Schematic representation of the model and its different compartments and their functions. Arrows show the flow of data between compartments

## 2.2. Simulated ISF

Previously, we developed the model of the ISF reactions that focused on four components involved in pH regulation, calcium ( $\text{Ca}^{2+}$ ), phosphate ( $\text{PO}_4^{3-}$ ), carbonate ( $\text{CO}_3^{2-}$ ), and hydrogen( $\text{H}^+$ ) [9]. However, the ionic strength of the solution containing four components is 0.017, which is notably lower than 0.15-0.16 reported experimentally [12]. Since ionic strength directly affects the calculation of activity coefficients and thus the equilibrium concentrations, to improve model precision, we included the additional chemical components and examined how their inclusion affected the ionic strength of the ISF (**Table 1**). The resulting ISF was defined as a solution containing seven major components: calcium

( $Ca^{2+}$ ), phosphate ( $PO_4^{3-}$ ), carbonate ( $CO_3^{2-}$ ), sodium ( $Na^+$ ), chloride ( $Cl^-$ ), magnesium ( $Mg^{2+}$ ), and potassium ( $K^+$ ) (**Table 1**). These components interact through reversible reactions forming 22 different chemical species listed here:  $H_3PO_4$ ,  $H_2PO_4^-$ ,  $HPO_4^{2-}$ ,  $H_2CO_3(aq)$ ,  $HCO_3^-$ ,  $CaHCO_3^+$ ,  $CaCO_3(aq)$ ,  $CaOH^+$ ,  $CaH_2PO_4^+$ ,  $CaHPO_4(aq)$ ,  $CaPO_4^-$ ,  $NaHPO_4^-$ ,  $NaH_2PO_4(aq)$ ,  $MgHCO_3^+$ ,  $MgCO_3(aq)$ ,  $MgOH^+$ ,  $MgH_2PO_4^+$ ,  $MgHPO_4(aq)$ ,  $MgPO_4^-$ ,  $NaCl$ ,  $KHPO_4^-$ ,  $OH^-$ . The equilibrium constants for the 22 reactions were obtained from experimental studies; where reported, we used the value at the body temperature of 37 °C (**Table 2**). Seven equations for the principle of mass conservation for total amounts of calcium (TCa), phosphate (TPO<sub>4</sub>), carbonate (TCO<sub>3</sub>), magnesium (TMg), sodium (TNa), potassium (TK), and chloride (TCl) in addition to pH value completed the description of ISF (**Table 2**). The total amounts of these components were matched to those reported in human plasma [12](**Table 1**). The ISF is an ionic solution which requires the inclusion of activity coefficients in calculating its equilibrium concentrations. Ionic strength of a solution is defined as:

$$I = \frac{1}{2} \sum_{i=1}^n c_i \cdot z_i^2 \quad (1)$$

where  $c_i$  is the molar concentration of ion  $i$ ,  $z_i$  is its valence, and  $n$  is the number of different ions in the solution. The activity coefficients were calculated as follows:

$$\log \gamma_i = -Az_i^2 \left( \frac{\sqrt{I}}{(1+\sqrt{I})} - 0.3I \right) \quad (2)$$

$\gamma_i$  is the activity coefficient of ion  $i$ , which depends on ionic strength  $I$  of the solution, ion valence  $z_i$ , and temperature and the dielectric constant of the solvent expressed in parameter  $A$ . This parameter was previously approximated [13] for a solution with water as the solvent as:

$$A = 0.486 + 6.07 \times 10^{-4}T_c + 6.43 \times 10^{-6}T_c^2 \quad (3)$$

where  $T_c$  is temperature in Celsius (37 °C in this study). Equation 2 is only valid for  $I \leq 0.5$  M [14], which is applicable in this case (**Table 1**). Finally, equilibrium concentrations are calculated as:

$$Q_i = c_i \cdot \gamma_i \quad (4)$$

where  $Q_i$ , the corrected concentration is a product of nominal concentration  $c_i$  of each ion and its activity coefficient  $\gamma_i$ .

**Table 1** Model components and their effect on the ionic strength of the solution. Reported are solution components in their ionic forms, nomenclature for their total concentrations, physiological total plasma concentrations and ionic strength of the solution following the inclusion of the specific component from top to down of the list. The reported ionic strength of human plasma is 0.15-0.16 [12]. Systemic pH was set to 7.4

| <b>Solution components</b> | <b>Total concentration</b> | <b>Physiological concentration (mM)</b> | <b>Solution ionic strength</b> |
|----------------------------|----------------------------|---|--------------------------------|
| $CO_3^{2-}$                | TCO <sub>3</sub>           | 27                                      | 0.017                          |
| $PO_4^{3-}$                | TPO <sub>4</sub>           | 1.0                                     |                                |
| $Ca^{2+}$                  | TCa                        | 1.6                                     |                                |
| $Na^+$                     | TNa                        | 142                                     | 0.089                          |
| $Cl^-$                     | TCl                        | 103                                     | 0.140                          |

|           |     |   |       |
|-----------|-----|---|-------|
| $K^+$     | TK  | 5 | 0.143 |
| $Mg^{2+}$ | TMg | 1 | 0.145 |

For the calculation of the equilibrium concentrations a system of non-linear equation had to be formed and solved. Using the reaction rate law and equilibrium constants for the 22 reactions (**Table 2**), one equation from pH definition, in addition of 7 equations derived from mass conservation law for total concentration of calcium (TCa), phosphate (TPO<sub>4</sub>), carbonate (TCO<sub>3</sub>), magnesium (TMg), sodium (TNa), potassium (TK), chloride (TCl), and hydrogen (TH), a system of 30 equations was formed. Using the definition of equilibrium constants, the system was later simplified to a system of 7 nonlinear equations with 7 variables (the components of in Table 1). The system of equation was solved for these 7 variables and the rest of chemical species were later calculated by reversing the simplifying step using equilibrium constants.

**Table 2** ISF Reactions and their equilibrium constants

| Reaction  | Equilibrium constants | Reference |
|---|-----------------------|-----------|
| $H_2CO_3(aq) \rightleftharpoons 2H^+ + CO_3^{2-}$ | $10^{-6.31}$          | [15]      |
| $HCO_3^- \rightleftharpoons H^+ + CO_3^{2-}$      | $10^{-10.25}$         | [15]      |
| $H_3PO_4 \rightleftharpoons H^+ + H_2PO_4^-$      | $10^{-2.196}$         | [15]      |
| $H_2PO_4^- \rightleftharpoons H^+ + HPO_4^{2-}$   | $10^{-7.185}$         | [15]      |
| $HPO_4^{2-} \rightleftharpoons H^+ + PO_4^{3-}$   | $10^{-12.19}$         | [15]      |
| $Ca^{2+} + HCO_3^- \rightleftharpoons CaHCO_3^+$  | $10^{1.16}$           | [15]      |

|   |                       |      |
|---|-----------------------|------|
| $\text{Ca}^{2+} + \text{CO}_3^{2-} \rightleftharpoons \text{CaCO}_3(\text{aq})$               | $10^{3.38}$           | [15] |
| $\text{Ca}^{2+} + \text{OH}^- \rightleftharpoons \text{CaOH}^+$                               | 25.12                 | [16] |
| $\text{Ca}^{2+} + \text{H}_2\text{PO}_4^- \rightleftharpoons \text{CaH}_2\text{PO}_4^+$       | 31.9                  | [17] |
| $\text{Ca}^{2+} + \text{HPO}_4^{2-} \rightleftharpoons \text{CaHPO}_4(\text{aq})$             | $6.81 \times 10^2$    | [17] |
| $\text{Ca}^{2+} + \text{PO}_4^{3-} \rightleftharpoons \text{CaPO}_4^-$                        | $3.46 \times 10^6$    | [17] |
| $\text{Mg}^{2+} + \text{HCO}_3^- \rightleftharpoons \text{MgHCO}_3^+$                         | $10^{0.62}$           | [18] |
| $\text{Mg}^{2+} + \text{CO}_3^{2-} \rightleftharpoons \text{MgCO}_3(\text{aq})$               | $10^{1.87}$           | [18] |
| $\text{Mg}^{2+} + \text{OH}^- \rightleftharpoons \text{MgOH}^+$                               | $10^{2.19}$           | [18] |
| $\text{Mg}^{2+} + \text{H}_2\text{PO}_4^- \rightleftharpoons \text{MgH}_2\text{PO}_4^+$       | $10^{0.4}$            | [19] |
| $\text{Mg}^{2+} + \text{HPO}_4^{2-} \rightleftharpoons \text{MgHPO}_4(\text{aq})$             | $10^{1.8}$            | [19] |
| $\text{Mg}^{2+} + \text{PO}_4^{3-} \rightleftharpoons \text{MgPO}_4^-$                        | $10^{3.3}$            | [19] |
| $\text{Na}^+ + \text{HPO}_4^{2-} \rightleftharpoons \text{NaHPO}_4^-$                         | 0.21                  | [14] |
| $\text{Na}^+ + \text{H}_2\text{PO}_4^- \rightleftharpoons \text{NaH}_2\text{PO}_4(\text{aq})$ | $10^{-6.82}$          | [20] |
| $\text{Na}^+ + \text{Cl}^- \rightleftharpoons \text{NaCl}(\text{aq})$                         | $3.41 \times 10^{-2}$ | [21] |
| $\text{K}^+ + \text{HPO}_4^{2-} \rightleftharpoons \text{KHPO}_4^-$                           | 2.5                   | [22] |
| $\text{H}_2\text{O} \rightleftharpoons \text{H}^+ + \text{OH}^-$                              | $10^{-14}$            | [23] |

### 2.3. Saturation

The simulated ISF includes the possibility of mineral formation. Physiochemically speaking, mineral formation requires the solution to be at a supersaturated state, meaning that there must be more solute available than the amount that can be dissolved in the solvent at a defined physical condition (temperature and pressure). To investigate the state of

saturation, the minerals of interest must be known. Although there have been many studies on the formation of intermediate calcium phosphate precipitates prior to or simultaneous with the formation of hydroxyapatite [24], in the current model we did not take into account the intermediate precipitates and their gradual transition into the stable hydroxyapatite form. In this study we assumed that hydroxyapatite with the chemical formula of  $Ca_{10}(PO_4)_6(OH)_2$  is the only form of mineral that could be formed. With that, to investigate the state of saturation we calculated supersaturation using the following equation:

$$S = (IP/K_{SP})^{1/9} \quad (5)$$

S in equation 5 is the solution supersaturation which depends on the ionic product and the solubility product of hydroxyapatite. Ionic product is calculated as:

$$IP = (C_{Ca} \times \gamma_{Ca})^5 (C_{PO_4} \times \gamma_{PO_4})^3 (C_{OH} \times \gamma_{OH})^1 \quad (6)$$

where C and  $\gamma$  stand for the equilibrium concentration and the activity coefficient for each ion in the mineral structure. Solubility product,  $K_{SP}$ , is the equilibrium constant for a chemical reaction in which a solid ionic compound dissolves to yield its ions and is measured experimentally.  $K_{SP}$  for hydroxyapatite at 37°C is reported  $2.03 \times 10^{-59} \text{ mol}^9/\text{l}^9$  [12]. For other precipitates, we used the following  $K_{SP}$ : brushite (DCPD)  $10^{-7}$  [25], octacalcium phosphate (OCP)  $1.05 \times 10^{-47}$  [26],  $\beta$ -tricalcium phosphate (TCP)  $2.83 \times 10^{-30}$  [27], and calcium carbonate ( $CaCO_3$ )  $3.36 \times 10^{-9}$  [28]. Supersaturation, S, greater than one in a solution indicates a supersaturated state where mineral precipitation occurs until  $S = 1$  (or  $IP = K_{SP}$ ) and the system rests at equilibrium. In a biological system like the human body, availability of mineralization inhibitors can affect this behavior. For example, this threshold at human urine is estimated at  $\sim 10$  [29], while for human plasma it is calculated in the range

of 1.5 to 13 [12, 14]. The difference in the reported values comes also from the fact that different studies considered different values for plasma concentrations and did the calculations with different levels of simplification. In the current study, supersaturation  $S$  was calculated at 14.9 for the concentrations introduced at **Table 1**.

It is worth noting here that different studies report the saturation state of the solution using slightly different methods, although they are all addressing the same phenomenon. Some studies use solution supersaturation defined as  $(IP/K_{SP})^{1/\vartheta}$ , where  $\vartheta$  is the sum of stoichiometric coefficients of cations and anions involved in the mineral, some other use the saturation index defined as  $\log(IP/K_{SP})$ , and in some cases, they just looked at the saturation ratio defined by  $IP/K_{SP}$ . It is obvious that the interpretation of the values calculated differs depending on the method used, for example while solution supersaturation of 1 means the solution is in equilibrium, the saturation index of value of 0 means the same state. In this study we used the solution supersaturation method.

#### **2.4. Mineral precipitation**

A supersaturated solution proceeds with mineral precipitation. Calcium phosphates and among them biologically important ones like hydroxyapatite have been studied over the years and different theoretical and experimental studies tried to address their rate of precipitation [30, 31]. In the current study, we relied on experimental study of hydroxyapatite precipitation rate at a solution with pH 7.4 to 8.4 [30] considering human physiology. The precipitation rate equation was reported as:

$$R = k_f s \gamma_2 \gamma_3 [Ca^{2+}] [PO_4^{3-}] \quad (7)$$

where  $R$  is rate of hydroxyapatite precipitation ( $\text{mol HAP L}^{-1}\text{s}^{-1}$ ),  $k_f$  is the rate constant ( $\text{L}^2\text{mol}^{-1}\text{m}^{-2}\text{s}^{-1}$ ),  $s$  is surface area ( $\text{m}^2\text{L}^{-1}$ ),  $\gamma_2$  and  $\gamma_3$  are the divalent and trivalent activity coefficients, and brackets are the concentrations of  $\text{Ca}^{2+}$  and  $\text{PO}_4^{3-}$  ( $\text{mol L}^{-1}$ ).

## 2.5. Model simulation and analysis (Numerical solution)

Due to the high level of non-linearity and large number of variables, the Newton-Raphson (NR) method was used to solve the system of equations.

To avoid divergence in the NR solver, as proposed by Morel and Morgan [32], in cases that  $[X_j]^n + \Delta X_j^n < 0$ , the next iteration would be calculated using  $[X_j]^{n+1} = \frac{[X_j]^n}{10}$ . The initial guess of equal concentrations and equal activity coefficients of 0.5 was made to initiate solving the system. During an iterative process, the calculated concentrations and coefficients of each iteration were used to initiate the next iteration of calculations. This iterative process was repeated to the point where the maximum difference between the last two iterative values of activity coefficients were smaller than an arbitrary value of  $\varepsilon_{act} = 10^{-8}$ . At this point, the equilibrium concentrations of all chemical species in the solution were calculated.

## 3. Results

We investigated how the changes in total concentrations of 7 model components, TCa, TPO4, TCO3, TMg, TNa, TK, TCl (**Table 1**), affect ISF composition, hydroxyapatite saturation and hydroxyapatite precipitation. We explored the range of changes corresponding to

physiologically reported mild and severe decreases and increases in individual components (**Table 3**). In addition, we studied the effect of physiological variation in systemic pH from pH7.3 to pH7.55 [33] on ions distribution.

**Table 3** physiological and pathophysiological levels of total calcium, total phosphate, total carbonate, and systemic pH

|                              | <b>Normal<br/>(mM)</b> | <b>Reference</b> | <b>Hypo<br/>(mM)</b>                                | <b>Reference</b> | <b>Hyper<br/>(mM)</b>                           | <b>Reference</b> |
|------------------------------|------------------------|------------------|---|------------------|---|------------------|
| <b>Ionized calcium</b>       | 1-1.4                  | [34]             | Mild: > 0.8<br>Sever: <0.62                         | [35]             | Mild: 1.4 - 2 -<br>Mod: 2- 2.5<br>Severe: 2.5-3 | [34]             |
| <b>Inorganic phosphorous</b> | 0.8 - 1.45             | [36]             | Mild: 0.65 - 0.8<br>Mod: 0.32-0.65<br>Severe: <0.32 | [36]             | Mild to mod: >1.45<br>Severe: >2                | [36]             |
| <b>Carbonate</b>             | 22-28                  | [37]             | Mild: 18- 21  | [37]             | Mild: 28- 32                                    | [37]             |

|  |  |  |                                  |  |                                   |  |
|--|--|--|----------------------------------|--|-----------------------------------|--|
|  |  |  | Mod: 10-<br>17<br>Severe:<br><10 |  | Mod: 32-<br>36<br>Severe: ><br>36 |  |
|--|--|--|----------------------------------|--|-----------------------------------|--|

### 3.1. Distribution of ions

We focused on the effect of total concentrations of individual components on the concentrations of ions relevant to hydroxyapatite precipitation, i.e.,  $Ca^{2+}$  and  $PO_4^{3-}$  (**Fig. 2**). Changes in TCa positively correlated with ionized calcium concentration (**Fig. 2A**) and negatively correlated with ionized phosphate level (**Fig. 2B**), although the effect of TCa on  $PO_4^{3-}$  was less prominent than on  $Ca^{2+}$ . The  $TPO_4$  positively correlated with ionized phosphate concentration and negatively correlated with ionized calcium and had a stronger effect on ionized phosphate (**Fig. 2C,D**). Changes in total concentrations of other components in the model had minimal effect on ionized calcium and phosphate with the exception of carbonate that demonstrated negative association with ionized calcium and no association with ionized phosphate (**Fig. 2E,F**). The effect of systemic pH was negligible for the ionized calcium, while ionized phosphate level was considerably influenced by pH level (**Fig. 2**).

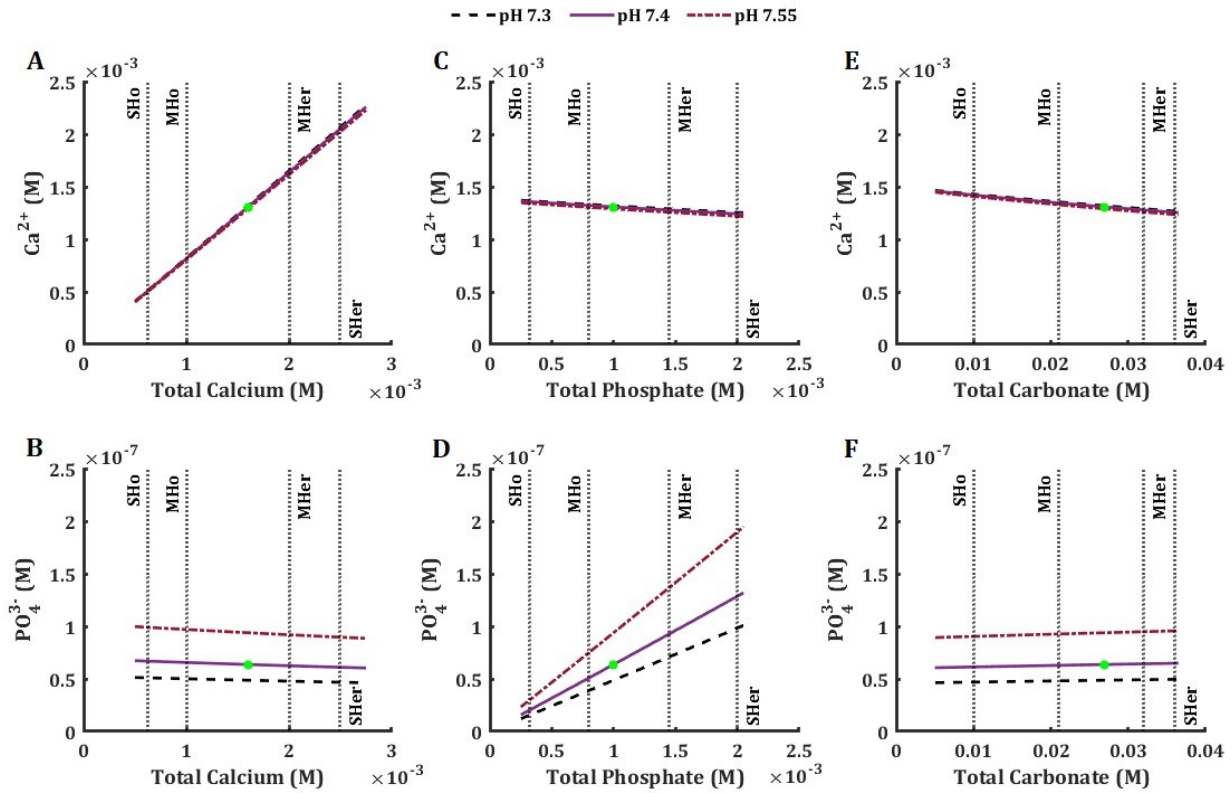


**Figure 2** Effect of physiological and pathophysiological total concentration of calcium (A,B), phosphate (B,D), and carbonate (E,F) on the equilibrium concentration of ionized calcium (A,C,E), and ionized phosphate (B,D,E) at physiological pH7.4 (solid line), low pH 7.3 (dashed line) and high pH 7.55 (dashed-dotted line). The vertical lines are the mild and severe levels for low and high total concentrations (**Table 3**)

### 3.2. Saturation

We next examined how total concentrations of individual components affect hydroxyapatite solution supersaturation (equation 5). Solution supersaturation for HAP at the physiological levels of ions was 16.4, which is consistent with previously reported values [12, 38] and demonstrates that the action of mineralization inhibitors is critical for preventing

precipitation in biological fluids [6]. The HAP solution supersaturation was positively associated with the levels of total calcium (**Fig. 3A**) and total phosphate (**Fig. 3B**). It was also mildly affected by total carbonate (negative association) (**Fig. 3C**), but not by any other model components. Mild and severe hypercalcemia and hyperphosphatemia showed a similar effect in increasing the HAP solution supersaturation. Mild and severe hypocalcemia and hypophosphatemia lead to a decrease in HAP solution supersaturation, with total calcium having a more prominent effect (**Table 4**). We also considered the solution supersaturation for other mineral species, including DCPD, OCP, TCP and CaCO<sub>3</sub> (**Fig. 3D-F**). For all these components the level of solution supersaturation was lower than that of HAP, and for DCPD specifically, it was below 1 in the physiological ranges of total calcium, phosphate, and carbonate.

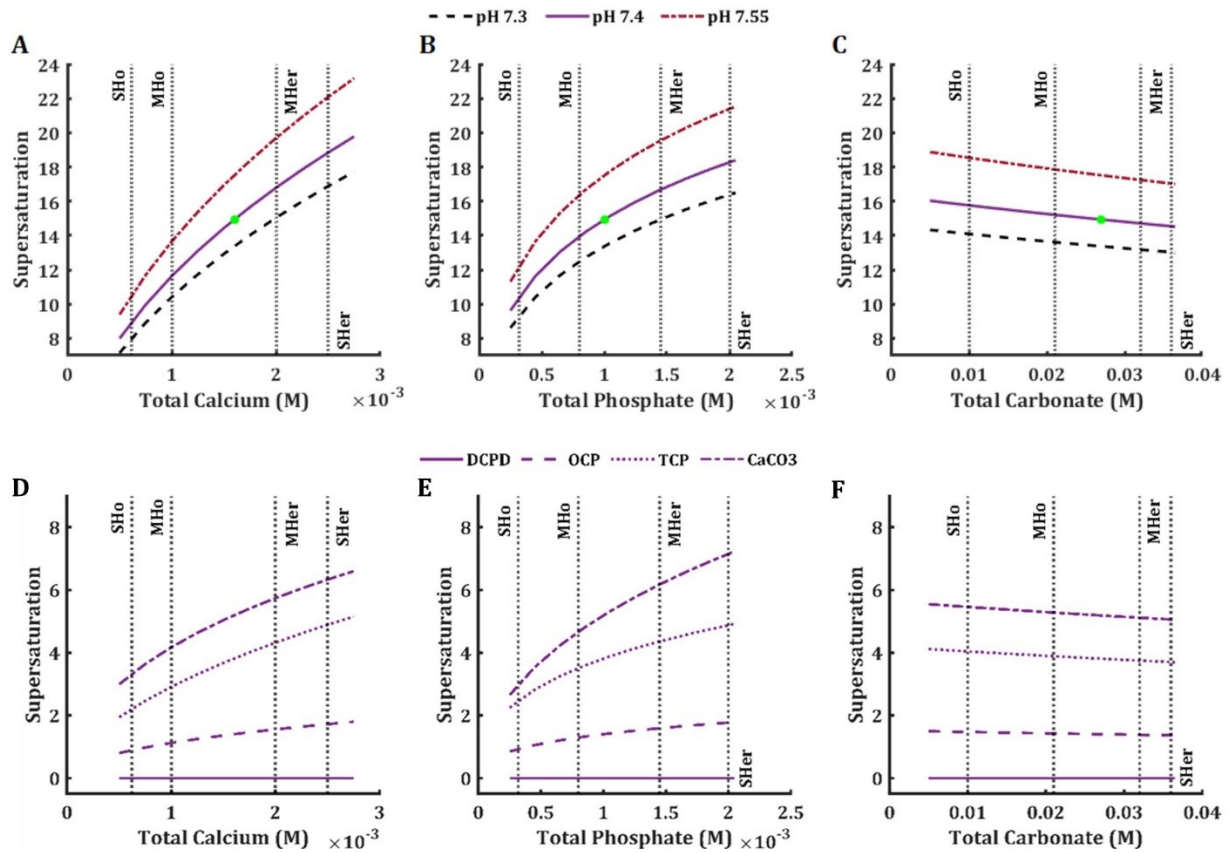


**Figure 3** Effect of physiological and pathophysiological total concentration of calcium (A,D), phosphate (B,E), and carbonate (C,F) on the solution supersaturation (equation 5) of hydroxyapatite (A-C) in the ISF at physiological pH 7.4 (solid line), low pH 7.3 (dashed line) and high pH 7.55 (dash-dotted line), and brushite (D-F, solid line), octacalcium phosphate (D-F, dashed line), tricalcium phosphate (D-F, dotted line), and calcium carbonate (D-F, dash-dotted line) in the ISF at physiological pH 7.4. The vertical lines are the mild and severe levels for low and high total concentrations (**Table 3**)

**Table 4** Percentage of saturation ratio changes in hypo/hyper levels of blood calcium, phosphate, and carbonate compared to normal concentrations at physiological pH (7.4)

|             | Severe hypo (%) | Mild hypo (%) | Mild hyper (%) | Severe hyper (%) |
|-------------|-----------------|---------------|----------------|------------------|
| <b>TCa</b>  | -39.88          | -22.14        | 12.40          | 26.14            |
| <b>TP04</b> | -30.31          | -6.63         | 11.71          | 22.39            |
| <b>TCO3</b> | 5.61            | 1.88          | -1.50          | -2.65            |

### 3.3. Precipitation

Precipitation starts with nucleation and proceeds with crystal growth [39]. In the biological context of bone mineralization, the nucleation step is mostly controlled biologically by the extracellular matrix proteins including collagens [11], while the physicochemical processes are involved in the growth phase. Thus, we assumed that the number of nucleators were not limiting and examined how hydroxyapatite precipitation rate was affected by change in the ISF total concentrations of different components (**Fig. 4**). Increase in total calcium (**Fig. 4A**) and total phosphate (**Fig. 4B**) concentrations led to higher hydroxyapatite precipitation rate, and this increase was considerably influenced by the pH of the ISF. A more basic environment favored higher precipitation rate, while an acidic environment decreased the precipitation rate, although the lower physiological pH limit caused less change in the rate compared to the higher physiological limit. While both hypercalcemia and hyperphosphatemia caused the precipitation rate to increase, hyperphosphatemia (both mild and severe) led to an almost two-fold higher increase in the rate compared to hypercalcemia (**Table 5**). Hypocalcemia and hypophosphatemia led to decrease of the precipitation rate (**Table 5**). Changes in total concentrations of other model components did

not affect the hydroxyapatite precipitation rate, except for total carbonate (Fig. 4C, Table 5) which showed a mild negative association with the precipitation rate.

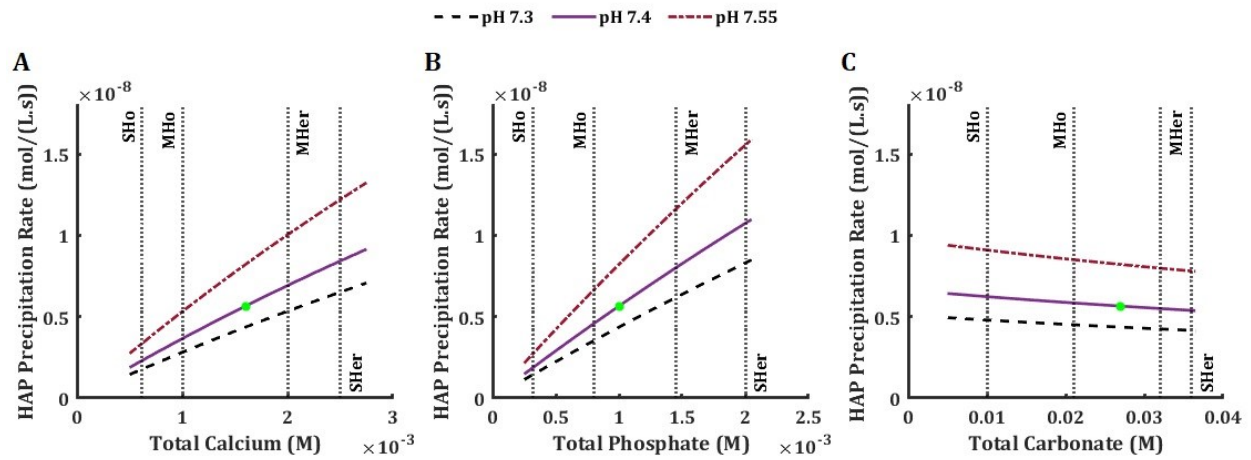


**Figure 4** Effect of physiological and pathophysiological total concentration of calcium (A), phosphate (B), and carbonate (C) on the precipitation rate of hydroxyapatite in the ISF, at physiological pH7.4 (solid line), low pH 7.3 (dashed line) and high pH 7.55 (dashed-dotted line). The vertical lines are the mild and severe levels for low and high total concentrations (Table 3)

**Table 5** Percentage of hydroxyapatite precipitation rate change in hypo/hyper levels of blood calcium, phosphate, and carbonate compared to normal concentrations at physiological pH (7.4)

|            | Severe hypo (%) | Mild hypo (%) | Mild hyper (%) | Severe hyper (%) |
|------------|-----------------|---------------|----------------|------------------|
| <b>TCa</b> | -59.07          | -35.39        | 22.33          | 48.94            |

|             |        |        |       |       |
|-------------|--------|--------|-------|-------|
| <b>TPO4</b> | -67.02 | -19.20 | 41.74 | 90.17 |
| <b>TCO3</b> | 10.45  | 3.46   | -2.72 | -4.80 |

Since from 7 model components, only two, total calcium and total phosphate, considerably influenced the hydroxyapatite precipitation in ISF, we examined how simultaneous changes in these two components affect hydroxyapatite supersaturation and precipitation rate. The simultaneous changes of TCa and TPO4 had non-linear effect on both hydroxyapatite supersaturation and especially on the hydroxyapatite precipitation rate, which increased synergistically when both TCa and TPO4 increased, but was only mildly affected when both TCa and TPO4 decreased (**Fig. 5**).

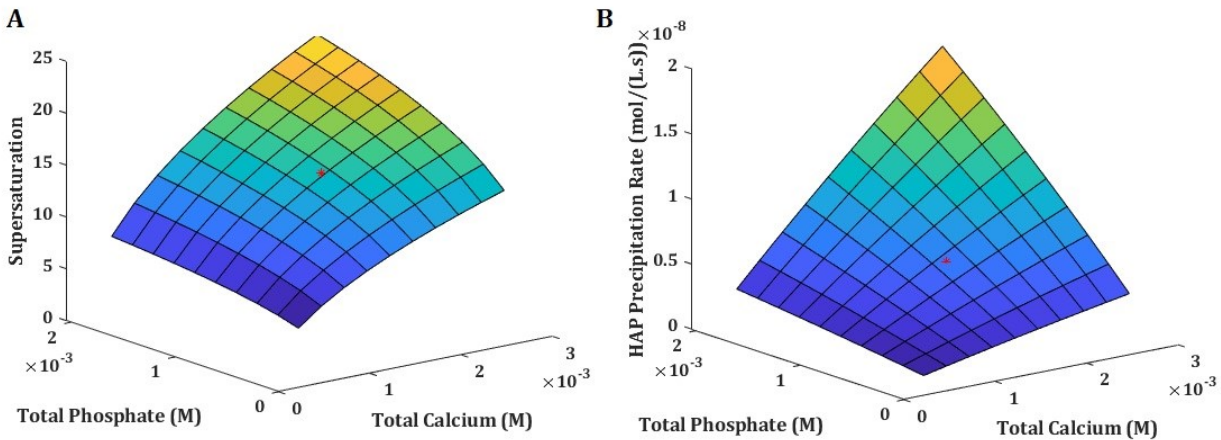


**Figure 5** Solution supersaturation (A) and precipitation rate (B) influenced by simultaneous changes in total calcium and total phosphate concentration in physiologically relevant concentrations at normal 7.4 pH

### 3.4. The Case of Isolated ISF

So far in this study, we investigated the behavior of the system under the assumption that ISF is in constant contact with the blood circulation, and the ions involved in the mineral formation will be immediately replenished. This assumption is supported by the fact that the rate of precipitation is much slower than the rate of ion delivery to the ISF. Nonetheless, many experimental studies are performed in a closed environment, where there is no continuous delivery of ions consumed in mineral formation. Thus, we adapted the model to simulate such scenarios by employing the following modifications. We assumed that an ISF unit has the volume of  $1 \mu\text{m}^3$  and the smallest time step to measure changes in the ISF was equal to 1 second. Given the initial total concentrations of model components, we calculated the equilibrium concentrations, supersaturation, and precipitation rate (equations 4, 5, and 7). Then, the amounts of ions that would have been removed by precipitation in the defined time step (1 s) were calculated and subtracted from the initial total concentrations of model components to produce the updated total concentrations of model components for the next iteration. This process was repeated to investigate the model behavior for a desired time length. This modified model was used to examine the temporal dynamics of hydroxyapatite precipitation in the closed system under different pH levels and initial component concentrations (**Fig. 6**). Initial precipitation rate in closed system strongly depended on pH, resulting in more hydroxyapatite precipitation at alkaline pH, which is similar to experimental observations [40].

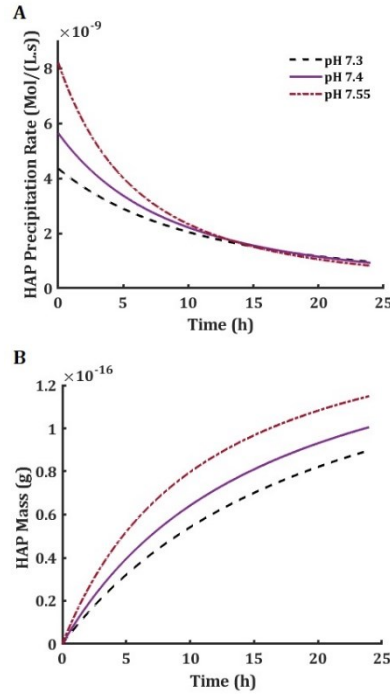


**Figure 6** Hydroxyapatite precipitation rate in a 24-hour precipitation period of the isolated ISF (A) and the accumulated mass of hydroxyapatite in a cube of 1  $\mu\text{m}^3$  volume (B) at physiological pH7.4 (solid line), low pH 7.3 (dashed line) and high pH 7.55 (dashed-dotted line)

Next, we compared our model predictions to previously published experimental data. First, we modeled the dependence of ionized calcium on pH reported by Miyajima et al [41]. We used in the model the reported values of component concentrations and pH for the experimental study and calculated the concentration of  $\text{Ca}^{2+}$  as a function of pH (**Fig. 7A**). Our model agreed well with the experimental values at pH 7.4-7.8 but deviated at higher pH levels. Next, we modeled the pH dependence of ion distributions reported by Boistelle et al [42]. We have similarly used the experimental values reported in the paper and calculated the resulting ionic concentrations of model species (**Fig. 7B**), and the solution

supersaturation for hydroxyapatite (**Fig. 7C**). Our findings were consistent with reported experimentally for pH 5-8 and deviated from reported values at higher pH. Thus, our model predictions were consistent with experimental findings for pH values in the physiological range.

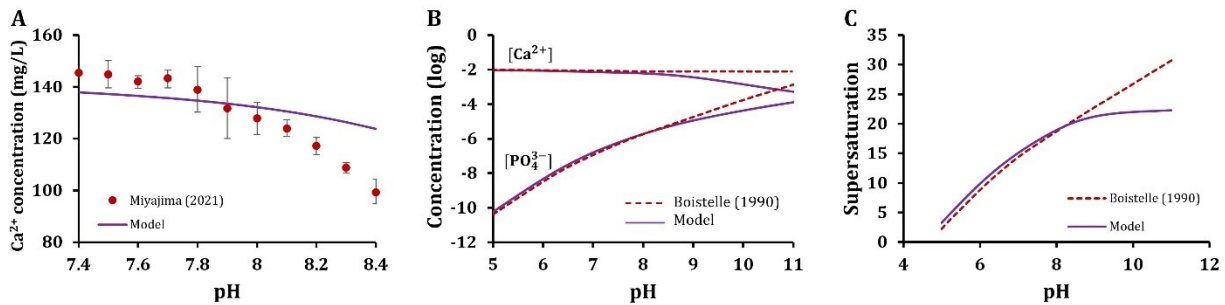


**Figure 7** Model validation with prior experimental data. Simulations were performed with experimental data reported by (A) Miyajima et al [41] or (B) Boistelle et al [42]. Model predictions are plotted as solid line and published data (circles with experimental errors for A and dashed lines for B,C) were extracted from the published papers and replotted with permission

#### 4. Discussion

The goal of this study was to investigate the role of physicochemical factors in the precipitation of bone hydroxyapatite in an environment that resembles bone interstitial fluid. We demonstrate that of the 7 components taken into consideration, only total calcium, total phosphate and to a lesser degree total carbonate affected ion availability, solution supersaturation and hydroxyapatite precipitation rate. Strong effect of systemic pH on

solution supersaturation and hydroxyapatite precipitation was due to its effect on ionized phosphate level since ionized calcium was not affected by pH. Hydroxyapatite precipitation was more strongly affected by availability of phosphate than availability of calcium within physiological range of changes in these components. Simultaneous change in total calcium and phosphate had synergetic effect on hydroxyapatite precipitation rate. Thus, while both calcium and phosphate levels affected hydroxyapatite precipitation directly, phosphate also demonstrated susceptibility to changes in pH, which additionally influenced hydroxyapatite precipitation.

Building a chemically sound model of interactions among different chemical species present in the ISF allowed us to investigate their effect on ionized calcium and phosphate, which are critical for hydroxyapatite formation. While it was challenging to find experimental or computational works that had the exact same solution parameters as the ones implemented in the model, using values from similar experimental studies, we were able to reproduce experimentally observed ion distribution for physiological levels of pH [41, 42]. The negative association between total phosphate and pH with ionized calcium observed previously [43], was also confirmed by the model. Our study suggests that only levels of total calcium and phosphate and to a lesser degree total carbonate affect availability of ionized calcium and phosphate relevant for hydroxyapatite precipitation. However, the chemical complexity of ISF should still be taken into account to obtain correct predictions of the ionic strength and interactions in the solution.

The distribution of ions matters not only because they define the properties of the ISF, but also as they can affect the precipitation behavior by modifying the solution saturation status. Building on previous findings that total calcium, phosphate and carbonate influence the

ionized calcium and phosphate availability, we investigated their consequent effect on saturation state of the ISF. At physiological levels of model components, the model predicted the solution supersaturation of 16.4, which is close to reported experimental values [12]. While the model confirmed the state of supersaturation normally observed in human plasma [44], it also provided a broader understanding of how this supersaturation state could be influenced when total concentration of model components (i.e., their plasma or ISF levels) change. Moreover, the model predicts and explains the previously reported [40, 45] relationship of increased supersaturation values when pH increases at constant calcium and phosphate levels. In the future, the model predictions can be improved by a more precise incorporation of different parameters, such as accounting for the variability in  $K_{sp}$  due to pH, temperature, and solution composition [46]. Investigating the effect of ion distribution and saturation status on hydroxyapatite precipitation behavior demonstrated that precipitation rate is driven by the values of ionized calcium and phosphate, which in turn depend on pH. Model predictions were consistent with previous findings that an increase in ionized phosphate at high pH levels increases the deposition rate of hydroxyapatite and that decrease in phosphate availability interferes with hydroxyapatite precipitation [47]. Thus, our findings are consistent with the well-recognized role of phosphate in regulating bone mineralization in physiological condition and in hypophosphatemic osteomalacia.

While many simplifications are implemented in constructing this model, the fact that its findings are in line with experimental works and current understanding of human physiology reassure us that the findings are reliable and that the model is suitable further developed. Combining this model with models of bone mineralization that account for biological factors such as collagen maturation [48] and bone cells-derived regulators [49]

will provide a powerful tool in studying the formation of bone hydroxyapatite or other biological mineralized tissues. Another field of modeling that could potentially benefit from the combined physicochemical and biological model is the whole-body calcium and phosphate homeostasis models. Bone is a major component of calcium and phosphate homeostasis, and its behavior is regulated by hormonal regulation by PTH, vitamin D, FGF23, calcitonin which directly or indirectly affect calcium and phosphate concentration in the body [50].

Taken together, we developed a mathematical model that captures the physiochemical factors involved in hydroxyapatite precipitation. We demonstrated how factors such as availability of ions in the environment and their distribution of these ions, as well as pH levels affect hydroxyapatite precipitation. Integrating this model with biological models of bone mineralization will allow in silico studies of complex clinical scenarios associated with alterations in ISF ion composition, such as osteomalacia, osteogenesis imperfecta, rickets, hypophosphatemia, and chronic kidney disease. Moreover, with minor adaptations, it could be used to understand mineralization in other physiological tissues, such as dentin and enamel, and in pathological conditions such as kidney stones and atherosclerotic plaques [51].

## **5. Additional Resources**

Implementation of current bone physicochemical model in MATLAB is available on GitHub: [https://github.com/Hosseinpoorhemati/bone\\_physicochemical\\_regulation.git](https://github.com/Hosseinpoorhemati/bone_physicochemical_regulation.git)

### **Data availability statement**

The original contributions presented in the study are included in the article, further inquiries can be directed to the corresponding author.

### **Author contributions**

HP: Conceptualization, Formal analysis, Investigation, Methodology, Software, Validation, Visualization, Writing—original draft, Writing—review & editing. SVK: Conceptualization, Funding acquisition, Methodology, Project administration, Writing—review & editing.

### **Funding**

The author(s) declare financial support was received for the research, authorship, and/or publication of this article. This work was supported by the operating grant from the Natural Sciences and Engineering Research Council of Canada (NSERC, RGPIN-288253).

### **Conflict of interest**

The authors declare that the research was conducted in the absence of any commercial or financial relationships that could be construed as a potential conflict of interest.

### **Publisher's note**

All claims expressed in this article are solely those of the authors and do not necessarily represent those of their affiliated organizations, or those of the publisher, the editors and the reviewers. Any product that may be evaluated in this article, or claim that may be made by its manufacturer, is not guaranteed or endorsed by the publisher.

## References

1. Boskey, A.L., *Bone composition: relationship to bone fragility and antiosteoporotic drug effects*. BoneKEY reports, 2013. **2**.
2. Willie, B.M., et al., *Bone adaptation: Safety factors and load predictability in shaping skeletal form*. Bone, 2020. **131**: p. 115114.
3. Boskey, A.L. and P.G. Robey, *The composition of bone*. Primer on the metabolic bone diseases and disorders of mineral metabolism, 2013: p. 49-58.
4. Vassiliou, V., E. Chow, and D. Kardamakis, *Bone metastases: a translational and clinical approach*. Vol. 21. 2013: Springer Science & Business Media.
5. Ambre, A.H., D.R. Katti, and K.S. Katti, *Biomaterialized hydroxyapatite nanoclay composite scaffolds with polycaprolactone for stem cell-based bone tissue engineering*. Journal of Biomedical Materials Research Part A, 2015. **103**(6): p. 2077-2101.
6. Murshed, M., *Mechanism of Bone Mineralization*. Cold Spring Harb Perspect Med, 2018. **8**(12).
7. Collin, C.B., et al., *Computational models for clinical applications in personalized medicine—guidelines and recommendations for data integration and model validation*. Journal of personalized medicine, 2022. **12**(2): p. 166.
8. Komarova, S.V., et al., *Mathematical model for bone mineralization*. Front Cell Dev Biol, 2015. **3**: p. 51.
9. Poorhemati, H. and S.V. Komarova, *Mathematical modeling of the role of bone turnover in pH regulation in bone interstitial fluid*. Computational Biology and Chemistry, 2021. **94**: p. 107564.
10. Hunter, G.K., C.L. Kyle, and H.A. Goldberg, *Modulation of crystal formation by bone phosphoproteins: structural specificity of the osteopontin-mediated inhibition of hydroxyapatite formation*. Biochemical Journal, 1994. **300**(3): p. 723-728.
11. Olszta, M.J., et al., *Bone structure and formation: A new perspective*. Materials Science and Engineering: R: Reports, 2007. **58**(3-5): p. 77-116.
12. Söhnel, O. and F. Grases, *Supersaturation of body fluids, plasma and urine, with respect to biological hydroxyapatite*. Urological research, 2011. **39**: p. 429-436.
13. Drake, F., G. Pierce, and M. Dow, *Measurement of the dielectric constant and index of refraction of water and aqueous solutions of KCl at high frequencies*. Physical Review, 1930. **35**(6): p. 613.

14. Granjon, D., O. Bonny, and A. Edwards, *Coupling between phosphate and calcium homeostasis: a mathematical model*. American Journal of Physiology-Renal Physiology, 2017. **313**(6): p. F1181-F1199.
15. Oyane, A., et al., *Preparation and assessment of revised simulated body fluids*. Journal of Biomedical Materials Research Part A, 2003. **65**(2): p. 188-195.
16. Koutsoukos, P. and G. Nancollas, *Crystal growth of calcium phosphates-epitaxial considerations*. Journal of crystal growth, 1981. **53**(1): p. 10-19.
17. Chughtai, A.R., R. Marshall, and G.H. Nancollas, *Complexes in calcium phosphate solutions*. The Journal of physical chemistry, 1968. **72**(1): p. 208-211.
18. Butler, J.N., *Ionic equilibrium: solubility and pH calculations*. 1998: John Wiley & Sons.
19. Childs, C., *Potentiometric study of equilibria in aqueous divalent metal orthophosphate solutions*. Inorganic Chemistry, 1970. **9**(11): p. 2465-2469.
20. Salaun, F., B. Mietton, and F. Gaucheron, *Influence of mineral environment on the buffering capacity of casein micelles*. Milchwissenschaft Milk Science International, 2007. **62**(1): p. 20-23.
21. Crundwell, F.K., *Path from Reaction Control to Equilibrium Constraint for Dissolution Reactions*. ACS Omega, 2017. **2**(8): p. 4845-4858.
22. Guynn, R.W., *Equilibrium constants under physiological conditions for the reactions of choline kinase and the hydrolysis of phosphorylcholine to choline and inorganic phosphate*. Journal of Biological Chemistry, 1976. **251**(22): p. 7162-7167.
23. Silverstein, T.P. and S.T. Heller, *p K a Values in the Undergraduate Curriculum: What Is the Real p K a of Water?* Journal of Chemical Education, 2017. **94**(6): p. 690-695.
24. Castro, F., et al., *Characterization of intermediate stages in the precipitation of hydroxyapatite at 37 C*. Chemical engineering science, 2012. **77**: p. 150-156.
25. Nancollas, G. and B. Tomazic, *Growth of calcium phosphate on hydroxyapatite crystals. Effect of supersaturation and ionic medium*. The journal of physical chemistry, 1974. **78**(22): p. 2218-2225.
26. Moreno, E.C., W.E. Brown, and G. Osborn, *Stability of dicalcium phosphate dihydrate in aqueous solutions and solubility of octocalcium phosphate*. Soil Science Society of America Journal, 1960. **24**(2): p. 99-102.
27. Gregory, T., et al., *Solubility of  $\beta$ -Ca<sub>3</sub>(PO<sub>4</sub>)<sub>2</sub> in the System Ca(OH)<sub>2</sub>-H<sub>3</sub>PO<sub>4</sub>-H<sub>2</sub>O at 5, 15, 25, and 37° C*. Journal of Research of the National Bureau of Standards. Section A, Physics and Chemistry, 1974. **78**(6): p. 667.
28. Gal, J.-Y., et al., *Calcium carbonate solubility: a reappraisal of scale formation and inhibition*. Talanta, 1996. **43**(9): p. 1497-1509.
29. Herbert, F.K., H. Miller, and G. Richardson, *Chronic renal disease, secondary parathyroid hyperplasia, decalcification of bone and metastatic calcification*. The Journal of Pathology and Bacteriology, 1941. **53**(2): p. 161-182.
30. Inskip, W.P. and J.C. Silvertooth, *Kinetics of hydroxyapatite precipitation at pH 7.4 to 8.4*. Geochimica et Cosmochimica Acta, 1988. **52**(7): p. 1883-1893.
31. Yun, J., et al., *A kinetic model for hydroxyapatite precipitation in mineralizing solutions*. Crystal Growth & Design, 2018. **18**(5): p. 2717-2725.
32. Morel, F. and J. Morgan, *A Numerical Method for Computing Equilibria in Aqueous Chemical Systems Environmental Science & Technology*. 1972.
33. Mehta, A.N. and M. Emmett, *Approach to acid-base disorders*, in *National Kidney Foundation Primer on Kidney Diseases*. 2018, Elsevier. p. 120-129.

34. Carroll, M.F. and D.S. Schade, *A practical approach to hypercalcemia*. American family physician, 2003. **67**(9): p. 1959-1966.
35. Pepe, J., et al., *Diagnosis and management of hypocalcemia*. Endocrine, 2020. **69**: p. 485-495.
36. Koumakis, E., et al., *The causes of hypo-and hyperphosphatemia in humans*. Calcified Tissue International, 2021. **108**: p. 41-73.
37. NARINS, R.G. and M. EMMETT, *Simple and mixed acid-base disorders: a practical approach*. Medicine, 1980. **59**(3): p. 161-182.
38. Aleš, H., J. Lenka, and Š. Ludvík, *The influence of simulated body fluid composition on carbonated hydroxyapatite formation*. Ceram.-Silik, 2002. **46**(1): p. 9-14.
39. Eanes, E.D., *Dynamics of calcium phosphate precipitation*. Calcification in biological systems, 2020: p. 1-17.
40. Lei, Y., et al., *Electrochemical induced calcium phosphate precipitation: importance of local pH*. Environmental science & technology, 2017. **51**(19): p. 11156-11164.
41. Miyajima, H., H. Touji, and K. Iijima, *Hydroxyapatite particles from simulated body fluids with different pH and their effects on mesenchymal stem cells*. Nanomaterials, 2021. **11**(10): p. 2517.
42. Boistelle, R. and I. Lopez-Valero, *Growth units and nucleation: the case of calcium phosphates*. Journal of crystal growth, 1990. **102**(3): p. 609-617.
43. Lehmann, M. and F. Mimouni, *Serum phosphate concentration. Effect on serum ionized calcium concentration in vitro*. Am J Dis Child, 1989. **143**(11): p. 1340-1.
44. Zhu, P., et al., *Investigation of apatite deposition onto charged surfaces in aqueous solutions using a quartz-crystal microbalance*. Journal of the American Ceramic Society, 2003. **86**(5): p. 782-790.
45. Nancollas, G.H. and J. Zhang, *Formation and dissolution mechanisms of calcium phosphates in aqueous systems*, in *Hydroxyapatite and related materials*. 2017, CRC Press. p. 73-81.
46. Ito, A., et al., *Solubility product of OH-carbonated hydroxyapatite*. Journal of Biomedical Materials Research: An Official Journal of The Society for Biomaterials and The Japanese Society for Biomaterials, 1997. **36**(4): p. 522-528.
47. Bhadada, S.K. and S.D. Rao, *Role of phosphate in biomineralization*. Calcified tissue international, 2021. **108**: p. 32-40.
48. Oosterlaken, B.M., M.P. Vena, and G. de With, *In vitro mineralization of collagen*. Advanced Materials, 2021. **33**(16): p. 2004418.
49. Staines, K.A., et al., *Identification of novel regulators of osteoblast matrix mineralization by time series transcriptional profiling*. Journal of bone and mineral metabolism, 2014. **32**: p. 240-251.
50. Case, R.M., et al., *Evolution of calcium homeostasis: from birth of the first cell to an omnipresent signalling system*. Cell calcium, 2007. **42**(4-5): p. 345-350.
51. Hinterdobler, J., et al., *Acute mental stress drives vascular inflammation and promotes plaque destabilization in mouse atherosclerosis*. European Heart Journal, 2021. **42**(39): p. 4077-4088.

## **Bridging Chapter 4 and 5**

The work presented in chapter 4 provided a model with sufficient complexity and predictive performance to satisfy the first two objectives of my research, i.e. a reliable simulation of chemical and physicochemical aspects involved in the process of bone mineralization. This model was superior to the previous one in both prediction reliability and computation time. While the number of components was almost twice that of the model presented in chapter 3, due to the implementation of better algorithms and mathematical solutions, the computations in this model were much faster and lighter, which eliminated the need for high computational power and made the use of the model more convenient.

While the model was developed according to relevant biological and physiological criteria, biological regulators were not a part of it, and the model by itself could not yet provide the ideal description of the bone mineralization process. Thus, the integration between the physicochemical model and a biological model was the next logical step. The biological model developed by Komarova et al. in 2015, which was introduced in chapter 2, was the biological model appropriate for this integration. Integrating these two models required re-imagining the process in a single model with two compartments and the possibility of flow of information among them. The physiological compartment had to be responsible for informing the biological model and particularly the mineral formation component of it of the limitations of the ionic solution and to guide the mineral formation process. Fine-tuning the model and further minor improvements on the biological compartment after the integration is achieved could improve the overall performance and usability of the integrated model, which is conducted and discussed in the following chapter.

## **Chapter 5. Mathematical Model Capturing Physicochemical and Biological Regulation of Bone Mineralization**

### **Mathematical Model Capturing Physicochemical and Biological Regulation of Bone Mineralization**

**Hossein Poorhemati<sup>1,2</sup>, Svetlana Komarova<sup>1,2,3,4\*</sup>**

<sup>1</sup>Biological and Biomedical Engineering, McGill University, Montreal, Canada

<sup>2</sup>Shriners Hospital for Children - Canada, Montreal, QC, Canada

<sup>3</sup>Faculty of Dental Medicine and Oral Health Sciences, McGill University, Montreal, Canada

<sup>4</sup>Department of Biomedical Engineering, Faculty of Engineering, University of Alberta,  
Edmonton, Canada

**\* Correspondence:**

Svetlana V. Komarova

[komarova@ualberta.ca](mailto:komarova@ualberta.ca)

**Keywords:** mathematical modeling, bone biomineralization, hydroxyapatite, mineralization inhibitors, physicochemical regulation

## **Abstract**

**Introduction:** Bone mineralization is a complex process tightly regulated by both biological factors such as collagen maturation as well as physicochemical factors such as pH. A previous model of biological mineralization captured the biological regulation of bone mineralization dynamics, but not the impact of bone microenvironment such as ion availabilities observed in hypo or hyperphosphatemia.

**Methods:** To build an integrated model of bone mineralization, we utilized two previously developed models which addressed a distinct aspect of bone mineralization. The first model described the processes of the extracellular matrix formation and maturation, inhibitor and nucleator formation and removal and their combined action in regulating bone mineralization. The second model simulated the bone interstitial fluid (BIF) permissive to precipitation of hydroxyapatite and described the physicochemical process of hydroxyapatite precipitation. The resulting bone mineralization model accounts for biological and physicochemical aspects of the process.

**Results:** The integrated model was analyzed for the impact of physicochemical factors (pH, levels of calcium and phosphate) on the mineralization dynamics. Model predictions were compared to experimental findings using two outcomes characterizing mineralization dynamics: mineralization delay that corresponds to histomorphometry measures of osteoid volume or thickness, and mineralization degree that corresponds to bone mineral density distribution. We identified the limitation of the previously developed model in predicting the mineralization delay observed in the situations of hypophosphatemia and hypocalcemia and proposed a model adaptation that predicts these outcomes.

**Conclusions:** The resulting mathematical model can be used for in silico testing of hypotheses regarding the role of different physicochemical, molecular, or cellular factors in causing a specific disruption in mineralization dynamics.

## 1. Introduction

Bone mineralization is a complex and multifaceted process that adheres to the principles of minerals chemistry yet occurs within a biological framework. In this biological framework, a group of biological factors directly promote or interrupt the mineral precipitation process in an environment that is permissive to it. For example, in the bone interstitial fluid (BIF), collagen molecules play a major role by providing the nucleation sites for mineral crystals at their intra and interfibrillar spaces [1]. However, genetic abnormalities that cause changes in collagen molecules production or post-translational processing, which are observed in the osteogenesis imperfecta (OI), affect the mineralization process resulting in altered quality and strength of the OI patients' bones [2]. There are also biological molecules, such as Osteopontin (OPN) [3] or Matrix Gla Protein (MGP) [4, 5] that are known for their inhibitory roles in bone mineralization. Bone mineralization dynamics can also be altered by impacting the BIF composition and physicochemical properties. For example, elevated systemic pH or hypophosphatemia shift the chemical equilibriums and ionic strength of the BIF, potentially leading to changes in supersaturation status and precipitation rate of hydroxyapatite [6]. Indeed, plasma levels of calcium and phosphate – ionic mineral constituents of bone hydroxyapatite mineral are critically important for successful mineralization [7]. Thus, both physicochemical and biological context can impact and regulate bone mineralization.

Mathematical models offer a valuable solution for studying multifaceted processes that occur at multiple time scales. Previously, our team developed a biological model that captured the observed dynamics of bone mineralization by accounting for four major biological components: naïve and mature collagen matrix, inhibitors and nucleators [8]. The mineral formation in the first model was positively regulated by the presence of nucleators arising

on the mature matrix and negatively regulated by the inhibitors, however, the ionic composition or pH that influence the BIF environment was not considered. Based on the established models of mineral precipitation [9], we have next developed a model to simulate the BIF and predict how different physicochemical conditions relevant to human physiology affect mineral precipitation [6, 10]. The objective in the current study was to develop an integrated model of bone mineralization that combines biological and physicochemical regulation of bone mineralization.

## 2. Model Development

The model has two main compartments, one for the physicochemical processes, which is based on Poorhemati & Komarova, 2024 [6], and another for the biological processes based on Komarova et al., 2015 [8].

**The physicochemical compartment** is comprised of four sections: initiation, equilibrium, saturation, and precipitation described in detail in [6]. Briefly, in the initiation section, we define the environment where bone formation process occurs, also known as bone interstitial fluid (BIF). BIF includes seven major components: calcium ( $Ca^{2+}$ ), phosphate ( $PO_4^{3-}$ ), carbonate ( $CO_3^{2-}$ ), sodium ( $Na^+$ ), chloride ( $Cl^-$ ), magnesium ( $Mg^{2+}$ ), and potassium ( $K^+$ ). In the equilibrium section, the equilibrium concentrations of all components and of the 22 chemical species resulting from their chemical reactions (**Table 1**) are calculated. Chemical species include  $H_3PO_4$ ,  $H_2PO_4^-$ ,  $HPO_4^{2-}$ ,  $H_2CO_3(aq)$ ,  $HCO_3^-$ ,  $CaHCO_3^+$ ,  $CaCO_3(aq)$ ,  $CaOH^+$ ,  $CaH_2PO_4^+$ ,  $CaHPO_4(aq)$ ,  $CaPO_4^-$ ,  $NaHPO_4^-$ ,  $NaH_2PO_4(aq)$ ,  $MgHCO_3^+$ ,  $MgCO_3(aq)$ ,  $MgOH^+$ ,  $MgH_2PO_4^+$ ,  $MgHPO_4(aq)$ ,  $MgPO_4^-$ ,  $NaCl$ ,  $KHPO_4^-$ ,  $OH^-$ . The pH of the environment

is chosen to resemble that of human body. Since BIF is an ionic solution, we calculated its the ionic strength ( $IS$ ):

$$IS = \frac{1}{2} \sum_{i=1}^n c_i \cdot z_i^2 \quad (1)$$

where  $c_i$  and  $z_i$ , are the molar concentration and valence of ion  $i$ , and  $n$  is the number of ions in the solution. This allowed us to calculate the activity coefficients  $\gamma_i$  for each ion:

$$\log \gamma_i = -Az_i^2 \left( \frac{\sqrt{IS}}{(1+\sqrt{IS})} - 0.3IS \right) \quad (2)$$

where  $IS$  is ionic strength,  $z_i$  is ion valence, and  $A$  is the dielectric constant of the solvent which depends on the temperature, and for a given the temperature in Celsius ( $T_c$ ), can be approximated using equation 3 [11].

$$A = 0.486 + 6.07 \times 10^{-4}T_c + 6.43 \times 10^{-6}T_c^2 \quad (3)$$

The corrected ion concentrations  $Q_i$  are defined as  $Q_i = c_i \cdot \gamma_i$ .

The equilibrium section includes 30 equations: 22 equations from reaction rate law and corresponding equilibrium constants, 1 equation from pH definition and 7 equations from mass conservation law for the total concentration of each of seven major components. This set of equations is then simplified to a system of 7 equations using the definition of equilibrium constants and solved using the Newton-Raphson method [6, 12].

In the saturation section, the solution supersaturation for hydroxyapatite,  $Ca_{10}(PO_4)_6(OH)_2$ , which we assumed to be the only precipitate in the system, is calculated based on the ionic product,  $IP$ , and the solubility constant of hydroxyapatite,  $K_{sp}$ , at 37°C. The ionic product is

calculated as presented in equation 4 where  $C$  and  $\gamma$  are respectively the equilibrium concentration and the activity coefficient for each ion involved in the mineral structure.

$$IP = (C_{Ca} \cdot \gamma_{Ca})^5 (C_{PO_4} \cdot \gamma_{PO_4})^3 (C_{OH} \cdot \gamma_{OH})^1 \quad (4)$$

If the solution is supersaturated, precipitation is permitted. Solution supersaturation was calculated using equation 5 where  $\theta$  is the sum of stoichiometric coefficients of cations and anions involved in the mineral.

$$S = \left(\frac{IP}{K_{sp}}\right)^{\frac{1}{\theta}} \quad (5)$$

In the precipitation section, the rate of hydroxyapatite precipitation ( $R$ ) in mol HAP  $L^{-1}s^{-1}$  is calculated using an experimentally derived equation [13], for which we assumed that the precipitation surface area is proportional to the number of nucleators described in the biological compartment.

$$R = k_p \gamma_2 \gamma_3 [Ca^{2+}] [PO_4^{3-}] \quad (6)$$

where  $k_p$  is the rate constant ( $L \text{ mol } s^{-1}$ ),  $\gamma_2$  and  $\gamma_3$  are the divalent and trivalent activity coefficients ( $\text{mol } L^{-1}$ ) for the concentrations of  $[Ca^{2+}]$  and  $[PO_4^{3-}]$ .

**Table 1. Physicochemical compartment variables, parameters, and values**

| Item  | Value    |
|---|----------|
| <b>Major components</b> (value represent total concentration in mM) |          |
| TCO <sub>3</sub>  | 27 [14]  |
| TPO <sub>4</sub>  | 1.0 [14] |

|   |                         |
|---|-------------------------|
| TCa   | 1.6 [14]                |
| TNa   | 142 [14]                |
| TCl   | 103 [14]                |
| TK  | 5 [14]                  |
| TMg   | 1 [14]                  |
| <b>Chemical species, reaction</b> (value represent equilibrium constant)                |                         |
| $\text{H}_2\text{CO}_3(\text{aq}) \rightleftharpoons 2\text{H}^+ + \text{CO}_3^{2-}$    | $10^{-6.31}$ [15]       |
| $\text{HCO}_3^- \rightleftharpoons \text{H}^+ + \text{CO}_3^{2-}$                       | $10^{-10.25}$ [15]      |
| $\text{H}_3\text{PO}_4 \rightleftharpoons \text{H}^+ + \text{H}_2\text{PO}_4^-$         | $10^{-2.196}$ [15]      |
| $\text{H}_2\text{PO}_4^- \rightleftharpoons \text{H}^+ + \text{HPO}_4^{2-}$             | $10^{-7.185}$ [15]      |
| $\text{HPO}_4^{2-} \rightleftharpoons \text{H}^+ + \text{PO}_4^{3-}$                    | $10^{-12.19}$ [15]      |
| $\text{Ca}^{2+} + \text{HCO}_3^- \rightleftharpoons \text{CaHCO}_3^+$                   | $10^{1.16}$ [15]        |
| $\text{Ca}^{2+} + \text{CO}_3^{2-} \rightleftharpoons \text{CaCO}_3(\text{aq})$         | $10^{3.38}$ [15]        |
| $\text{Ca}^{2+} + \text{OH}^- \rightleftharpoons \text{CaOH}^+$                         | 25.12 [16]              |
| $\text{Ca}^{2+} + \text{H}_2\text{PO}_4^- \rightleftharpoons \text{CaH}_2\text{PO}_4^+$ | 31.9 [17]               |
| $\text{Ca}^{2+} + \text{HPO}_4^{2-} \rightleftharpoons \text{CaHPO}_4(\text{aq})$       | $6.81 \times 10^2$ [17] |
| $\text{Ca}^{2+} + \text{PO}_4^{3-} \rightleftharpoons \text{CaPO}_4^-$                  | $3.46 \times 10^6$ [17] |
| $\text{Mg}^{2+} + \text{HCO}_3^- \rightleftharpoons \text{MgHCO}_3^+$                   | $10^{0.62}$ [18]        |
| $\text{Mg}^{2+} + \text{CO}_3^{2-} \rightleftharpoons \text{MgCO}_3(\text{aq})$         | $10^{1.87}$ [18]        |
| $\text{Mg}^{2+} + \text{OH}^- \rightleftharpoons \text{MgOH}^+$                         | $10^{2.19}$ [18]        |
| $\text{Mg}^{2+} + \text{H}_2\text{PO}_4^- \rightleftharpoons \text{MgH}_2\text{PO}_4^+$ | $10^{0.4}$ [19]         |
| $\text{Mg}^{2+} + \text{HPO}_4^{2-} \rightleftharpoons \text{MgHPO}_4(\text{aq})$       | $10^{1.8}$ [19]         |

|   |  |
|---|--|
| $\text{Mg}^{2+} + \text{PO}_4^{3-} \rightleftharpoons \text{MgPO}_4^-$                        | $10^{3.3}$ [19]  |
| $\text{Na}^+ + \text{HPO}_4^{2-} \rightleftharpoons \text{NaHPO}_4^-$                         | 0.21 [20]  |
| $\text{Na}^+ + \text{H}_2\text{PO}_4^- \rightleftharpoons \text{NaH}_2\text{PO}_4(\text{aq})$ | $10^{-6.82}$ [21]  |
| $\text{Na}^+ + \text{Cl}^- \rightleftharpoons \text{NaCl}(\text{aq})$                         | $3.41 \times 10^{-2}$ [22, 23]   |
| $\text{K}^+ + \text{HPO}_4^{2-} \rightleftharpoons \text{KHPO}_4^-$                           | 2.5 [23]   |
| $\text{H}_2\text{O} \rightleftharpoons \text{H}^+ + \text{OH}^-$                              | $10^{-14}$ [24]  |
| <b>Precipitation parameters</b>   |  |
| Rate constant, $k_p$  | $2469 \text{ L mol s}^{-1}$ [13]                                       |
| $K_{SP}$ for hydroxyapatite   | $2.03 \times 10^{-59} \text{ mol}^9/\text{l}^9$ [14]                   |
| Activity coefficients $\gamma_2$ and $\gamma_3$   | Calculated for $\text{Ca}^{2+}$ and $\text{PO}_4^{3-}$ by equation (2) |

Based on the total concentration of these seven components and systemic pH, the physicochemical compartment calculates the maximum rate of hydroxyapatite formation possible under the defined circumstances.

**The biological regulation compartment** takes into account naïve and mature collagen, mineralization nucleators, and mineralization inhibitors [8]. The mineral precipitation rate is informed by the concentrations of nucleators and inhibitors as well as by the physicochemically-defined hydroxyapatite precipitation rate.

The biological compartment is based on the previous model [8]. Briefly, we assumed that bone formation process starts with osteoblasts producing the naïve extracellular matrix ( $x_1$ ), which undergoes a series of transformations that take up to almost two weeks [8, 25] to form mature matrix ( $x_2$ ) that support mineral formation. Equations (7), (8) describe the removal

of naïve matrix and the corresponding appearance of mature matrix with the characteristic rate constant  $k_1$ .

$$\frac{dx_1}{dt} = -k_1x_1 \quad (7)$$

$$\frac{dx_2}{dt} = k_1x_1 \quad (8)$$

Mineralization inhibitors are critical to prevent mineralization in the generally supersaturated environment of the human body [6, 14, 26]. Numerous mineralization inhibitors with different mechanisms of action have been described [4, 27, 28], which are combined in the model as a single variable  $I$ . We assumed that the available inhibitors are proportional to the naïve matrix,  $x_1$ , which is described by the term  $v_1x_1$ , where  $v_1$  is the characteristic rate constant of diffusion of inhibitors through the immature matrix. During mineralization, inhibitors can be cleaved enzymatically or removed by other methods such as binding to other molecules, being trapped or masked [29, 30]. The removal of inhibitors was initially assumed to be proportional to mature matrix  $x_2$  and the number of inhibitors  $I$ , with the characteristic rate constant of  $r_1$ :

$$\frac{dI}{dt} = v_1x_1 - r_1x_2I \quad (9)$$

Alternative description of the removal of mineralization inhibitors is proposed in this work. We hypothesized that a higher rate of mineral formation may be associated with faster removal of inhibitors from the environment with the characteristic constant  $t_1$ :

$$\frac{dI}{dt} = v_1x_1 - t_1 \frac{dy}{dt} I \quad (9b)$$

Given that precipitation conditions are met (which is identified by the supersaturation in the physicochemical compartment), precipitation of biological hydroxyapatite is driven by the presence of nucleators in the extracellular matrix [29]. We assumed that appearance of nucleators ( $N$ ) is proportional to the rate of matrix maturation as described by the term  $k_2 dx_2/dt$  in which  $k_2$  represents the number of nucleators per collagen molecule [8]. It is assumed that nucleators become trapped in the crystal as they initiate mineralization, thus their removal is proportional to the rate of the appearance of the mineral ( $y$ ),  $dy/dt$ , and the number of nucleators, with the characteristic rate constant of  $r_2$ :

$$\frac{dN}{dt} = k_2 \frac{dx_2}{dt} - r_2 \frac{dy}{dt} N \quad (10)$$

**Integration of physicochemical and biological compartments.** The rate of mineral formation depends on the physicochemical factors, equation (6), as well the number of available nucleators, which we assume to define the mineralizing surface. Inhibitors inversely affect mineralization, which is captured by a Hill type function, which approaches 0 as the inhibitor amount tends to infinity;  $a$  and  $b$  are constants regulating the Hill type function behavior. Equation (11) presents mineral formation dynamics.

$$\frac{dy}{dt} = f(R) \cdot \left( \frac{b}{b+I^a} \right) N \quad (11)$$

where  $R$  is the precipitation rate calculated in equation (6) and  $f(R)$  is the characteristic rate constant for mineral formation that represents a conversion function to change the unit of  $R$  to *molecule HAP/(day.  $\mu m^3$ )* as required by the equation (11) of biological compartment.

**Table 2** shows the variables, parameters, and their corresponding values relevant to this enhanced model. An insight to the process of obtaining values is explained elsewhere [6, 8].

**Table 2. Variables and parameters of the biology compartment**

| Item   | description                                      | Value                                 |
|--|--|---------------------------------------|
| <b>Variables</b> (Value is the characteristic value and the unit is $\frac{\text{molecules}}{\mu\text{m}^3}$ , otherwise provided) |  |                                       |
| $x_1$  | Naïve collagen matrix                            | $9.4 \times 10^5$                     |
| $x_2$  | Mature collagen matrix                           | $9.4 \times 10^5$                     |
| $I$  | Inhibitors                                       | $\sim 10^6$                           |
| $N$  | Nucleators                                       | 1-10 per assembled collagen           |
| $y$  | Hydroxyapatite mineral                           | $0.8 \times 10^9$                     |
| <b>Parameters</b>  |  |                                       |
| $k_1$  | Collagen assembly                                | $0.1 \text{ day}^{-1}$                |
| $k_2$  | Number of nucleators per collagen molecule       | 1                                     |
| $v_1$  | Production of inhibitors by osteoblasts          | $0.1 \text{ day}^{-1}$                |
| $r_1$  | Degradation of inhibitors                        | $2 \times 10^{-7} \text{ day}^{-1}$   |
| $r_2$  | Use of nucleators by mineralized bone            | $1.7 \times 10^{-8} \text{ mol}^{-1}$ |
| $t_1$  | Removal of inhibitors by mineralized bone        | $1.5 \times 10^{-8} \text{ mol}^{-1}$ |
| $b$  | Hill coefficient                                 | 10                                    |
| $a$  | Apparent dissociation constant for Hill function | $10^{57}$                             |

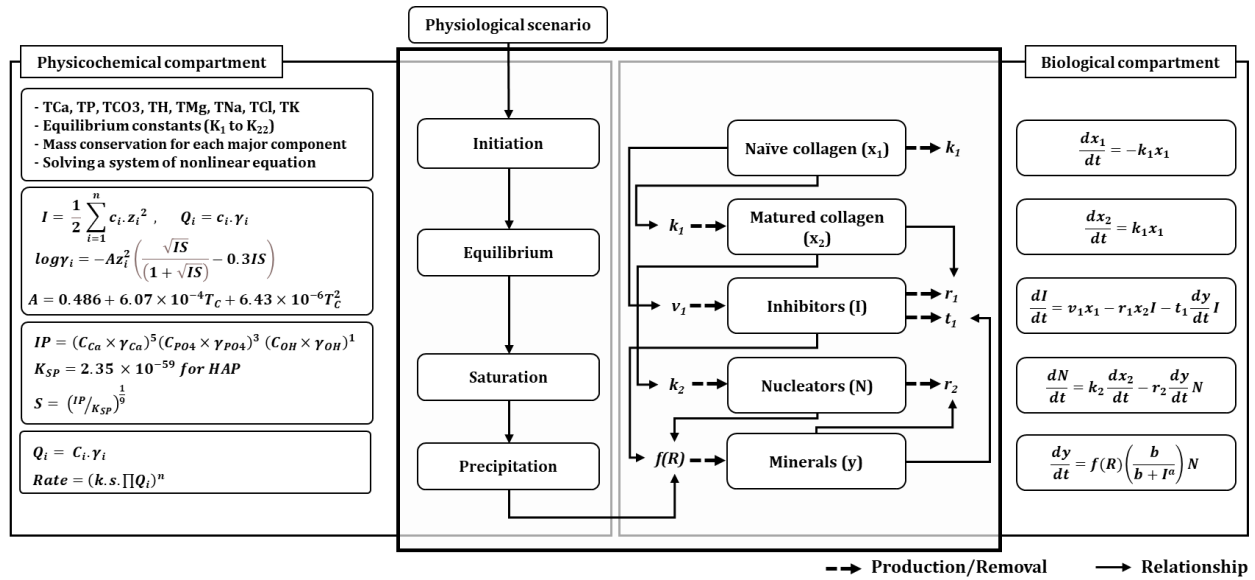


**Figure 1. Schematic representation of the integrated model and governing equations**

### Model simulation and analysis:

The schematic description of the integrated model including both the physicochemical and biological compartments is provided in **Figure 1**. The two compartments of this model have their own numerical solution. In the physicochemical one, a system of 8 non-linear equations is solved by implementing a Newton-Raphson solver in MATLAB [6]. For the biological compartment, a system of 5 first-order ordinary differential equations is solved using *ode15s*, a built-in MATLAB ODE solver. The version of MATLAB used for the current work was R2023b. For better comparison of the influence of different changes on the mineralization dynamics, the values of the biological components plotted in current work figures were non-demonopolized by using characteristic values presented in **Table 1**. For details, please check the relevant MATLAB code published on the model GitHub repository.

### 3. Results

First, we examined how the physicochemical compartment influences the behavior of different components of biological compartment of the model. Changing the pH of the BIF from physiological to low levels (acidic) to high levels (basic), we observed no change in matrix (**Figure 2A**) or inhibitors dynamics (**Figure 2B**). However, the rate of nucleator depletion depended on pH, and was faster in a more acidic environment, and slower in more basic conditions (**Figure 2C**). Formation of hydroxyapatite was strongly affected by pH (**Figure 2D**). Examining the rate of change in mineral formation demonstrated that the higher mineral content achieved in more basic environment corresponded with a sharper fast growth phase and higher formation rate in the fast-growth phase (**Figure 2E**). We identified two outcomes that characterize the mineralization dynamics: *i*) mineralization delay identified from plots in Figure 2E as time to reach the maximal rate of mineralization and *ii*) mineralization degree, identified as the ratio between mineralization level at  $t=200$  between the investigated and standard physiological conditions. Mineralization degree was only marginally affected by the environment pH (from ~14 days in pH 6.8 to ~11 days in pH 8.0), while the degree of mineralization was significantly impacted by pH (**Figure 2D**). When we plotted the dependence of mineralization delay and degree as a function of pH, we observed a non-linear decrease in the mineralization delay and a linear increase in degree of mineralization with an increase in pH (**Figure 2F**).

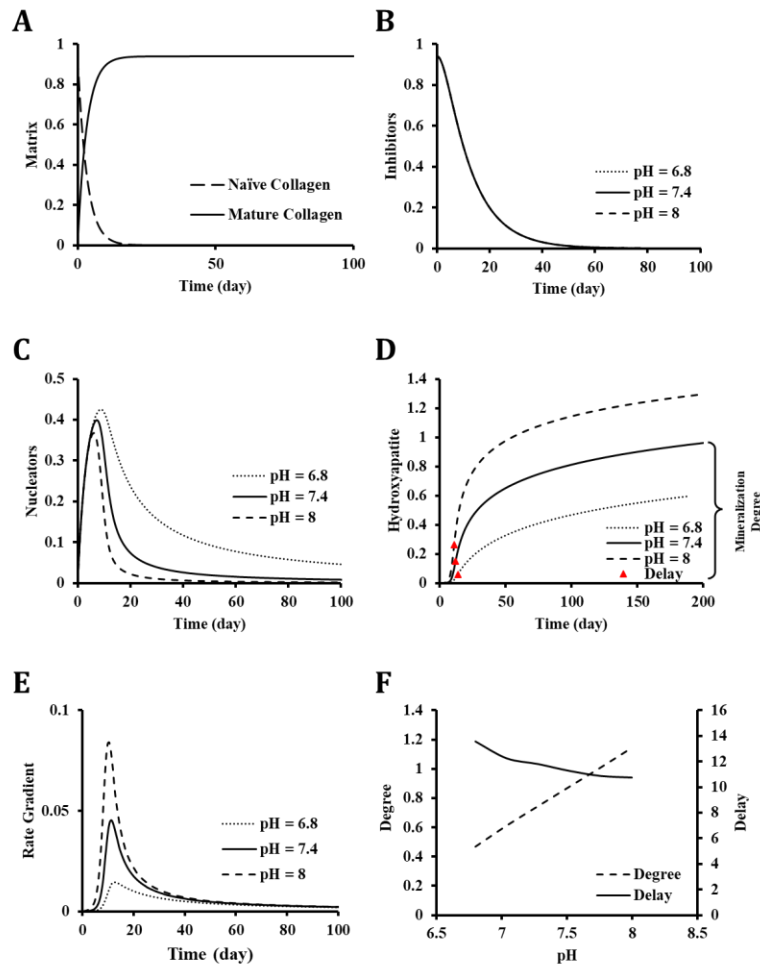


**Figure 2. Bone mineralization model behavior influenced by changes in pH level of the BIF.** Plotted are changes in time in naïve and mature collagen (A), inhibitors (B), nucleators (C), hydroxyapatite (D), and the rate of mineral formation (E) at physiological pH 7.4 (solid line) and physiologically relevant levels of acidic pH 6.8 (dotted line) and basic pH 8.0 (dashed line). (F) pH dependence for mineralization delay (solid line, right scale) identified from plots in E as time to reach maximal rate of mineralization, and mineralization degree (dashed line, left scale) identified as mineralization level at  $t=200$  normalized to that observed in standard physiological conditions.

Next, we performed a sensitivity analysis for model parameters by examining the changes in mineralization dynamics, delay and degree upon varying individual model parameters (**Figure 3**). Matrix maturation characteristic rate,  $k_1$  strongly effected mineralization dynamics (**Figure 3 A,B**). Decrease in  $k_1$  led to remarkable increase the delay time ( $\sim 100$  days for  $k_1 = 0.003$ ) associated with an increase in mineralization degree (1.5 for  $k_1 = 0.03$ ), however increasing  $k_1$  had a limited effect (no significant changes between  $k_1$  values of 3 or 30) (**Figure 3 A,B**). The inhibitors production rate  $v_1$  also strongly affected mineralization delay times, but the mineralization degree was not considerably affected (**Figure 3 C,D**). The inhibitors removal characteristic rate  $r_1$  affected both mineralization delay and degree, but in this case lower delay times were associated with higher degree of mineralization (**Figure 3 E,F**). The nucleator production rate  $k_2$  showed no significant impact on delay time, while higher  $k_2$  values caused much higher mineral formation (**Figure 3 G,H**). The nucleators removal characteristic rate  $r_2$  did not affect the delay time, but decreasing its value within the same order of magnitude, led up to 2.5 times higher mineralization degree (**Figure 3 I,J**). Changes in the maximum physicochemical precipitation rate  $f(R)$  strongly affected mineralization degree and slightly delay times (**Figure 3 K,L**).

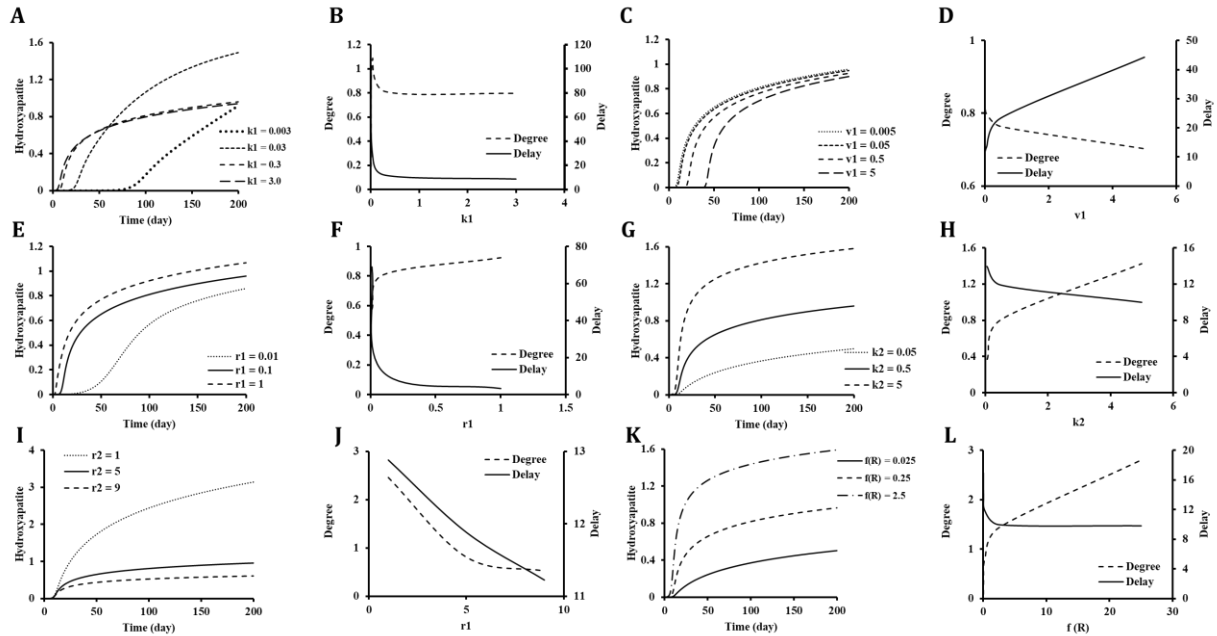


**Figure 3. Sensitivity analysis for the parameter changes in the integrated model.** Model parameters, including characteristic rates of matrix maturation,  $k_1$  (A, B), inhibitors production  $v_1$  (C, D), inhibitors removal  $r_1$  (E, F), nucleator production  $k_2$  (G, H), nucleator removal  $r_2$  (I, J) as well as the maximum physicochemical precipitation rate  $f(R)$  (K, L) were varied as indicated on the corresponding plots, and the mineralization dynamics (A, C, E, G, I, K), delay (B, D, F, H, J, L, solid lines, right axes) and degree (B, D, F, H, J, L, dashed lines, left axes) were examined.

Next, we investigated how the mineralization dynamics is affected when BIF levels of calcium and phosphorus are changed from the physiologically normal, clinically observed low and high levels [31]. The change from the normal range of phosphate concentration (0.8-1.45 mM) to the hypophosphatemic condition (0.3-0.8 mM) or the hyperphosphatemic condition (1.45-2.0 mM) slightly affected the mineralization delay and strongly affected the degree of

mineralization (**Figure 4 A, B**). Similarly, the change from the normal range of calcium concentration (1.0-1.4 mM) to the hypocalcemic (0.6-1.0 mM) or the hypercalcemic (1.4-3.0 mM) conditions had minimal effect on the mineralization delay and strong effect on mineralization degree (**Figure 4 C, D**). Thus, the model predicted bone hypomineralization in rickets due to hypophosphatemia [32] or hypocalcemia [33], but failed to predict the significant delay in mineralization offset observed in histomorphometry studies [32],

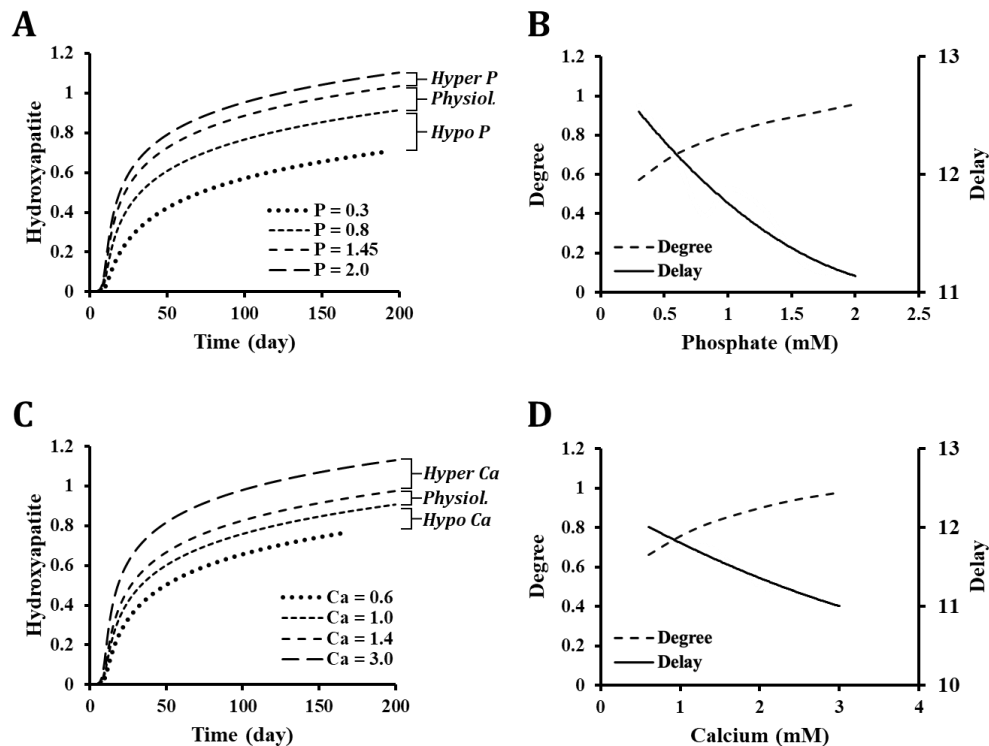


**Figure 4. Mineralization dynamics under normal, hypo- and hyper- physiological calcium and phosphate levels at BIF.** BIF phosphate (**A, B**) or calcium (**C, D**) were varied as indicated on the corresponding plots, and the mineralization dynamics (**A, C**), delay (**B, D**, solid lines, right axes) and degree (**B, D**, dashed lines, left axes) were examined.

We next examined how the model can be updated to predict the mineralization delay observed in the conditions of hypophosphatemia and hypocalcemia. Since the sensitivity analysis indicated that the delay is strongly affected by the dynamics of inhibitors (**Figure 3**), we tested if associating the inhibitor removal term with mineral formation would improve model predictions. The new term for the removal of inhibitors was introduced (equation 9b):  $t_1(dy/dt)I$  where  $t_1$  is inhibitor removal characteristic rate,  $dy/dt$  is the rate of mineral formation, and  $I$  is the current concentration of inhibitors. Matrix maturation was not affected by introducing the new term, or by changes in  $t_1$  (**Figure 5 A**). Both inhibitors (**Figure 5 B**) and nucleators (**Figure 5 C**) were removed faster when  $t_1$  was increased. Change in  $t_1$  minimally affected the degree of mineralization (**Figure 5 D**), however the mineralization delay was strongly affected (**Figure 5 D, E**). An interesting observation was the mineral formation rate behavior, which kept a similar behavior and intensity at different  $t_1$  values, but in the lower  $t_1$  side, the behavior appeared in an later time (**Figure 5 E**). The dependence of mineralization delay and degree on  $t_1$  (**Figure 5 F**) was qualitatively similar to that observed with the original equation for the inhibitor removal (**Figure 3 F**).

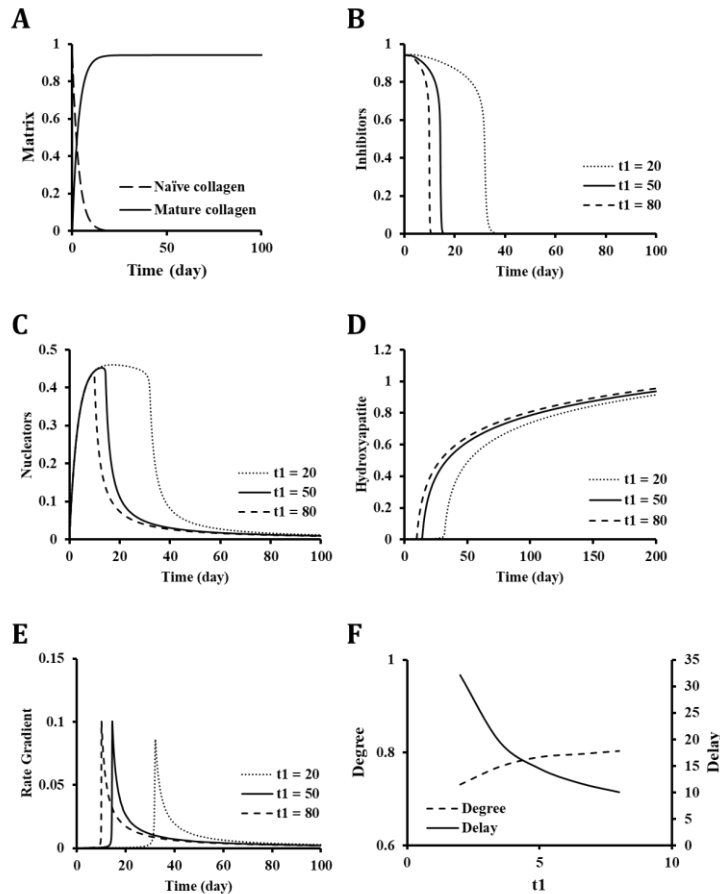


**Figure 5. Bone mineralization model behavior with an alternative inhibitor removal term.** Plotted are changes in time in naïve and mature collagen (A), inhibitors (B), nucleators (C), hydroxyapatite (D), and the rate of mineral formation (E) at indicated levels of  $t_1$ . (F) Mineralization delay (solid line, right scale), and mineralization degree (dashed line, left scale) as function of  $t_1$ .

Next, we compared how the models with different inhibitor removal terms predict the effect of severe hypo- and hyperphosphatemia. When equation (9a) was used, changing phosphate level showed no impact on the value or dynamics of inhibitors. In contrast, when we used equation (9b), change in phosphate concentration led to change in the behavior of inhibitors

(Figure 6 A). As a result, there was a mineralization delay in hypophosphatemic conditions that was much more prominent when the equation (9b) was used compared to equation (9a), while mineralization degree was affected similarly (Figure 6C, D).

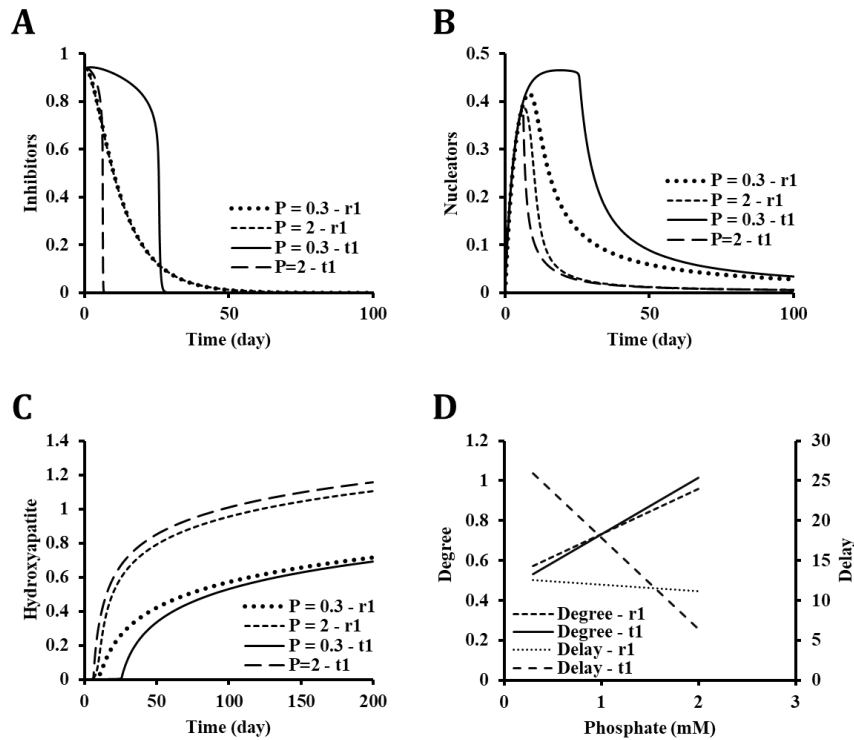


**Figure 6. Comparison of model predictions with different inhibitor removal terms at severe hypo- and hyperphosphatemia.** Plotted are changes in time in inhibitors (A), nucleators (B), hydroxyapatite (C) at indicated levels of BIF phosphate. (F) Mineralization delay (solid line, right scale), and mineralization degree (dashed line, left scale) as function of BIF phosphate levels.

Lastly, we examined the predictions of updated model for the effect of physicochemical changes, including BIF pH and levels of calcium and phosphate on bone mineralization. The updated model predicted stronger effects of pH (**Figure 7 A,B**), BIF phosphate (**Figure 7 C,D**) and calcium (**Figure 7 E,F**) on mineralization delay compared to the original model (**Figure 2** and **Figure 4**), while the changes in mineralization degree were similar between the models.

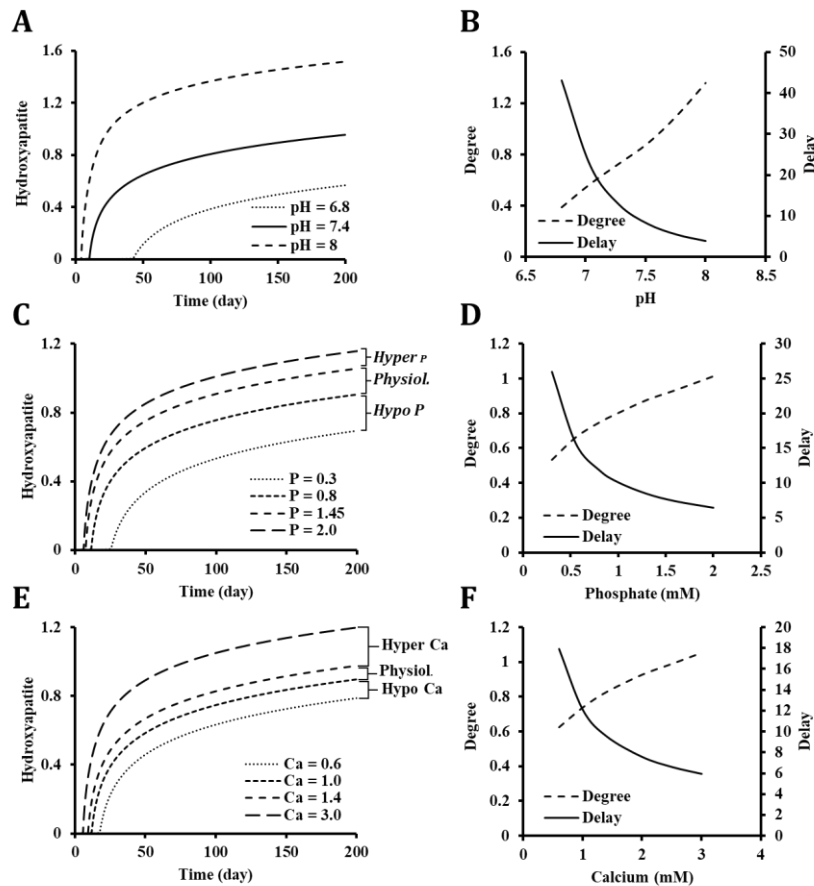


**Figure 7. Predictions of the updated model for the effects of physicochemical factors on bone mineralization.** BIF pH (**A, B**), phosphate (**C, D**) or calcium (**E, F**) were varied as

indicated on the corresponding plots, and the mineralization dynamics (**A, C, E**), delay (**B, D, F**, solid lines, right axes) and degree (**B, D, F**, dashed lines, left axes) were examined.

#### **4. Discussion**

In this study we developed a mathematical model that integrates the physicochemical and biological aspects of regulation of bone mineralization. We analyzed the model behavior and predictions with regard to experimentally measurable outcomes of the delay in the offset of bone mineralization and the degree of achieved mineralization. We identified the limitation of the previously developed model and proposed a model adaptation that allows us to correctly predict the mineralization delay observed in the situations of hypophosphatemia and hypocalcemia. The resulting mathematical model can be used to study the influence of alterations in physicochemical (pH, electrolyte levels) and biological (mutations, expression levels) factors on the outcome of bone mineralization.

Connecting the models of physicochemical regulation in BIF [6, 10] and biological regulation of bone mineralization [8] allowed us to examine the clinically relevant scenarios of osteomalacia in rickets due to hypophosphatemia [32] or hypocalcemia [33]. In both situations, the bone histomorphometry analysis demonstrated significant delay in mineralization offset as evident by accumulation of unmineralized osteoid [32], as well as low degree of mineralization [33]. However, just combining the previously developed models did not allow for predicting an observed delay in the mineralization offset. In the revised model, we introduced a new description of the inhibitors dynamics by associating their removal term with rate of mineral formation.

Multiple mineralization inhibitors have been identified to date, including pyrophosphate (PPi) [34], Matrix Gla Protein (MGP) [4, 5], Osteopontin (OPN) [35], and Dentin Matrix Protein 1 (DMP1) [28]. These inhibitors exhibit different mechanisms of action. PPi, which is produced both intra and extracellularly by enzymatic reactions, inhibits formation and growth of calcium and phosphate crystals. However, alkaline phosphatase mediated hydrolysis of PPi results in production of phosphate that promotes mineralization. Similar to PPi, OPN binds to crystals and prevents their growth, and loses its inhibitory properties through the action of tissue nonspecific alkaline phosphatase [35-37]. MGP is a circulating mineralization inhibitor. MGP overexpression was shown to cause moderate osteomalacia [5], and its ablation resulted in ectopic mineralization [4]. DMP1 was shown to act as an inhibitor of mineralization when present in the solution [28], or as a promotor of mineralization when it is absorbed onto the collagen surface [38, 39]. Thus, the removal of inhibitors is required to permit mineral formation, however since the nature of these inhibitors is very different, it is difficult to predict which processes could dominate in determining the kinetics of overall removal of the inhibitors. Our study suggests that biological processes that link inhibitor removal to the mineralization rate are important in predicting an observed delay in the mineralization at low Ca and PO<sub>4</sub> levels.

In the current model, shift in the mineralization dynamics appears in the form of changes in the mineralization delay, degree of mineralization, or both. Mineralization delay in an experimental setting could be represented by histomorphometry measures of osteoid volume per bone volume (OV/BV) or osteoid thickness (O.Th.). Bone mineral density distribution (BMDD) could be seen as a measure relevant to mineralization degree [40]. Manipulating single parameters in the model results in different behavioral paradigms of the

pair of mineralization delay/degree. In general, we observed two patterns of changes: *i)* shorter mineralization delay was associated with higher mineralization degree and vice versa, when we changed inhibitor removal rate, nucleators production rate, or maximum mineral precipitation rate; *ii)* shorter mineralization delay was associated with lower mineralization degree and vice versa when we changed the removal characteristics rate of nucleators, or the matrix maturation characteristic rate. In the future, the model can be used to study the combinations of parameters that might have synergistic or opposing effect on either mineralization degree or delay time. This is beneficial in fine-tuning the model to reproduce specific cases where an observed hydroxyapatite formation dynamic is not reproduced by changing a single parameter. Importantly, introduction of BIF provides an opportunity to understand at least in part the interactions between the BIF and mineralization dynamics. The model successfully showed that pH plays a crucial role in mineralization dynamics, allowing its application for diseases in which altered systemic pH is associated with bone abnormalities, such as metabolic acidosis, respiratory acidosis, renal tubular acidosis, hyperparathyroidism, chronic kidney disease [41]

The current model, being an integration of two other models, naturally comes with limitations relevant to previous models, as well as new ones adopted to make the integration possible. For the biological compartment, major limitations are: 1) matrix maturation steps such as collagen cross-linking, and post-translational modifications of proteins are not explicitly taken into account; 2) different mechanisms of action of different inhibitors are combined into one term; 3) different mechanisms of inter and intrafibrillar nucleation are not described; 4) no physical limitation is put for the maximum capacity of the matrix to store deposited minerals. On the physicochemical compartment side, the major limitations

are: 1) no influence of biological factors on the equilibrium established in the BIF; 2) inhibitors and nucleators of mineralization are only regulated biologically; 3) the BIF is homogenous, and ions are immediately distributed within it; 4) hydroxyapatite is the only form of mineral allowed to be formed in the BIF. For the integrated model the main limitation is that the flow of information is a one-way from the physicochemical to the biological compartment, so that changes in the latter do not affect the former. It is important to note that while developing and fine tuning a multi-aspect model takes more resources, it comes with the benefit of performing more comprehensive investigations, thus improving the reliability of predictions.

## **5. Conclusion**

In this work, building upon our previous studies, we developed a mathematical model that captures the synergistic impact of major biological and physicochemical factors involved in bone mineralization. This model can be used to further investigate different physiological conditions relevant to hydroxyapatite precipitation. The modular structure of this model makes it possible to easily adjust it for any relevant mineral of interest in other calcified tissues. Control of the user of the model over different parameters involved in each compartment of the model makes it possible to determine all combinations of factors that would cause a specific phenotype or mineralization dynamics, and use it for *in silico* testing of hypotheses regarding different molecular, cellular, or clinical experiments. These studies will deepen our understanding of the relationship between calcium and phosphate

homeostasis and bone mineralization dynamics in normal and pathophysiological scenarios  
accelerating discoveries of the mechanisms of relevant diseases.

## References

1. Fratzl, P., et al., *Nucleation and growth of mineral crystals in bone studied by small-angle X-ray scattering*. *Calcified tissue international*, 1991. **48**: p. 407-413.
2. Rauch, F. and F.H. Glorieux, *Osteogenesis imperfecta*. *The Lancet*, 2004. **363**(9418): p. 1377-1385.
3. Hunter, G.K., C.L. Kyle, and H.A. Goldberg, *Modulation of crystal formation by bone phosphoproteins: structural specificity of the osteopontin-mediated inhibition of hydroxyapatite formation*. *Biochemical Journal*, 1994. **300**(3): p. 723-728.
4. Marulanda, J., et al., *Matrix Gla protein deficiency impairs nasal septum growth, causing midface hypoplasia*. *Journal of Biological Chemistry*, 2017. **292**(27): p. 11400-11412.
5. Murshed, M., et al., *Extracellular matrix mineralization is regulated locally; different roles of two gla-containing proteins*. *The Journal of cell biology*, 2004. **165**(5): p. 625-630.
6. Poorhemati, H. and S.V. Komarova, *Mathematical model of physicochemical regulation of precipitation of bone hydroxyapatite*. *Mathematical modeling and optimization for real life phenomena*, 2024: p. 89.
7. Bonjour, J.-P., *Calcium and phosphate: a duet of ions playing for bone health*. *Journal of the American College of Nutrition*, 2011. **30**(sup5): p. 438S-448S.
8. Komarova, S.V., et al., *Mathematical model for bone mineralization*. *Front Cell Dev Biol*, 2015. **3**: p. 51.
9. Ostapienko, B.I., D. Lopez, and S.V. Komarova, *Mathematical modeling of calcium phosphate precipitation in biologically relevant systems: scoping review*. *Biomech Model Mechanobiol*, 2019. **18**(2): p. 277-289.
10. Poorhemati, H. and S.V. Komarova, *Mathematical modeling of the role of bone turnover in pH regulation in bone interstitial fluid*. *Computational Biology and Chemistry*, 2021. **94**: p. 107564.
11. Drake, F., G. Pierce, and M. Dow, *Measurement of the dielectric constant and index of refraction of water and aqueous solutions of KCl at high frequencies*. *Physical Review*, 1930. **35**(6): p. 613.
12. Morel, F. and J. Morgan, *A Numerical Method for Computing Equilibria in Aqueous Chemical Systems Environmental Science & Technology*. 1972.
13. Inskeep, W.P. and J.C. Silvertooth, *Kinetics of hydroxyapatite precipitation at pH 7.4 to 8.4*. *Geochimica et Cosmochimica Acta*, 1988. **52**(7): p. 1883-1893.
14. Söhnel, O. and F. Grases, *Supersaturation of body fluids, plasma and urine, with respect to biological hydroxyapatite*. *Urological Research*, 2011. **39**(6): p. 429-436.
15. Oyane, A., et al., *Preparation and assessment of revised simulated body fluids*. *Journal of Biomedical Materials Research Part A*, 2003. **65**(2): p. 188-195.
16. Koutsoukos, P. and G. Nancollas, *Crystal growth of calcium phosphates-epitaxial considerations*. *Journal of crystal growth*, 1981. **53**(1): p. 10-19.
17. Chughtai, A.R., R. Marshall, and G.H. Nancollas, *Complexes in calcium phosphate solutions*. *The Journal of physical chemistry*, 1968. **72**(1): p. 208-211.
18. Butler, J.N., *Ionic equilibrium: solubility and pH calculations*. 1998: John Wiley & Sons.
19. Childs, C., *Potentiometric study of equilibria in aqueous divalent metal orthophosphate solutions*. *Inorganic Chemistry*, 1970. **9**(11): p. 2465-2469.

20. Granjon, D., O. Bonny, and A. Edwards, *Coupling between phosphate and calcium homeostasis: a mathematical model*. American Journal of Physiology-Renal Physiology, 2017. **313**(6): p. F1181-F1199.
21. Salaun, F., B. Mietton, and F. Gaucheron, *Influence of mineral environment on the buffering capacity of casein micelles*. Milchwissenschaft Milk Science International, 2007. **62**(1): p. 20-23.
22. Crundwell, F.K., *Path from Reaction Control to Equilibrium Constraint for Dissolution Reactions*. ACS Omega, 2017. **2**(8): p. 4845-4858.
23. Guynn, R.W., *Equilibrium constants under physiological conditions for the reactions of choline kinase and the hydrolysis of phosphorylcholine to choline and inorganic phosphate*. Journal of Biological Chemistry, 1976. **251**(22): p. 7162-7167.
24. Silverstein, T.P. and S.T. Heller, *p K a Values in the Undergraduate Curriculum: What Is the Real p K a of Water?* Journal of Chemical Education, 2017. **94**(6): p. 690-695.
25. Christiansen, D.L., E.K. Huang, and F.H. Silver, *Assembly of type I collagen: fusion of fibril subunits and the influence of fibril diameter on mechanical properties*. Matrix Biology, 2000. **19**(5): p. 409-420.
26. Aleš, H., J. Lenka, and Š. Ludvík, *The influence of simulated body fluid composition on carbonated hydroxyapatite formation*. Ceram.-Silik, 2002. **46**(1): p. 9-14.
27. Murshed, M., *Mechanism of Bone Mineralization*. Cold Spring Harb Perspect Med, 2018. **8**(12).
28. He, G., et al., *Spatially and temporally controlled biomineralization is facilitated by interaction between self-assembled dentin matrix protein 1 and calcium phosphate nuclei in solution*. Biochemistry, 2005. **44**(49): p. 16140-16148.
29. Reznikov, N., et al., *Biological stenciling of mineralization in the skeleton: local enzymatic removal of inhibitors in the extracellular matrix*. Bone, 2020. **138**: p. 115447.
30. Gericke, A., et al., *Different forms of DMP1 play distinct roles in mineralization*. Journal of dental research, 2010. **89**(4): p. 355-359.
31. McKee, T.J. and S.V. Komarova, *Is it time to reinvent basic cell culture medium?* Am J Physiol Cell Physiol, 2017. **312**(5): p. C624-C626.
32. Robinson, M.-E., et al., *Mineralized tissues in hypophosphatemic rickets*. Pediatric Nephrology, 2020. **35**: p. 1843-1854.
33. Lambert, A. and A. Linglart, *Hypocalcaemic and hypophosphatemic rickets*. Best Practice & Research Clinical Endocrinology & Metabolism, 2018. **32**(4): p. 455-476.
34. Sapir-Koren, R. and G. Livshits, *Bone Mineralization and Regulation of Phosphate Homeostasis*. Ibms Bonekey, 2011. **8**(6).
35. Boskey, A., et al., *Osteopontin-hydroxyapatite interactions in vitro: inhibition of hydroxyapatite formation and growth in a gelatin-gel*. Bone and mineral, 1993. **22**(2): p. 147-159.
36. McKEE, M.D. and A. Nanci, *Osteopontin and the bone remodeling sequence. Colloidal-gold immunocytochemistry of an interfacial extracellular matrix protein*. Annals of the new York Academy of Sciences, 1995. **760**: p. 177-189.
37. Nanci, A., et al., *Ultrastructural characterization and immunolocalization of osteopontin in rat calvarial osteoblast primary cultures*. Microscopy research and technique, 1996. **33**(2): p. 214-231.
38. He, G., et al., *Nucleation of apatite crystals in vitro by self-assembled dentin matrix protein I*. Nature materials, 2003. **2**(8): p. 552-558.

39. Hunter, G.K. and H.A. Goldberg, *Nucleation of hydroxyapatite by bone sialoprotein*. Proceedings of the National Academy of Sciences, 1993. **90**(18): p. 8562-8565.
40. Roschger, P., et al., *Bone mineralization density distribution in health and disease*. Bone, 2008. **42**(3): p. 456-466.
41. Bushinsky, D.A. and N.S. Krieger, *Effects of acid on bone*. Kidney international, 2022. **101**(6): p. 1160-1170.

## **Chapter 6. Final Discussion, Conclusion, and Future Directions**

### **6.1. Advancing the mathematical modeling of bone formation**

The main goal of my research was to improve the clinical applicability of the mathematical model of bone mineralization [1]. The previous model was able to successfully capture the nonlinear behavior of bone mineral formation as it begins with a period of matrix maturation and no mineral formation, equivalent to the osteoid formation, followed by a fast mineral growth phase that represent the primary bone mineralization state, and finally by a third phase where the mineral formation slows, consistent with the secondary mineralization stage [2]. The model performed well in capturing the dynamic of bone formation and several diseases, however, it lacked the required components to be able to describe different scenarios of hypo or hyper-mineralization due to alterations in pH or ion availability. It must be noted that abnormal mineralization is not always caused by abnormal levels of required ions. There are cases where abnormal mineralization occurs while physiologically normal levels of calcium and phosphate are available. For example, osteogenesis imperfecta (OI), a condition characterized by high bone fragility due to brittleness caused by high mineral content [3], is generally characterized by normal levels of blood calcium and phosphorus. The previous model was successful in characterizing different hypermineralization dynamics observed in osteogenesis imperfecta. However, that model was not applicable to examine osteomalacia resulting from systemic low levels of calcium or phosphate or deficiency in their regulating hormones like vitamin D or FGF23 [4]. Thus, my goal was to build a mathematical model able to capture both physicochemical and biological aspects of bone mineralization thus improving its applicability to the full range of clinical scenarios.

To address the model limitations, different steps needed to be taken. First, there was a need to include an aqueous environment that resembles the bone microenvironment, where a supersaturated solution of different calcium and phosphate species can make the hydroxyapatite mineral formation possible. As presented in chapter 3, initially an aqueous environment containing a limited number of known chemical species of bone interstitial fluid was conceptualized and simulated. Provided the total concentrations of calcium, phosphate, carbonate, and hydrogen (pH), the physicochemical properties of the system were investigated. Particularly, the effect of processes equivalent to bone resorption or formation on the pH of the solution was of interest. Although the first model had no provision for mineral formation, and it was not capable of predicting the hydroxyapatite precipitation rate, it provided significant insights into important chemical interactions occurring the bone aqueous microenvironment.

Building upon the initial model, a comprehensive model of bone interstitial fluid was developed, as presented in chapter 4. This model included the total concentration of seven major components (calcium, phosphate, carbonate, magnesium, sodium, potassium, chloride) plus pH of the environment to be able to characterize the physicochemical properties of the environment and the rate of mineral formation under the defined scenario. The equilibrium in this model includes a total of 30 chemical species, and hydroxyapatite is the only form of mineral this environment is permissive to its precipitation. It is important to note that mathematical model of such complexity, which includes both large number of variables and the high level of non-linearity, requires extensive computational resources. One important modeling effort described in Chapter 4, is the implementation of a new numerical approach, which allowed to drastically reduce the resources and time required to

perform simulations. This reduced the needs from hours on supercomputers for the simple model described in Chapter 3 to the minutes on regular computers for the much more complex model described in Chapter 4. The model describing the physicochemical processes in BIF was successful at investigating ion distribution, supersaturation, and precipitation rate of hydroxyapatite at physiologically normal levels of ions as well as in pathological conditions. Importantly, the model prediction was validated against experimental data. Thus, the simulated bone interstitial fluid model provided insights into the aqueous phase behavior and was trustworthy to be integrated with other relevant models of bone mineralization.

Finally, the model introduced in chapter 5 successfully integrates the descriptions of both biological and physicochemical factors that regulate bone mineralization. The model is built so that the physicochemical compartment (aqueous phase model) calculates the maximum rate at which hydroxyapatite precipitation is feasible in the bone interstitial fluid and informs the equation governing the mineral formation in the biological compartment. The biological compartment considers other regulators including maturation of extracellular matrix, and formation and removal of nucleation sites and inhibitors. Eventually the bone mineralization dynamics is impacted by both the physicochemical and biological processes. The integrated model was used to examine the bone mineralization outcome of low calcium or phosphate levels, which clinically is known to result in osteomalacia, a mineralization disorder characterized by high mineralization lag time and lower mineralization degree [5-8]. While the model predicted the lower mineral content, it could not predict a change in the mineralization lag time, which led us to develop an alternative term to describe the dynamics of mineralization inhibitors. Associating inhibitor removal term with mineralization rate

made a significant impact on model prediction of mineralization delay. Since different mechanisms of action and removal of various bone mineralization inhibitors were previously described [9-12], the model predicts that inhibitor removal proportional to mineralization is critical.

The integrated model developed in this work provides the opportunity to investigate various scenarios of physiological and pathological bone mineralization. This includes examining the outcomes of genetic alterations that might affect the biological factors as well as physicochemical factors arising from an altered environmental condition. Importantly, the model captures the interconnected nature of the physicochemical and biological processes that occur during bone mineralization. This model can also be adapted to other processes of biologically-regulated mineralization, such as physiological formation of other mineralized tissues including dentin, enamel or eggshell, as well pathophysiological calcification observed in kidney stone formation and atherosclerosis.

The overall conclusions of my studies are summarized as follows:

1. Bone aqueous microenvironment (bone interstitial fluid) affects and is affected by bone mineralization and demineralization
2. Carbonate buffer is relatively more important than phosphate buffer in bone interstitial fluid
3. Novel approach is developed to mathematically model physicochemical aspects of bone mineralization

4. The contribution of biological and physicochemical factors in regulating hydroxyapatite precipitation under physiological and pathophysiological conditions can be examined.
5. Accounting for chemical reactions in bone interstitial fluid allows to demonstrate why deviations of phosphate blood concentration from normal ranges has particularly strong effect on bone mineralization.
6. A more realistic depiction of bone mineralization processes facilitates development of treatment strategies for diseases exhibiting abnormal mineralization.
7. An easily available and re-usable tool generated in these studies will help researchers to further investigate various scenarios of abnormal mineralization, to hypothesize on the cause and to design experimental and clinical studies to validate their hypothesis.

## **6.2. Application of the model**

Mathematical modeling has become a cornerstone of scientific discoveries in life sciences. Translating intricate biological systems into a framework of equations and computational simulations not only provides the opportunity to do rigorous analysis on the observed behavior of the system under investigation, but also facilitates and accelerates the generation of new predictions to be later experimentally tested. Mathematical modeling also fosters a deeper understanding of biological phenomena by bridging the established knowledge and emerging ideas. Models can seamlessly incorporate data generated in meticulously controlled laboratory experiments alongside with real-world observations. They can integrate different aspects or description of a process into one cohesive unit, take

advantage of our current state of knowledge in many different fields and help us illuminate areas where our knowledge remains incomplete. We can bring our established knowledge of chemistry, physics and biology and use mathematics, statistics and computation to perform virtual experiments to test new hypotheses in a controlled environment without spending significant time or financial resource.

The bone mineralization model developed and presented in chapter 5 offers great potential in investigating different physiologically relevant scenarios of bone mineralization in healthy or pathological conditions. However, it must be noted that to interpret the outcomes and predictions, one must always consider the assumptions implemented in developing this model and limitations that are inherent to this model, which are extensively discussed in chapter 5. We identified two measures to compare the model predictions and the experimental observations regarding the change in bone mineralization behavior: mineralization delay and mineralization degree. These metrics were chosen to correspond to commonly measured experimental outcomes: the presence of non-mineralized matrix (osteoid), osteoid volume per bone volume (OV/BV) and/or osteoid thickness (O.Th.) that could be considered as a measure of mineralization lag time, and bone mineral density distribution (BMDD) that represents a measure of mineralization degree. Using these two measures, one can systematically manipulate different parameters of physicochemical and biological compartments of the model to reproduce the combination of phenotypes shown in **Figure 1**. More than one set of parameters might lead to a specific phenotype. This could show that a specific dynamic could be caused by different combinations of regulators. Such a systematic search will provide a possible mechanism behind specific phenotypes. Interpreting the model predictions and proposed mechanisms, researchers can move

forward to experimentally test the model prediction for each phenotype-mechanism pair. This will potentially accelerate the discovery of underlying mechanisms of many abnormal bone diseases or provide new insights into the process. In a complimentary approach, diseases of abnormal bone mineralization can be characterized according to the two outcome measures: delay and degree of mineralization. Then, the algorithm presented on Figure 1 could be used in reverse, right to left, by first identifying the relevant outcomes and then examining potential mechanisms that can underly its development. Combining these two steps together, different diseases or conditions could match with specific mechanisms, i.e. the combination of parameters, to eventually design targeted experimental and clinical studies to validate these predictions.

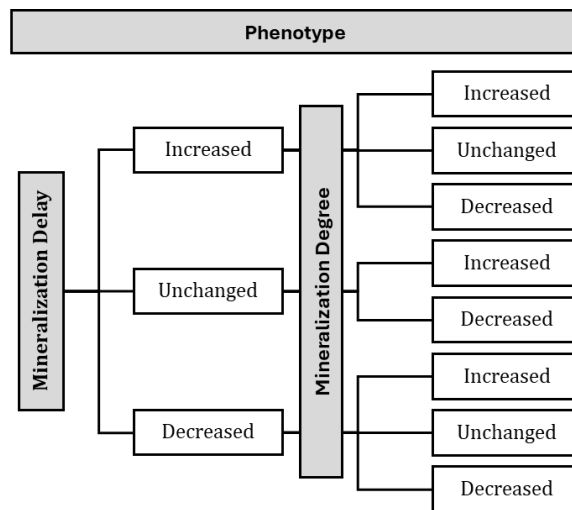


**Figure 1.** Breakdown of different bone mineralization phenotype based on model outcome measures: mineralization delay and mineralization degree

While taking these steps is not in the scope of current work, it is worth providing a brief list of potential diseases to be later studied by the model. First, we suggest separating these diseases into two categories: 1. Characterized by abnormal levels of calcium and phosphate. Some of the diseases of the first category which are characterized by abnormal levels of calcium or phosphate in the blood are: hyperparathyroidism [13], hypoparathyroidism [14], and chronic kidney disease (CKD) [15]. 2. Characterized by normal levels of calcium and phosphate. Of the diseases belonging to the second category which are characterized by normal levels of calcium and phosphate in the blood, some are: Rickets/Osteomalacia [4], Fibrous dysplasia [16], Osteogenesis imperfecta (OI) [17], and McCune-Albright syndrome [18]. While this separation makes it easier to direct parameter space search toward the physicochemical or biological compartments, it is important to remember that these compartments are interconnected and that in a specific condition both types of regulators can contribute. Since the model allows easy investigation of the contribution of single or combination of different parameters, as well as quantitative estimate of the effect size, model simulations will provide insights for the outcome of complex scenarios.

Investigating different abnormal mineralization with the model, alongside the new discoveries in the field of bone mineralization will direct potential improvements necessary to make future bone mineralization models even more reliable, which in turn help the advancement of discoveries in the field. As described, the interaction and communication among researchers employing in-silico, in-vitro and in-vivo models as well as clinicians is necessary and beneficial for everyone.

### **6.3. Accessibility of research**

Science thrives on the open exchange of ideas and information making research accessibility of critical importance. Accessibility goes beyond simply making research free to read, even though open access publications are a crucial step. It is also about ensuring that scientific findings are presented in a way that can be understood and utilized by a broad audience. Researchers can take further action to tailor their work for different audiences. This might involve creating lay summaries that break down complex concepts into easily understandable language for the public, interactive presentations that provide an engaging learning experience for students. During my PhD studies, I have employed these strategies when I presented my findings at the conferences focused on potential users of my research, including biologists at the International Conference on the Chemistry and Biology of Mineralized Tissues and clinicians at the International Association for Dental Research Meeting.

One of the most compelling reasons for accessible research is to drive efficiency and prevent wasting resources. When research findings and tools are readily available, others can avoid duplicating efforts and effectively build upon existing knowledge. Accessible research fosters collaboration and accelerates scientific progress. I have consistently provided the MATLAB implementation of the models in online public code repositories to facilitate their reuse in the future.

The benefits of accessible research extend far beyond the scientific community. For example, in a scenario where a patient can access a user-friendly app that summarizes the results of a new medical study relevant to their condition, could empower the individuals to take a more

active role in their own health. Similarly, accessible research findings can inform public policy decisions, leading to more effective solutions for a range of societal challenges. One of the future goals for me is to create a graphical user interface to save significant time and effort of fellow researchers (**Figure 2**). Such graphical user interface will improve the accessibility of the model for non-mathematicians and will allow them to alter model parameters and investigate the outcome of the model.

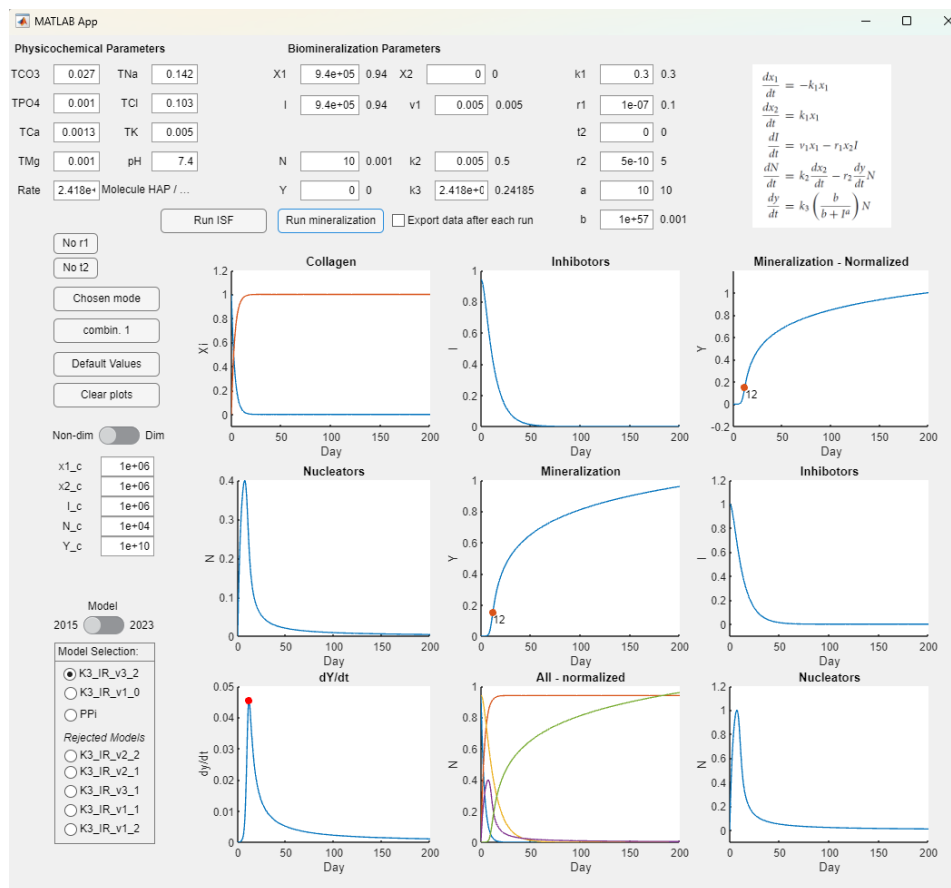


**Figure 2.** A Screen shot of the beta version of the graphical user interface of the integrated model of bone mineralization

Ultimately, the goal of accessible research is not to dumb down science, but to make it more inclusive and impactful. By fostering collaboration, preventing duplication of efforts, and empowering individuals with knowledge, accessible research paves the way for a brighter future where scientific advancements benefit all of humanity. The call to action is clear: researchers, institutions, and funding bodies must all work together to break down barriers and unlock the full potential of scientific discovery. By embracing accessibility, we can ensure that science continues to be a powerful force for positive change in the world.

## References

1. Komarova, S.V., et al., *Mathematical model for bone mineralization*. Front Cell Dev Biol, 2015. **3**: p. 51.
2. Roschger, P., et al., *Bone mineralization density distribution in health and disease*. Bone, 2008. **42**(3): p. 456-466.
3. Roschger, P., et al., *Evidence that abnormal high bone mineralization in growing children with osteogenesis imperfecta is not associated with specific collagen mutations*. Calcified tissue international, 2008. **82**(4): p. 263-270.
4. Cianferotti, L., *Osteomalacia is not a single disease*. International Journal of Molecular Sciences, 2022. **23**(23): p. 14896.
5. Arnala, I., et al. *Bone histomorphometry in celiac disease*. in *Annales Chirurgiae et Gynaecologiae*. 2001.
6. Roschger, P., et al., *Constant mineralization density distribution in cancellous human bone*. Bone, 2003. **32**(3): p. 316-323.
7. Rabelink, N.M., et al., *Bone pain and extremely low bone mineral density due to severe vitamin D deficiency in celiac disease*. Archives of osteoporosis, 2011. **6**: p. 209-213.
8. Cheung, M., et al., *Cortical and trabecular bone density in X-linked hypophosphatemic rickets*. The Journal of Clinical Endocrinology & Metabolism, 2013. **98**(5): p. E954-E961.
9. Boskey, A., et al., *Osteopontin-hydroxyapatite interactions in vitro: inhibition of hydroxyapatite formation and growth in a gelatin-gel*. Bone and mineral, 1993. **22**(2): p. 147-159.
10. Murshed, M., et al., *Extracellular matrix mineralization is regulated locally; different roles of two gla-containing proteins*. The Journal of cell biology, 2004. **165**(5): p. 625-630.
11. Sapir-Koren, R. and G. Livshits, *Bone Mineralization and Regulation of Phosphate Homeostasis*. Ibms Bonekey, 2011. **8**(6).
12. Marulanda, J., et al., *Matrix Gla protein deficiency impairs nasal septum growth, causing midface hypoplasia*. Journal of Biological Chemistry, 2017. **292**(27): p. 11400-11412.

13. Bilezikian, J.P., et al., *Hyperparathyroidism*. The Lancet, 2018. **391**(10116): p. 168-178.
14. Mannstadt, M., et al., *Hypoparathyroidism*. Nature Reviews Disease Primers, 2017. **3**(1): p. 1-21.
15. Kalantar-Zadeh, K., et al., *Chronic kidney disease*. The lancet, 2021. **398**(10302): p. 786-802.
16. Boyce, A.M., *Fibrous dysplasia*. 2015.
17. Rauch, F. and F.H. Glorieux, *Osteogenesis imperfecta*. The Lancet, 2004. **363**(9418): p. 1377-1385.
18. Hartley, I., et al., *Fibrous dysplasia of bone and McCune–Albright syndrome: a bench to bedside review*. Calcified tissue international, 2019. **104**: p. 517-529.